

**PEOPLE'S DEMOCRATIC REPUBLIC OF ALGERIA**  
**MINISTRY OF HIGHER EDUCATION AND SCIENTIFIC RESEARCH**  
**UNIVERSITY M'HAMED BOUGARA OF BOUMERDES**



**Faculty of Technology**  
**Department of Electrical Systems Engineering**

**Master's Thesis**

Presented by

**BELMESK MERYEM**  
**HADJ MOHAMED YOUSRA**

Course: Electrical engineering

Major: Electric Machines

---

**MODELING IRON LOSSES IN ROTATING  
ELECTRIC MOTORS**

---

**Defended publicly on 30 /06/2024 in front of a jury composed of:**

M'ZION	Nassima	Professeur	UMBB	President
ABDESLAME	Djamila	MCB	UMBB	Examiner
CHERAT	Nidhal	MCB	UMBB	Examiner
HAMEL	Meziane	MCA	UMBB	Supervisor
HADJAZ	Sadia	Engineer	Electro-industries	Co-Supervisor

**Academic year: 2023/2024**



# **ACKNOWLEDGEMENTS**

## **ACKNOWLEDGEMENTS**

I wanna thank ALLAH for everything, for being always here with me, listening to me, helping me and the most important thing is blessed me with all my gifts Al-HamdLALLAH, and here it is a the new one^^

We want to thank our supervisor, Sir Hamel Meziane, MCA at UMBB, for being a man with honor in his work, as well as for teaching us that hard and disciplined work leads to beautiful results.

A lot of Thanks to Ma'am HADJAZ Sadia, as well as Sir BENACER Mohand Ouamar, Engineers at the company Electro-Industries, for having supervised us within the company, we love to thank them of their endless support in every time we need them in our project of manufacturing induction motors, also Sir Bel Abbas for their advice and guidance in Epstein Frame and iron losses, without forgetting to thank all the Electro-Industries workers who helped us a lot in our period of stage

Our sincere thanks go to Ma'am M'ZIOU Nassima for having given us the honor of chairing the jury of our Graduation

We also thank Ma'am ABDESLAM Djamila and Sir CHERAT Nidhal, MCB at UMBB, for agreeing to examine our work

# **DEDICATIONS**

## Dedications

To the love of my life, "Vava" and "Yemma," there are no words on this planet that can express how much I am grateful and proud to be your little daughter. Thank you for making my life shine. Thank you for showing me what strength and resilience look like. Watching you face challenges with grace and sacrificed for us unconditionally has inspired me to be strong and never give up. Your courage and kindness is my inspiration. May Allah bless you both to us.

*Love you to the square of infinity, "mommy" and "daddy."<3*

To my backbone in this life, my cutest Sisters (Sousou, Kamo, Loulous), my lovely Brother Idir, and my Brothers and Sister in law (Said, Salim, Bouthina), as well as my little chocolates (Marouch, Mirou, Adam), being part of this family such an amazing thing, thank u all for being always here with me, for believing in me and being my biggest fan. May God bless us to us, *love u to the moon and back guys.*

To my crazy BFF (Ahlam, Maissa, Manel, Hayat, Roumissa, Lydia), and my Iraq friend Marwa, i don't know how i got so lucky to have a bestie as wonderful as you, your precious friendship has illuminated every step of this experience and made this path sweeter.

To my partner in crime, Yousra, your presence in my life was truly special for my heart. Thank you for always being here for me through all those years with your unlimited support. *LOVE U YOUTA*

**Meryem**

## **Dedications**

My Mama, to the light of my eyes, I want to thank you for your unconditional love and for your support every time. No matter what your condition is, whether you stay up late with me for encouragement, there's nothing that can explain my feelings of gratitude, and I thank you for always supporting me in all stages of my life. Without you, I wouldn't never be here, Mom.

to my Papa, my support in life, for who sacrificed his comfort for me, to the person who made me happy in my worst situation and was with me in every moment I needed him without complaint. If you collect all the languages of the world, they cannot express my love and gratitude to you. May you always be the sun of my life.

To my brother Fouzi and sister Hafsa, thank you for being with me on this path. With your constant support, I want to thank Fouzi, especially for those sentences, which were trivial but meant a lot to me. Thank you for everything, my lovely family.

I want to thank all my friends (Ahlam, Maissa, Manel, Hayat, Roumisa) who supported me, thank you very much BFF for everything.

To my reckless teenage friend and thin path, Eta (Meryomti), you have always been my sister, my support, and my best friend. You were and still are a healing force for my soul. Thank you for your support in every step of my life and for always pushing me to achieve my dreams.

***Yusra***

# **CONTENTS**

# CONTENTS

List of figures

List of Tables

List of Symbols and Acronyms

**GENERAL INTRODUCTION ..... 1**

## **CHAPTER I ELECTRIC MOTORS IN ELECTRIC VEHICLES**

**I.1 Introduction ..... 3**

**I.2 History of development of automobile ..... 3**

**I.2.1 Steam automobile..... 3**

**I.2.2 Thermal vehicles ..... 4**

**I.2.3 Electric vehicles..... 5**

**I.3 Battery electric vehicles ..... 5**

**I.4 Relationship between the Battery and Electric Motor ..... 6**

**I.5. Motors in electric vehicles..... 6**

**I.5.1. Permanent magnet synchronous motor (PMSM) ..... 7**

**I.5.2. Brushless DC motor (BLDC)..... 8**

**I.6. Induction motor ..... 8**

**I.6.1. Constitution..... 9**

**I.6.2. Stator..... 10**

**I.6.3. Rotor ..... 11**

**I.6.4. Principle of operation ..... 12**

**I.6.5. Rotating magnetic field..... 12**

**I.6.6. Slip..... 13**

**I.6.7. Power equation of induction motor ..... 14**

**a) Input power ..... 14**

**b) Air-gap power ..... 15**

**c) Output power ..... 15**

**I.6.8. Torque..... 15**

**I.6.9. Efficiency..... 16**

**I.7. Losses in induction motor ..... 16**

**I.8. Iron losses ..... 17**

II.8.1. Hysteresis losses.....	17
II.8.2. Eddy currents losses.....	18
II.8.3. Additional losses.....	18
<b>I.9. Conclusion.....</b>	<b>19</b>
<b>CHAPTER II MAGNETIC MATERIALS AND IRON LOSSES IN ELECTRIC MOTORS</b>	
<b>II.1 Introduction.....</b>	<b>20</b>
<b>II.2. Magnetism.....</b>	<b>20</b>
II.2.1. Intensity of Magnetization.....	20
<b>II.3. Orbital and Spin Magnetic Moment.....</b>	<b>21</b>
II.3.1. Orbital Magnetic Moment.....	21
II.3.2. Spin Magnetic Moment.....	22
II.3.3. Total Magnetic Moment.....	22
<b>II.4. Magnetic polarization and Magnetization.....</b>	<b>23</b>
II.4.1. Magnetic polarization.....	23
II.4.2. Magnetization.....	23
II.4.3. Magnetic Susceptibility.....	23
II.4.4. Flux density $B$ .....	24
<b>II.5. Type of Magnetic Materials.....</b>	<b>25</b>
II.5.1. Diamagnetism.....	26
II.5.2. Paramagnetism.....	26
II.5.3. Ferromagnetism.....	27
<b>II.6. Hysteresis.....</b>	<b>29</b>
II.6.1. Coercive Field $H_c$ .....	30
II.6.2. Remanent Induction $B_r$ .....	30
II.6.3. Hysteresis Mechanical.....	31
<b>II.7. Soft and Hard Magnetic Materials.....</b>	<b>32</b>
<b>II.8. Non-grain oriented iron and silicon iron sheets.....</b>	<b>32</b>
II.8.1. Non-Oriented Fully Processed Electrical Steel.....	33
II.8.2 Non-oriented semi-processed electrical steel.....	33
II.8.3. Principles of fabrication.....	33
<b>II.9. Grain-Oriented Iron-Silicon Sheets.....</b>	<b>34</b>
II.9.1. Principles of fabrication.....	34
II.9.2. Insulation of grain-oriented sheets.....	35

<b>II.10. Overview of Iron Losses Models .....</b>	<b>35</b>
<b>II.10.1. Steinmetz Equation .....</b>	<b>36</b>
<b>II.10.2. Standard losses separation approach.....</b>	<b>39</b>
<b>II.10.3. Epstein Frame.....</b>	<b>41</b>
<b>II.10.3. Method of work the epstein frame .....</b>	<b>42</b>
<b>II.11. Conclusion.....</b>	<b>43</b>

**CHAPTER III ELECTRO-INDUSTRIES COMPANY**

<b>III.1. Introduction.....</b>	<b>44</b>
<b>III.2. History of the company .....</b>	<b>44</b>
<b>III.3. Presentation of the company.....</b>	<b>44</b>
<b>III.4. Presentation of the motors unit .....</b>	<b>46</b>
<b>III.5. Cutting workshops .....</b>	<b>46</b>
<b>III.5.1. Cutting process .....</b>	<b>47</b>
<b>III.5.2. Packaging .....</b>	<b>47</b>
<b>III.5.3. Manufacturing of fan covers .....</b>	<b>48</b>
<b>III.6. Die casting workshops.....</b>	<b>48</b>
<b>III.7. Machining workshops .....</b>	<b>49</b>
<b>III.7.1. Manufacture of the shaft .....</b>	<b>50</b>
<b>III.8. Winding workshops .....</b>	<b>50</b>
<b>III.8.1. Insulation preparation sector .....</b>	<b>50</b>
<b>III.8.2. Coil preparation sector .....</b>	<b>51</b>
<b>III.8.3. Winding stator preparation sector .....</b>	<b>51</b>
<b>III.9. Assembly workshop .....</b>	<b>52</b>
<b>III.9.1. Pre-assembly sector .....</b>	<b>52</b>
<b>III.9.2. Final assembly sector .....</b>	<b>52</b>
<b>III.10. Final test .....</b>	<b>53</b>
<b>III.11. Conclusion .....</b>	<b>54</b>

**CHAPTER IV CALCULATION OF IRON LOSSES IN A 2.2 KW INDUCTION MOTOR**

<b>IV.1. Introduction.....</b>	<b>55</b>
<b>IV.2. Presentation of software motor-CAD .....</b>	<b>55</b>
<b>Part one: Calculating iron losses.....</b>	<b>56</b>
<b>IV.3. Epstein Frame .....</b>	<b>56</b>
<b>IV.4. Steel sheet M800-50A .....</b>	<b>57</b>

<b>IV.5. Steinmetz and bertotti equations .....</b>	<b>57</b>
<b>IV.6. Steel sheet M400-50A .....</b>	<b>61</b>
<b>IV.7. Comparison between steel sheets M800-50A and M400-50A .....</b>	<b>63</b>
<b>Part two Study on induction motor type 2.2 kW .....</b>	<b>65</b>
<b>IV.8. Presentation of the induction motor .....</b>	<b>65</b>
<b>IV.9. Machine geometry .....</b>	<b>66</b>
<b>IV.10. Patten distribution.....</b>	<b>68</b>
<b>IV.11. Curve of first magnetization .....</b>	<b>69</b>
<b>IV.12. Electromagnetic simulation results.....</b>	<b>70</b>
<b>IV.12.1. Mesh .....</b>	<b>70</b>
<b>IV.12.2. Magnetic field cartography .....</b>	<b>72</b>
<b>IV.12.3. Electromagnetic characteristics .....</b>	<b>72</b>
<b>IV.12.4. Magnetodynamic characteristics .....</b>	<b>75</b>
<b>IV.13. Airgap flux density .....</b>	<b>76</b>
<b>IV.14. Losses in the induction motor .....</b>	<b>77</b>
<b>IV.14.1. In the stator .....</b>	<b>77</b>
<b>IV.14.2. In the rotor .....</b>	<b>77</b>
<b>IV.15. Thermal study.....</b>	<b>78</b>
<b>IV.15.1. Geometry of the squirrel cage asynchronous machine.....</b>	<b>78</b>
<b>IV.15.2. Temperature distribution without of a cooling circuit.....</b>	<b>80</b>
<b>IV.15.3. Temperature distribution with cooling circuit .....</b>	<b>80</b>
<b>IV.16. Conclusion .....</b>	<b>83</b>
<b>GENERAL CONCLUSION.....</b>	<b>84</b>
<b>Bibliography .....</b>	<b>86</b>

# **LIST OF FIGURES**

# LIST OF FIGURES

## Chapter I Electric Motors in Electric Vehicles

Figure I.1. First electric car.....	4
Figure I.2. Electric car.....	4
Figure I.3. Electric vehicle components.....	5
Figure I.4. Relationship between the battery and electric motor.....	6
Figure I.5. Permanent magnet motor components.....	7
Figure I.6. Components of a BLDC motor.....	8
Figure I.7. Induction motor.....	9
Figure I.8. Components of the principal parts in the motor.....	10
Figure I.9. Induction motor stator construction.....	11
Figure I.10. Squirrel cage type rotor.....	11
Figure I.11. Construction working principle of induction motors.....	12
Figure I.12. Graph represent rotating magnetic field.....	13
Figure I.13. Power balance of the induction motor.....	14
Figure I.14. Losses in electrical machines.....	16
Figure I.15. (a) Measured iron loss data at 50 kHz and 100 kHz from silicon steel 50PN470. (b) The estimated hysteresis loss factor from two frequencies of iron loss data.....	17
Figure I.16. Hysteresis in magnetic.....	17
Figure I.17. Eddy currents losses.....	18

## Chapter II Magnetic materials and iron losses in electric motors

Figure II.1. Magnetic behavior of the atom.....	20
Figure II.2. Electron Orbit Magnetic Moment.....	21

Figure II.3. Magnetic moment of an electron.....22

Figure II.4. Behavior in a diamagnetic material.....26

Figure II.5. Behavior in a Paramagnetism material.....27

Figure II.6. Behavior in a Ferromagnetism material.....28

Figure II.7. Hysteresis Loop.....29

Figure II.8. Explication of Coercive Field.....30

Figure II.9. B-H diagram showing saturation (Bs), remanent induction flux density (Br),  
Coercive field strength (Hc), and a trail up from the unmagnetized material.....30

Figure II.10. Explication of Hysteresis Mechanical.....31

Figure II.11. Hysteresis mechanical in Soft and Hard Magnetic Materials.....32

Figure II.12. Model approaches to determine iron losses in electrical machines.....36

Figure II.13. Coils in epstein frame.....41

Figure II.14. Epstein frame measurement system.....42

Figure II.15. Epstein frame.....43

**Chapter III Electro-Industries Company**

Figure III.1. Logo of Electro-Industries.....44

Figure III.2. Satellite view of the company website.....45

Figure III.3. Factory units.....45

Figure III.4. UMA different workshops.....46

Figure III.5. Basic stages of the cutting workshop.....47

Figure III.6. Pictures from cutting process.....47

Figure III.7. Packaging of the stator package.....48

Figure III.8. fan covers.....	48
Figure III.9. Housing.....	49
Figure III.10. The basic stages of machining workshops.....	49
Figure III.11. Machining workshops.....	50
Figure III.12. Basic stages of Winding workshops.....	50
Figure III.13. Winding workshops.....	51
Figure III.14. Assembly workshop.....	53
Figure III.15. Resistance measurement and tests with load.....	53

**Chapter IV Calculation of iron losses in a 2.2 kW induction motor**

Figure IV.1. ANSYS Motor-CAD Software Window.....	56
Figure IV.2. Epstein Frame in the company Electro-Industries.....	56
Figure IV.3. Specific losses curve for M800-50A sheet from 30Hz to 200Hz.....	60
Figure IV.4. Specific losses curve for M800-50A sheet from 400Hz to 1000Hz.....	60
Figures IV.5. Loss density vs flux density for M400-50A.....	63
Figure IV.6. Housing.....	66
Figure IV.7. Rotor.....	66
Figure IV.8. Stator.....	66
Figure IV.9. Induction motor.....	66
Figure IV.10. Radial geometry of induction motor .....	67
Figure IV.11. Axial geometry of induction motor .....	67
Figure IV.12. 3D View of induction motor.....	68
Figure IV.13. Linear Patten Distribution.....	68
Figure IV.14. Radial Patten Distribution.....	69

Figure IV.15. Curve of first magnetization.....	70
Figure IV.16. Mesh of the motor.....	71
Figure IV.17. Distribution of the magnetic field.....	72
Figure IV.18. Stator current waveform.....	73
Figure IV.19. Line current versus speed.....	73
Figures IV.20. Torque versus speed.....	74
Figures IV.21. Single load point back FEM position.....	75
Figures IV.22. Torque variation curve as a function of time.....	75
Figures IV.23. Rotation speed curve as a function of time.....	76
Figures IV.24. Distribution of flux density in the airgap.....	76
Figures IV.25. Radial geometry of a squirrel cage induction motor according to ansys Motor-CAD.....	78
Figures IV.26. Axial geometry of a squirrel cage induction motor according to ansys Motor-CAD.....	79
Figures IV.27. 3D view of the induction motor.....	79
Figures IV.28. Radial view of motor temperature distribution by ansys Motor-CAD.....	80
Figures IV.29. Radial view of temperature distribution.....	81
Figures IV.30. Axial view of temperature distribution.....	81
Figures IV.31. Temperature variation in the motor housing.....	82
Figures IV.32. Temperature variation in the motor end winding front (C2) .....	82

# **LIST OF TABLES**

# LIST OF TABLES

## Chapter II Magnetic materials and iron losses in electric motors

Table I.1. Characteristics of magnetic material.....	25
Table I.2. Different stages of manufacturing conventional sheets.....	35

## Chapter IV Calculation of iron losses in a 2.2 kW induction motor

Table IV.1. Steinmetz loss method being used for Steel sheet M800-50A.....	58
Table IV.2. Core losses vs magnetic flux density for different method at 30Hz.....	58
Table IV.3. Core losses vs magnetic flux density for different method at 50 Hz.....	58
Table IV.4. Core losses vs magnetic flux density for different method at 60 Hz.....	59
Table IV.5. Core losses vs magnetic flux density for different method at 100 Hz.....	59
Table IV.6. Core losses vs magnetic flux density for different method at 200 Hz.....	59
Table IV.7. Steinmetz loss method being used for Steel sheet M400-50A.....	61
Table IV.8. Core losses vs magnetic flux density for different method at 50Hz.....	62
Table IV.9. Core losses vs magnetic flux density for different method at 60 Hz.....	62
Table IV.10. Core losses vs magnetic flux density for different method at 100 Hz.....	62
Table IV.11. Core losses vs magnetic flux density for different method at 200 Hz.....	62
Table IV.12. Comparison the value of iron losses between steel sheets M800-50A and M400-50A for 0.5 T.....	64
Table IV.13. Comparison the value of iron losses between steel sheets M800-50A and M400- 50A for 1T.....	64
Table IV.14. Specifications of the Machine Studied.....	65
Table IV.15. Losses in the stator.....	77
Table IV.16. Losses in the rotor.....	77

**LIST OF SYMBOLS  
AND  
ABBREVIATIONS**

## SYMBOLS

$\Omega_s$	Synchronous speed of the rotating field in [rad/s]
$\omega_s$	Synchronous electrical pulsation of the rotating field [rad/s]
$s$	The slip in [%]
$N$	The speed of rotation in [tr/min]
$N_s$	The Synchronous speed in [tr/min]
$f$	frequency [Hz]
$f_{eq}$	Equivalent frequency [Hz]
$U$	Supply voltage (compound) in [V]
$I$	Current absorbed (compound) in [A]
$\cos \alpha$	Power Factor
$P_{in}$	Input power in [W]
$P_{out}$	Output power in [W]
$p_{AG}$	The air-gap power of the motor in [W]
$\sum P_{Losses}$	Sum of losses in the stator and rotor in [W]
$TAG$	The electromagnetic torque developed by the machine in [Nm]
$\eta$	Efficiency in percentage [%]
$I$	Intensity of magnetization (A/m).
$M$	Total magnetic moment of the material ( $A \cdot m^3$ ).
$V$	Volume of the material ( $m^3$ ) .
$x$	Magnetic Susceptibility [emu/cm <sup>3</sup> ]
$\mu_r$	Is termed as the relative magnetic permeability of a material [H/m]
$\mu$	Orbital Magnetic Moment [ $A \cdot m^2$ ]

$\mu_B$	Fundamental unit of magnetism called the Bohr magneton [J/T] or $\left[\frac{eV}{T}\right]$
$\mu_0$	Vacuum permeability $\mu_0 = 4\pi \times 10^{-7}$ [HM]
$\mu_z$	Spin Magnetic Moment [Bm]
$\chi$	Magnetic susceptibility [ $\text{cm}^3/\text{mol}$ ]
$\vec{H}$	Magnetic field strength [A/m]
$\vec{H}_c$	Coercive Field
$\vec{B}$	Flux density [T]
$\vec{B}_r$	Remanent Induction
$V$	Volume of the material [ $\text{m}^3$ ]
$\vec{L}$	Angular momentum [ $\text{kg}\cdot\text{m}^2/\text{s}$ ]
$e$	Electron charge [C]
$g$	G-factor, a dimensionless quantity specific to the particle
$\vec{J}$	Magnetic polarization [T]
$\hbar$	Reduced Planck constant [J.s]
$m_e$	Electron mass [Kg]
CSE	Steinmetz coefficient
$p_{exe}$	Additional losses [W]
$p_{Fe}$	Total iron losses [W]
$p_{Fe}$	Specific iron losses [W/kg]
$p_{hyst}$	Specific hysteresis losses [W/kg]
$e$	Electromotive force in [V]
$S$	Section of the sample [ $\text{m}^2$ ]

$N_1$	Number of turns of the primary coil
$N_2$	Number of turns of the secondary coil
$V_2$	Voltage across the secondary coil [V]
$B$	Induction in the sample [T]
$\Phi$	Magnetic flux [Wb]
$dl$	Infinitesimal element of the loop, measured in meters [m]
$Z$	Number of slot
$m$	Number of phase
$q$	Number of slot per pole per phase
$\eta_{exc}$	Values range from 2 to 3
$T_n$	Nominal torque [N.m]
$N_n$	Nominal rotation speed [tr/min]
$I_n$	Nominal current [A]
$\Delta$	Electrical coupling
$m$	Mass [kg]
$K_h$	Hysteresis loss coefficient
$K_{eddy}$	Eddy current loss coefficient
$\beta$	Beta exponent for hysteresis loss
$\alpha$	Alpha exponent for hysteresis loss
$K_{exc}$	Excess loss coefficient
$P_{cu}$	Copper losses in [W]
$M$	magnetization [A/m]

## ABBREVIATIONS

EVs	Electric Vehicle
BEVs	Battery Electric Vehicles
RPM	Round per Minute
PF	Power Factor
AC	Alternating Current
DC	Direct Current
PMDCM	Permanent Magnetic Direct Current Motor
NGO	Non-Grain-Oriented NGO
FEM	Finite Element Method
GSE	Generalized Steinmetz Equation
MSE	Modified Steinmetz Equation
iGSE	Improved Generalized Steinmetz Equation
NSE	Natural Steinmetz Extension
PS	Power Supply
ADC	Analog to Digital Converter
DAC	Digital to Analog Converter
RMF	Rotating magnetic field
EMF	Electromotive force
ENEL	National Electro-Technical Industries Company
NEMA	National Electrical Manufactures Association

# **GENERAL INTRODUCTION**

## GENERAL INTRODUCTION

Electric vehicles (EVs) offer numerous advantages over traditional internal combustion engine vehicles. They are environmentally friendly, producing zero tailpipe emissions, which significantly reduces air pollution and greenhouse gas emissions, contributing to cleaner air and combating climate change. EVs also have lower operating costs due to cheaper electricity compared to gasoline, and they require less maintenance with fewer moving parts. In terms of performance, EVs often provide instant torque for quick acceleration and a quieter driving experience. As of 2023, global EV sales have been steadily increasing, with over 9 million electric cars sold worldwide, reflecting growing consumer interest and investment in sustainable transportation solutions (Source: International Energy Agency). These trends indicate a promising shift towards a cleaner and more efficient automotive future with electric vehicles at the forefront.

Electric motors constitute a fundamental component of electric vehicles (EVs), pivotal in their propulsion and efficiency. Unlike internal combustion engines, electric motors convert electrical energy from batteries into mechanical energy without combustion, resulting in minimal energy loss and higher efficiency. This direct conversion process enables EVs to deliver instant torque, providing swift acceleration and a responsive driving experience. Moreover, electric motors are compact, lightweight, and require less maintenance compared to traditional engines, contributing to the overall reliability and longevity of EVs.

Despite the numerous advantages of electric motors in EVs, they are not without inefficiencies. Different losses occur during their operation, impacting overall performance and efficiency. These losses can be broadly categorized into copper losses, iron losses, and mechanical losses. Copper losses occur due to the resistance in the motor windings, leading to heat generation and energy dissipation. Mechanical losses arise from friction and windage within the motor, further reducing efficiency. However, one of the most critical and complex types of losses to address are iron losses.

Evaluating iron losses accurately is paramount for enhancing the efficiency and performance of electric motors. Precise assessment allows for the optimization of motor designs, selection of appropriate materials, and implementation of advanced control strategies to minimize these losses. As the demand for high-efficiency EVs grows, addressing iron losses effectively

becomes increasingly important, contributing to the development of more reliable, durable, and energy-efficient electric vehicles.

This work is divided on two parts. In the first part of this work, we focus on evaluating the iron losses of M800-50A electrical steel using an Epstein frame. This method allows for precise measurement of core losses under controlled laboratory conditions, providing essential data on the material's performance in alternating magnetic fields. In the second part, we integrate the obtained data to calculate iron losses in a 2.2 kW induction motor manufactured by the national company Electro-industries.

In this thesis, in the first chapter we explore the intricacies of electric cars and their motors, focusing particularly on the widely-used induction motor and the critical role of batteries in powering these systems. We address the sources of inefficiency in electric motors and the persistent challenges in understanding and mitigating these losses. In the second chapter the study extends to magnetic materials and iron loss, emphasizing the complexity of modeling iron losses with traditional and contemporary approaches. Additionally, in the third chapter we present a detailed of the manufacturing process of electric motors at Electro-Industries company, from design to assembly and testing. Finally, in the fourth chapter we investigate the properties of silicon iron sheets using Epstein frame measurements, compare different types of silicon steel sheets, and employ Motor-CAD simulations to analyze the electromagnetic and thermal behavior of a 2.2kW induction motor.

# **CHAPTER I**

## **ELECTRIC MOTORS IN ELECTRIC VEHICLES**

**I.1 Introduction**

Thermal vehicles play a significant role in the creation of greenhouse gases, whereas global warming can largely be attributed to emissions from using fossil fuels in energy production. Because of this pollution and for protecting the ozone layer, humans thought and invented the electric vehicle to reduce the value of global warming resulting from the emission of gases. It was one of the most helpful technological revolutions of the twentieth century for protecting our environment.

In this chapter, we studied the history of the electric car and the different types of electric motors that are used in the manufacture of electric cars, the most important of which is the induction motor, the characteristics of which we studied. The relationship between the electric motor and the battery caught our attention. What interests us in the interactions between them that can affect energy consumption and car performance is losses in electric motors and how we can reduce iron losses in order to conserve power and battery life for a longer period of time

**I.2 History of development of automobile****I.2.1 Steam automobile**

The development of the automobile started at the end of the 18th and beginning of the 19th centuries. In 1769, Nicolas-Joseph Cugnot had the honor of creating the first steam automobile capable of human transportation. Cugnot built a steam-powered vehicle known as the "Fardier à vapeur" (steam dray). It was a large, three-wheeled vehicle designed to haul artillery for the French military. This invention is considered one of the earliest self-propelled vehicles and is often regarded as one of the first automobiles. However, its practicality and widespread adoption were limited due to various technical challenges and the infancy of steam-powered transportation technology at the time. Nevertheless, Cugnot's succeeded in making his mark in the history of automotive engineering [1].

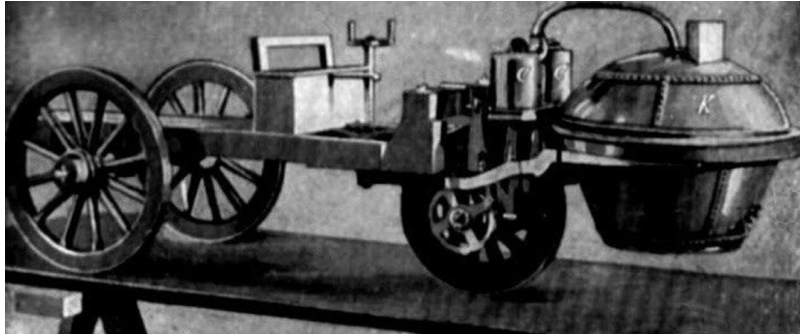


Figure I.1. First electric car

### I.2.2 Thermal vehicles

The history of the thermal car, which primarily refers to vehicles powered by internal combustion engines burning fossil fuels, is rich and spans several centuries. German engineer Nikolaus Otto is credited with developing the first practical internal combustion engine in the 1860s. He introduced the four-stroke engine cycle, known as the Otto cycle, which became the basis for many modern internal combustion engines. After this, Karl Benz, in 1885-1886, is often credited with creating the first true automobile powered by an internal combustion engine. His company, Benz & Cie., introduced the Motorwagen, a three-wheeled vehicle powered by a single-cylinder gasoline engine. Throughout the 20th century, there were continuous improvements in automobile design, engineering, and performance. This included advancements in motor efficiency, safety features, comfort, and environmental regulations. Innovations such as electric starters, pneumatic tires, hydraulic brakes, and improved fuel injection systems contributed to the evolution of thermal cars [1].

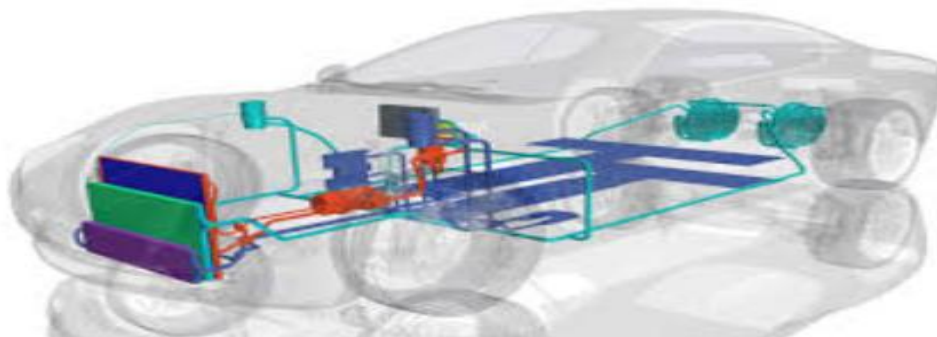
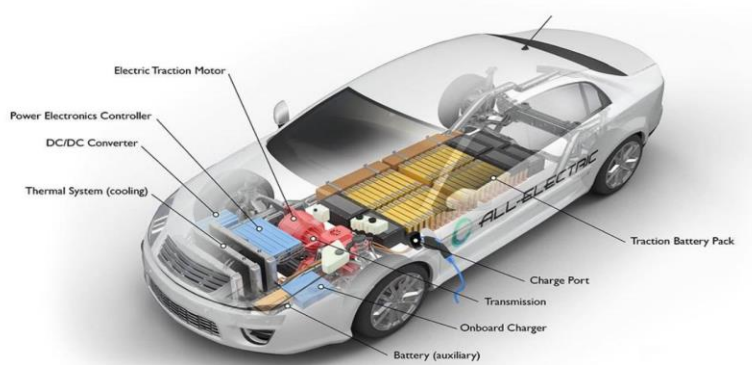


Figure I.2. Electric car

### I.2.3 Electric vehicles

Robert Anderson was the originator of the concept of the electric vehicle, he practical his idea in real life at 1830, but his car did not see the light because the battery designed can't be recharged. After improving the battery quality, the scientist Gustave Trouvé created the first model of electric vehicle in 1881, which was developed by German engineer Anders Flocken in 1888. It was the first car close to what exists today. After this, the world started manufacturing electric cars. The most popular brand is Tesla, but even the biggest companies are racing to create electric cars, like BMW, Audi, Mercedes, VW, etc. [1]

The operation of an EV is similar to that of an internal combustion vehicle, but they are different primarily in their power sources and propulsion systems. Electric cars are powered by electric motors fueled by electricity stored in batteries. They do not require fossil fuels and instead rely on charging from the electrical grid or renewable energy sources like solar or wind power [1].



**Figure I.3. Electric vehicle components**

### I.3 Battery electric vehicles

Electric vehicles (EVs), also known as battery electric vehicles (BEVs), are a key strategy for reducing air pollution and global warming emissions. They have zero tailpipe emissions, and these batteries are made from lithium-ion. This battery can live for about 10–20 years before needing to be replaced. There are three types of charging available: slow, fast, and rapid, and it's up to kilowatts. They are often used to measure the power created by a motor, which means the higher the kW, the quicker the charging point can move electricity into your car [2].

### I.4 Relationship between the Battery and Electric Motor

The lithium-ion battery pack is linked to single motor, dual motors, triple motors, or four motors, which in turn drive the wheels. When the driver presses the accelerator, the electric motor converts electrical energy from the battery into mechanical energy, and the amount of current flowing through the motor determines the speed and torque of the motor.

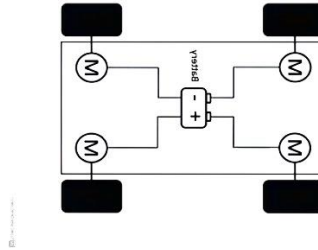


**Figure I.4. Relationship between the battery and electric motor**

However, due to their limited range, charging time, and high cost of battery replacement, EVs are not gaining traction in the market very quickly. This limitation causes an issue called "range anxiety," which refers to driver's fear of running out of energy while driving [2].

The impact of various factors on vehicle energy consumption can be categorized into two primary categories: internal factors pertaining to the vehicle itself, such as vehicle design parameters, characteristics, efficiency and inertia of the vehicle components, auxiliary device usage, etc.; and external factors pertaining to driving conditions, such as environmental and traffic conditions, road type and conditions, driving behavior, and so forth [3].

What interests us about the interactions between components that can affect the energy consumption and performance of the vehicle are the losses in electric motors and how we can minimize iron losses in order to conserve energy for a longer period of time.

### I.5. Motors in electric vehicles

There are three famous types of electric motors used by electric vehicles manufacturers, permanent magnet synchronous motor, brushless DC Motor, the induction motor, each motor has characteristics that distinguish it from the other so the companies chose the model they needed according to his specifications, those features impact in a lot of things, for example, great control, low upkeep cost, high speed, easy plan, and provide acceleration and torque management.

### I.5.1. Permanent magnet synchronous motor (PMSM)

The system works of a Permanent Magnet Synchronous Motor by relying on the interaction between the rotating magnetic field of the stator and the constant magnetic field of the rotor. However, when a three-phase AC power source is connected to the windings of the stator coils, a magnetic field is created that moves at a speed that matches the frequency of the power source, however, the rotor is referred to as "synchronous" because it is made to follow the same speed as the stator. This indicates that the speed of rotation of the rotor and the magnetic field move at the same speed. According to Ampere's Law, the torque produced by the interaction between the rotor's constant magnetic field and the stator's rotating magnetic field causes the rotor to rotate, this lead to converts electrical energy into mechanical energy [3] [5].

Permanent Magnet Synchronous Motor is one of the best motors for the usage in electric vehicles; it is a strong competitor in this industry. PMSM has many advantages, i mentioned some of them: since the magnets are very strong, agitation is limited to a small area, this makes the machine more profitable, has high torque, is very efficient, dissipates heat evenly, reduces the losses involved, and improves speed proficiently. The biggest disadvantage of this motor is the magnets used in it, the permanent magnet synchronous motor makes use of rare earth metals such as neodymium, which is extremely costly. Most electric companies use permanent magnet synchronous motors, for example, the Chevrolet Bolt EV, Ford Focus Electric, Nissan Leaf, and BMW i3 [4].

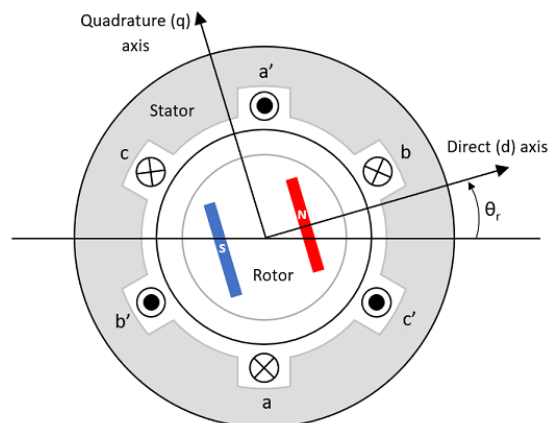


Figure I.5. Permanent magnet motor components

### I.5.2. Brushless DC motor (BLDC)

The term "brushless" refers to the absence of a commutator and brush arrangement, as the commutation is performed electronically, a Brushless DC Electric Motor is an electric motor powered by a direct current voltage, technically a BLDC is regarded as a kind of synchronous motor, which means that when the rotor and the stator's produce a magnetic field they rotate at the same synchronous speed, the rotation happens after the pair poled is energized in a sequential manner, in the way that the rotation commences automatically and stays fixed [3] [5].

Brushless DC Motor have as well many technology offers, longer lifetime, high power densities, and less maintenance because of the absence of brushes. It is also easy to control, lighter, has excellent speed torque, and has high efficiency between 95-98%. This makes BLDC the most preferred motor for use in small electric vehicles. However, BLDC had rare permanent magnets, and being so rare makes them so expensive. Overheating results in power loss, difficulty controlling or starting the motor, failure due to wear and tear, and short circuits. A brushless DC electric motor was used in cars like the Toyota Prius [4].

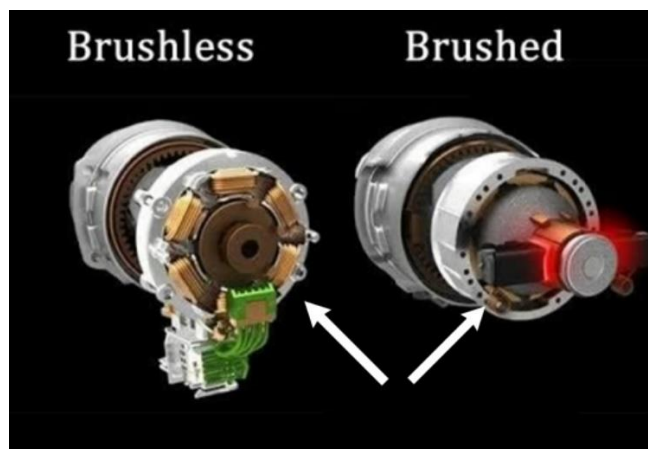


Figure I.6. Components of a BLDC motor

### I.6. Induction motor

Induction motors are some of the most famous types of alternative current. The induction motor is available in two types: slip ring type or wound rotor type and squirrel cage type or short-circuited rotor type, but we need in our education only the squirrel cage type. This motor is a synchronous speed machine. The term asynchronous comes from the fact that the rotation speed of the rotor is different from that of the stator rotating field. Induction motors are widely used in

industries due to the absence of commutator, which in turn means lesser maintenance, the motor is built tough and easy a squirrel cage inductor motor doesn't even need a slip ring arrangement, a rotating magnetic field is created by the stator's winding, which is connected to the three-phase AC supply [3] [5].

There are many advantages to the induction motor, which is what makes it so demanded for usage in industrial settings. According to the lack of brushes, there aren't a lot of maintenance issues, which reduces the cost of the motor and a long life for the squirrel cage induction motors. They also have a high efficiency of around 85–97%, which is excellent, excellent speed torque characteristics, and easy and well-constructed. However, this does not imply that induction motors are faultless. The drawback is that they need a complex inverter circuit and difficult control in the motor, a low starting torque, and rotor losses at higher speeds, but still because of the high reliability, this motor is the preferred choice for electric vehicles, Tesla model S is the best example to prove his worth add others like Toyota RAV4, GM EV1.... [4].

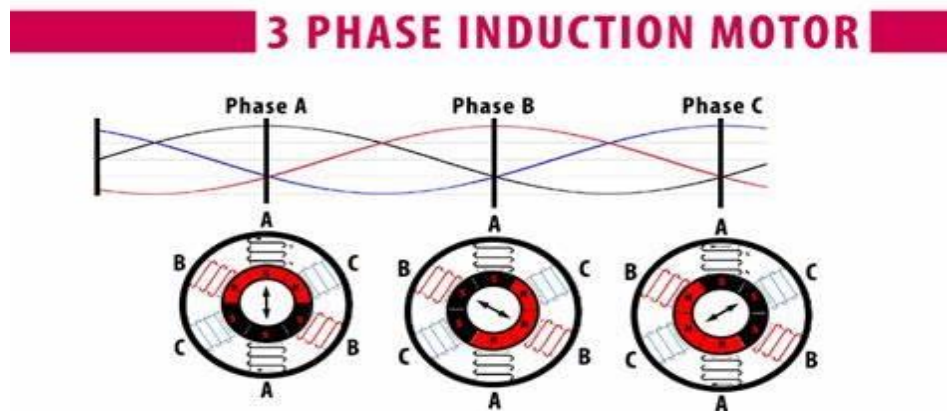


Figure I.7. Induction motor

### I.6.1. Constitution

Induction motor consists of two principal elements: the stator (fixed part) and the rotor (moved part), and those two are divided into different types of elements, Figure I.8 presents all of the existing elements in the motor:

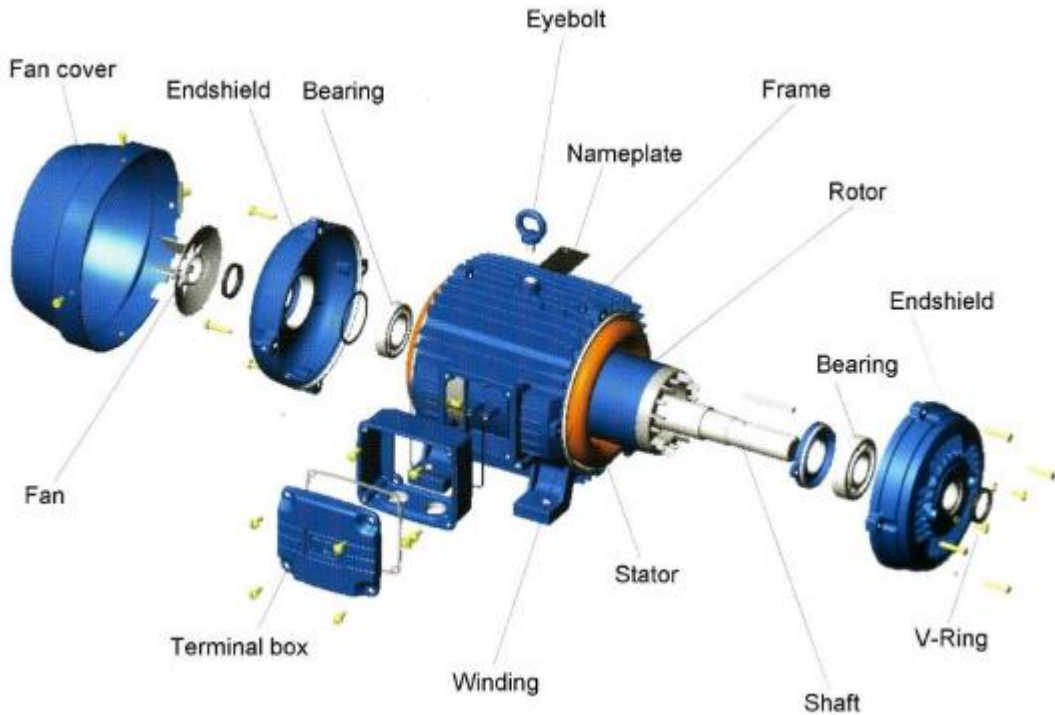


Figure I.8. Components of the principal parts in the induction motor

### I.6.2. Stator

The stator of an induction motor represents the fixed part and is divided into three components: the stator core, which is composed of high-grade steel and has a three-phase winding, the stator core, which is constructed from stacks of identical thin sheets isolated from each other by oxidation, and the stator winding which creates a magnetic field that rotates is produced by the three-phase winding, the last one is the body farmer offers support for structures [6].

Depending on the required speed, the 3-phase stator windings are wound for a specific number of poles, the higher the number of poles, the slower the motor speed, and vice versa [6].

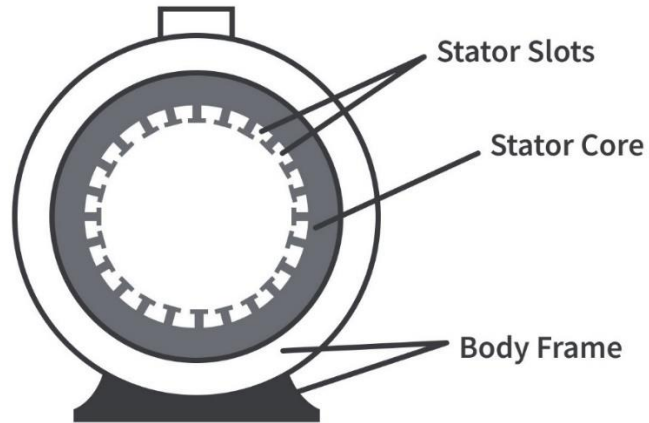


Figure I.9. Induction motor stator construction

### I.6.3. Rotor

The rotor of an induction motor represents the rotating part. The rotor consists of a shaft, which is the central part that rotates and transmits mechanical power, a balance ring, which gives balance to the rotor dynamically, making sure the rotation is smooth, an end ring, which represents the part that connects the bars of the squirrel cage and provides structural integrity, an aluminum bar, which is the part of the squirrel cage structure; these bars supply electricity and create a magnetic field when current passes through them; and a silicon steel core made of laminated silicon steel to reduce eddy currents, it supports the aluminum bars and concentrates the magnetic flux [6].

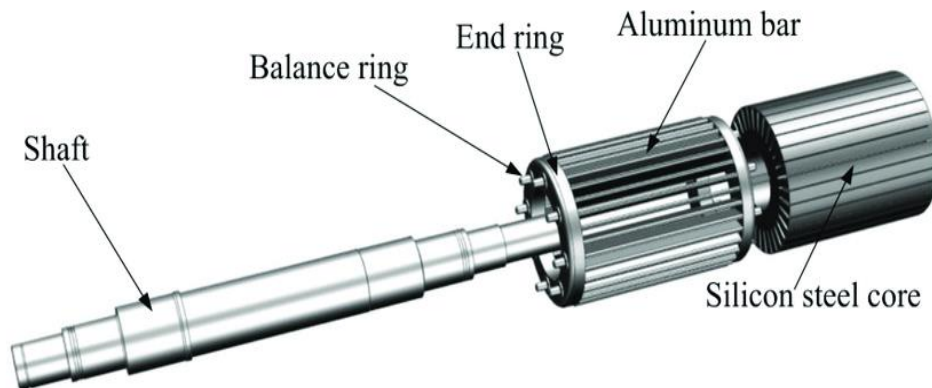


Figure I.10. Squirrel cage type rotor

### I.6.4. Principle of operation

The workings of an induction motor are based on the principle of electromagnetic induction. In an induction motor, there are two windings, namely, the stator winding and the rotor winding. The input AC supply is connected to the stator winding, and the current flowing in the stator winding produces a magnetic flux, called a rotating magnetic field. The rotor winding of the induction motor is a short-circuit winding. The rotating magnetic flux from the stator cuts the short-circuited conductors of the rotor winding. According to Faraday's law of electromagnetic induction, an EMF is induced in the rotor circuit, which causes a current to flow through it. When the current flows through the rotor winding, another magnetic flux is produced in the machine. Therefore, there are two magnetic fluxes inside the induction motor: one is stator flux and the other is rotor flux. These two magnetic fluxes interact with each other. Because of that, the rotor will experience torque, which makes the rotor rotate in the direction of the rotating magnetic field of the stator. In this way, an induction motor runs [6].

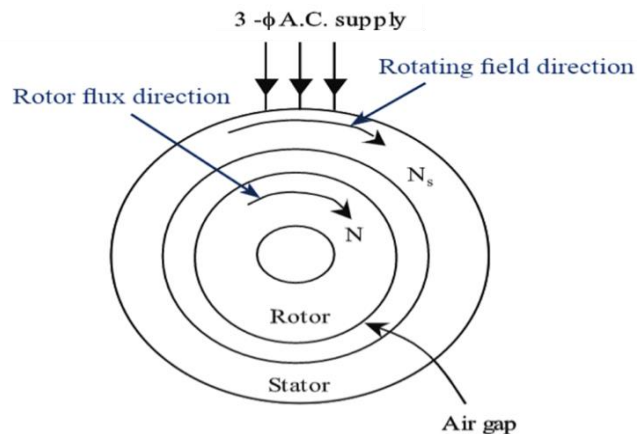


Figure I.11. Construction working principle of induction motors

### I.6.5. Rotating magnetic field

The rotating magnetic field (RMF) is the variation of the magnetic flux caused by the stator currents, and its rotation frequency is imposed by the frequency of the stator currents. This means its rotation speed is proportional to the power supply frequency [7].

The speed of this rotating field is called synchronous speed and is expressed as follows:

$$\Omega_s = \frac{\omega_s}{p} \quad (\text{I.1})$$

$$\Omega_s = \frac{2\pi N_s}{60} \quad (I.2)$$

With:

$\Omega_s$ : Synchronous speed of the rotating field in [rad/s]

$\omega_s$ : Synchronous electrical pulsation of the rotating field [rad/s]

$N_s$ : The Synchronous speed in [tr/min]

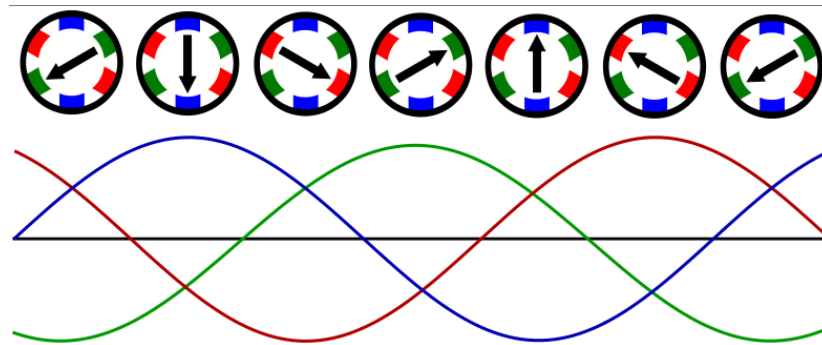


Figure I.12. Graph represent rotating magnetic field

### I.6.6. Slip

There is a difference in rotational speed between the stator-rotating field and the mechanical speed of the rotor, this difference is called slippage, symbolized by  $s$ ; it is a percentage and varies from one motor to another. The slip law is given by [7]:

$$s = \frac{N_s - N}{N_s} \cdot 100 \quad (I.3)$$

With:

$s$  : The slip in [%]

$N_s$ : The Synchronous speed in [tr/min]

$N$ : The speed of rotation in [tr/min]

### I.6.7. Power equation of induction motor

There are three types of power in the induction motor. Figure I.13. shows us the different types of power and losses in electric motors, however, the unit for measuring power and losses is the watt [W]

## Induction Motors

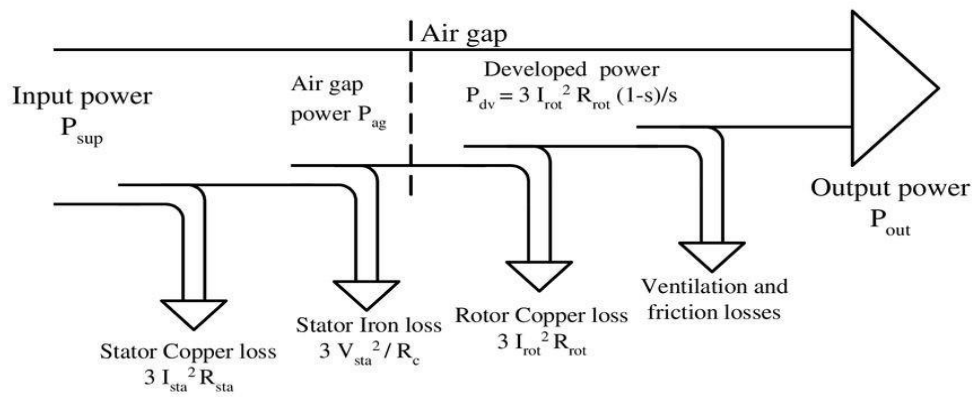


Figure I.13. Power balance of the induction motor

#### a) Input power

The input power of the induction motor supply to the stator, which consists of 3-phase currents (I) and voltages (V), is denoted as [6]:

$$P_{in} = \sqrt{3} \cdot U \cdot I \cdot \cos \alpha \quad (I.4)$$

U: supply voltage (compound) in [V]

I: current absorbed (compound) in [A]

$\cos \alpha$ : Power Factor

**b) Air-gap power**

After supplying input power to motor losses occur at the stator level, the power left over will go to the motor's rotor by crossing the air gap between its stator and rotor, this power is called the air-gap power ( $P_{AG}$ ) of the motor, and is defined as [6]:

$$P_{AG} = P_{in} - P_{cu} - P_{Fe} \quad (I.5)$$

$P_{cu}$ : Copper losses in [W]

$P_{Fe}$ : Iron losses in [W]

**c) Output power**

After the losses of the rotor (Mechanical and Winding Losses) are removed, the remaining power is transformed into mechanical power this power named, output power, is given by [6]:

$$P_{out} = P_{in} - \sum P_{losses} \quad (I.6)$$

$P_{in}$ : input power in [W]

$\sum P_{Losses}$  : Sum of losses in the stator and rotor in [W]

**I.6.8. Torque**

The torque of an induction motor represents the rotational force that the motor produces, allowing it to carry out mechanical work. However, there is a direct relationship between the overall volume of the motor and the torque, where the overall volume of the motor is determined by the torque it has to produce. If we wanted to change the value of torque, we would only change speed, which means that torque has a clear connection with speed and power and is given by the following relationship: [8]

$$T_{AG} = \frac{P_{AG}}{\Omega_s} \quad (I.7)$$

With:

$T_{AG}$ : the electromagnetic torque developed by the machine in [Nm]

$p_{AG}$ : The air-gap power of the motor in [KW]

### I.6.9. Efficiency

Efficiency is important when judging how well induction motors work because it affects how much energy they use and how well they work, the reason of there is efficiency is the amount of losses produced by the motor due to different reasons, this means the difference between electrical input power and mechanical output power, mathematically, it can be expressed as:

$$\eta = \frac{\text{Power Out}}{\text{Power In}} = \frac{P_{\text{out}}}{P_{\text{in}}} \quad (\text{I.8})$$

$\eta$  : Efficiency in percentage [%]

### I.7. Losses in induction motor

The losses in the induction motor are converted into heat, which increases the operating temperature of the machine. The longevity of insulation is strongly correlated with the operating temperature. Therefore, the machine must be designed to tolerate the heat generated by its losses. The electric motor losses can be divided into two types variable and constant losses [8].

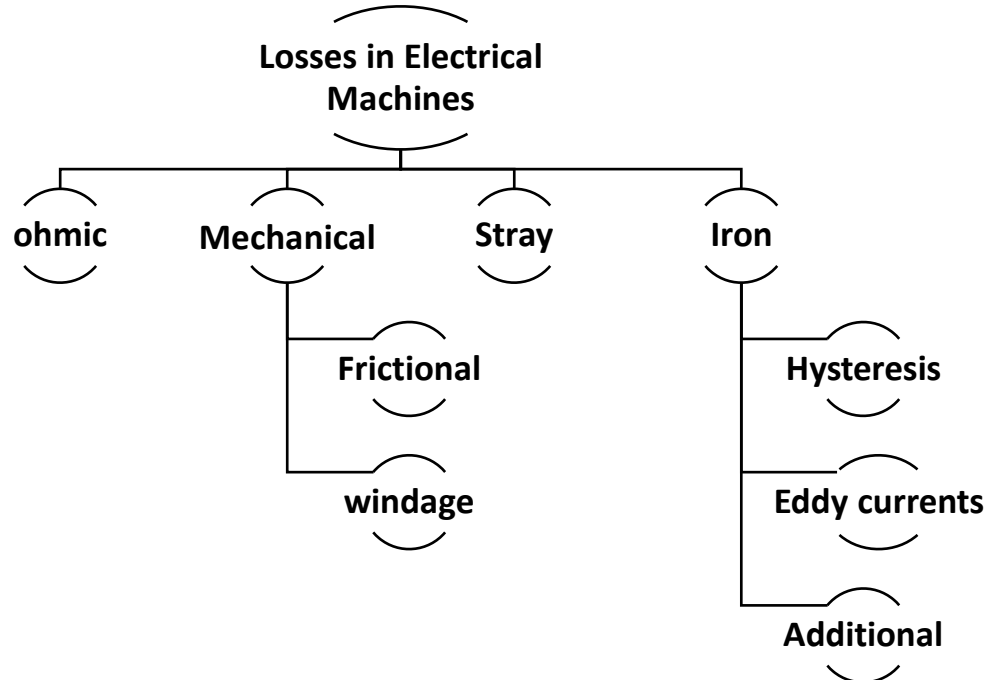


Figure I.14. Losses in induction motor

### I.8. Iron losses

Iron losses can be divided into hysteresis losses, eddy current losses and additional losses. Iron losses are given per weight and depend on the frequency and the maximum flux density. This means that the faster the motor rotates, the higher the iron losses. And the smaller the electric motor is designed, the less space is left for the magnetic flux and the higher the flux density becomes. The proportionality constants  $C$  depend on the material and its manufacturing. Iron losses occur mostly in the stator and rotor, but eddy current losses can also occur in permanent magnets. Losses in magnets are usually small, but critical because magnets usually do not have good temperature resistance [8].

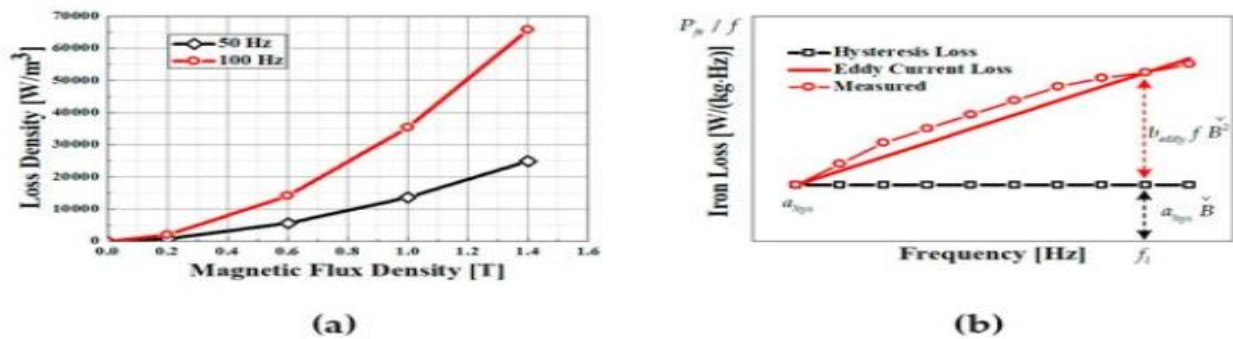


Figure I.15. (a) Measured iron loss data at 50 kHz and 100 kHz from silicon steel 50PN470.

(b) The estimated hysteresis loss factor from two frequencies of iron loss data

#### II.8.1. Hysteresis losses

Magnetic materials are divided into many small domains, each with a different magnetic orientation. When the magnetic orientation of the domains changes, these remagnetization losses are called hysteresis losses because the material passes through hysteresis during magnetization [8].

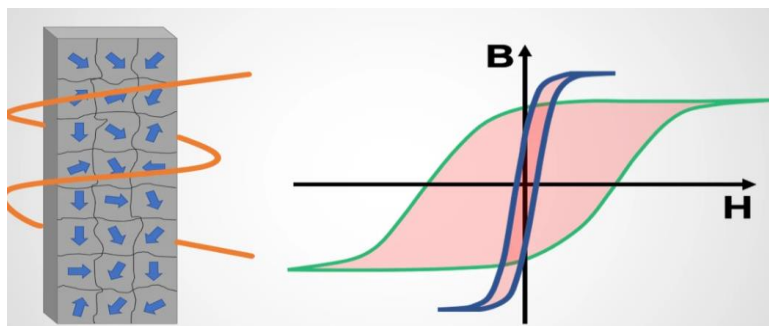


Figure II.16. Hysteresis in magnetic

### II.8.2. Eddy currents losses

Eddy currents happen when the magnetic flux in the stator changes. The eddy currents create losses in the stator and heat it up. To reduce the losses, the stator is divided into separate laminations that are insulated from each other. This significantly reduces eddy current losses.

The thinner the sheets are made, the lower the eddy current losses in the sheet. In order to have an excellent ability to convert electrical energy to mechanical energy for the electric motor, we must calculate the iron losses in order to improve the converted power and thus improve the operation of the electric motor [8].

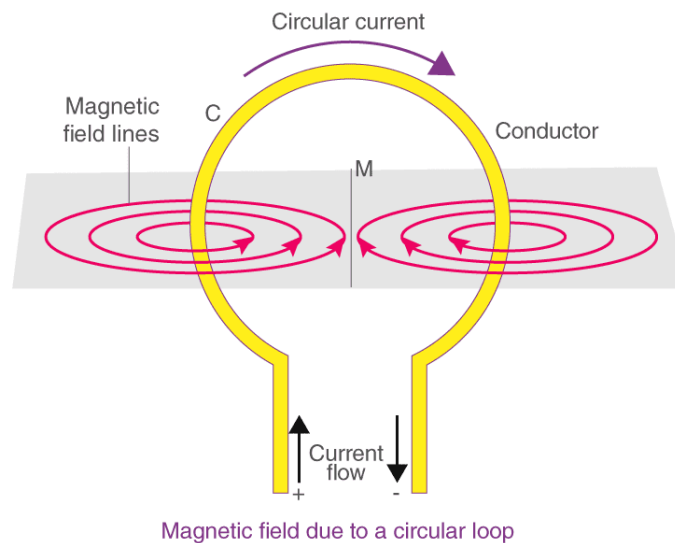


Figure II.17. Eddy currents losses

### II.8.3. Additional losses

In principle, additional loss is the difference between the total measured loss and the sum of calculated losses: the stator and rotor resistive losses, the stator and rotor iron losses, and the mechanical losses. These losses are caused by several different phenomena. Some of them are easy to model, but some are very difficult to calculate. The joule losses are calculated by using the DC resistance of the winding, and therefore, the additional losses also include the losses caused by the skin effect in the conductors [10].

Additional losses occur mainly in the form of eddy currents in those parts of the machine that are subjected to the flux. The rest of the additional losses comprise high-frequency hysteresis and rotating flux iron losses. In other words, the additional load losses can be divided into losses that are not accounted for by the sum of friction and windage losses, the stator and rotor losses, and the core losses [10].

### **I.9. Conclusion**

In conclusion, the principle source of power for an electric automobile is the electric motor, which transforms electrical energy from the battery into mechanical energy to drive the wheels and make the car move forward, instant acceleration and effective energy transfer are provided by the electric motor's torque and speed characteristics, which are tailored for the performance of the vehicle.

In addition to studying the relationship between the battery and the electric motor and the various losses in electric motors, the most important of which are iron losses, and how we can reduce them in order to preserve the battery for a longer period of time.

# **CHAPTER II**

## **MAGNETIC MATERIALS AND IRON LOSSES IN ELECTRIC MOTORS**

## II.1 Introduction

Magnetic materials play an essential role in many industrial applications, such as electrical transformers, motors, and various electronic devices. These materials are characterized by their ability to generate and maintain magnetic fields, which makes them essential in the conversion and distribution of electrical energy.

In practical applications, magnetic materials undergo continuous changes in the magnetic field, resulting in energy losses known as iron losses. These losses affect the efficiency of electrical appliances and cause unwanted heat generation.

In this chapter, we will review the characteristic and types of magnetic materials, in addition to studying the most popular methods for calculating iron losses in induction motors.

## II.2. Magnetism

Magnetism is a phenomenon associated with magnetic fields, which arise from the motion of electric charges. This motion can take many forms. It can be an electric current in a conductor or charged particles moving through space, or it can be the motion of an electron in an atomic orbital. Magnetism is also associated with elementary particles, such as the electron, that have a property called spin [15].

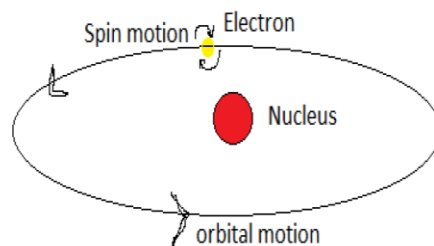


Figure II.1. Magnetic behavior of the atom

### II.2.1. Intensity of Magnetization

The Magnetic moment of a magnet undergoes a change when it is placed in a magnetic field. This change, that is, the magnetic moment change per unit volume, is the intensity of magnetization [15].

The formula for the intensity of magnetization is:

$$I = \frac{M}{V} \quad (\text{II.1})$$

I: Intensity of magnetization (A/m).

M: Total magnetic moment of the material ( $A.m^3$ ).

V: Volume of the material ( $m^3$ ).

### II.3. Orbital and Spin Magnetic Moment

An electron is a charged particle, and there is a magnetic moment associated with its angular momentum. Because the electron in an atom may have two types of angular momentum, there are two sources of magnetic moment [13].

-Spin Magnetic Moment

-Orbital angular momentum.

#### II.3.1. Orbital Magnetic Moment

The orbital magnetic moment is a measure of the strength of the magnetic field produced by the orbital angular momentum of an electron [13].

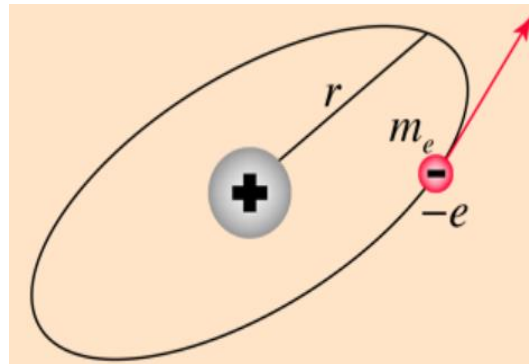


Figure II.2. Electron Orbit Magnetic Moment

$$\mu = -\left(\frac{e}{2m_e}\right) \vec{L} \quad (\text{II.2})$$

$$\mu = -\left(\frac{e}{2m_e}\right) m\hbar = -\mu_B m \quad (\text{II.3})$$

The quantity  $\mu_B$  is a fundamental unit of magnetism called the Bohr magneton, which has the value:  $\mu_B = 9.3 \times 10^{-24}$  [J/T] or  $\mu_B = 5.8 \times 10^{-5}$  [ $\frac{eV}{T}$ ]

### II.3.2. Spin Magnetic Moment

The electron magnetic moment, or more specifically, the electron magnetic dipole moment, is the magnetic moment of an electron resulting from its intrinsic properties of spin and electric charge [13].

$$\mu_z = \pm \left( \frac{e}{2m_e} \right) [J/T] \quad (\text{II.4})$$

$$\mu_z = \pm g\mu_B \quad (\text{II.5})$$

$$\mu_B = \left( \frac{eh}{2m_e} \right) = 9.3 \times 10^{-24} \text{ [J/T]} \quad \text{or} \quad \mu_B = 5.8 \times 10^{-5} \left[ \frac{eV}{T} \right]$$

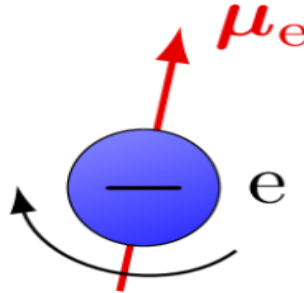


Figure II.3. Magnetic moment of an electron

### II.3.3. Total Magnetic Moment

The total magnetic moment of an atom is equal to the sum of the orbital magnetic moments and the spin moments of the peripheral electrons. For atoms with full electron orbits, the moments balance out each other globally, but in some cases, linked to the existence of incomplete sub-layers, the compensation of the moments is not total, and the atom is considered magnetic in those situations.

## II.4. Magnetic polarization and Magnetization

### II.4.1. Magnetic polarization

Magnetic polarization  $J$  (also denoted by  $I$  or  $B_i$ ) - is the value quantifying the response of matter to an applied magnetic field due to the alignment of internal magnetic dipole moments. Polarizations express the same quantity as magnetization  $M$  but are scaled by the permeability of vacuum  $\mu_0$ . [19]

$$\vec{J} = \mu_0 \vec{M} \text{ [T]} \quad (\text{II.6})$$

Where:

$\vec{M}$ : Magnetisation (A/m)

$\mu_0$  : Permeability of vacuum

### II.4.2. Magnetization

Magnetization, also termed magnetic polarization, is a vector quantity that measures the density of a permanent or induced dipole moment in a given magnetic material. As we know, magnetization results from the magnetic moment, which results from the motion of electrons in the atoms or the spin of electrons or the nuclei.

The net magnetization results from the response of a material to the external magnetic field, together with any unbalanced magnetic dipole moment that is inherent in the material due to the motion in its electrons, as mentioned earlier. The concept of magnetization helps us classify materials based on their magnetic properties [19].

$$B = \mu_0 (1 + x)H = \mu_0 \mu_r H = \mu H \quad (\text{II.7})$$

$x$ : Magnetic Susceptibility [emu/cm<sup>3</sup>]

$\mu_r$  : is termed as the relative magnetic permeability of a material [H/m]

### II.4.3. Magnetic Susceptibility

Magnetic susceptibility is a dimensionless proportionality constant that indicates the degree of magnetization of a material in response to an applied magnetic field. It is caused by the interactions of electrons and nuclei with the externally applied magnetic field [12].

The mathematical definition of magnetic susceptibility is the ratio of magnetization to applied magnetizing field intensity [12].

$$x = \frac{M}{H} \quad (\text{II.8})$$

$x$ : Magnetic susceptibility [cm<sup>3</sup>/mol]

$M$ : magnetization [A/m]

$H$ : Magnetic field strength [A/m]

#### II.4.4. Flux density $\vec{B}$

The magnetic induction intensity  $B$  is the total magnetic field "felt" by the magnet, which is the sum of the applied magnetic field  $H$  and the induced magnetic field  $M$  at this time. In a vacuum environment, the magnetic induction intensity is proportional to the external magnetic field, that is [12].

$$\vec{B} = \mu_0 \vec{H} \quad (\text{II.9})$$

$$\vec{B} = \mu_0 \vec{H} + \vec{J} \quad (\text{II.10})$$

We know:

$$\vec{J} = \mu_0 \vec{M} \quad (\text{II.11})$$

So:

$$\vec{B} = \mu_0 (\vec{H} + \vec{M}) \quad (\text{II.12})$$

We have:

$$\vec{M} = x \vec{H} \quad (\text{II.13})$$

So:

$$\vec{B} = \mu_0 (1 + x) \vec{H} \quad (\text{II.14})$$

Become:

$$\vec{B} = \mu_0 \mu_r \vec{H} \quad (\text{II.15})$$

With:

$$\mu_r = 1 + x \quad (\text{II.16})$$

Where:

$\mu_0$ : Vacuum permeability  $\mu_0 = 4\pi \times 10^{-7} [\text{HM}]$

$\mu_r$ : Relative magnetic permeability [H/m]

$\vec{H}$ : Magnetic field [A/m]

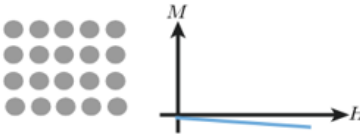
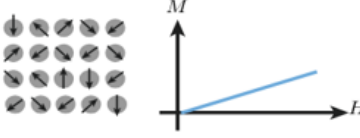
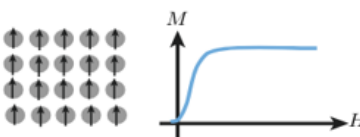
$\vec{B}$ : Flux density [T]

$\vec{M}$ : Magnetization [A/m]

$x$ : Magnetic susceptibility [ $\text{cm}^3/\text{mol}$ ]

## II.5. Type of Magnetic Materials

Table I.1. Characteristics of magnetic material

Type of Magnetism	Susceptibility	Atomic / Magnetic Behaviour		Example / Susceptibility	
<b>Diamagnetism</b>	Small negative	Atoms have no magnetic moment		Au Cu	$-2.74 \times 10^{-6}$ $-0.77 \times 10^{-6}$
<b>Paramagnetism</b>	Small positive	Randomly oriented magnetic moments		$\beta$ -Sn Pt Mn	$0.19 \times 10^{-6}$ $21.04 \times 10^{-6}$ $66.10 \times 10^{-6}$
<b>Ferromagnetism</b>	Large positive	Parallel aligned magnetic moments		Fe	$\sim 100,000$

### II.5.1. Diamagnetism

Diamagnetism is a kind of magnetism characteristic of materials that line up at right angles to a no uniform magnetic field and that partly expel from their interior the magnetic field in which they are placed. First observed by S.J. Brugmans (1778) in bismuth and antimony, diamagnetism was named and studied by Michael Faraday (beginning in 1845). He and subsequent experimenters found that some elements and most compounds exhibit this "negative" magnetism. Indeed, all substances are diamagnetic: the strong external magnetic field speeds up or slows down the electrons orbiting in atoms in such a way as to oppose the action of the external field in accordance with Lenz's law [20].

The diamagnetism of some materials, however, is masked either by a weak magnetic attraction (paramagnetism) or a very strong attraction (ferromagnetism). Diamagnetism is observable in substances with symmetric electronic structure (as ionic crystals and rare gases) and no permanent magnetic moment. Diamagnetism is not affected by changes in temperature [16].

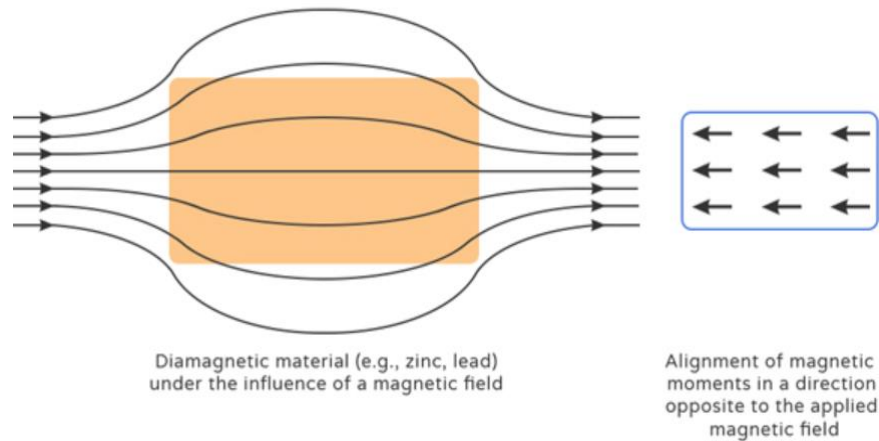


Figure II.4. Behavior in a diamagnetic material

### II.5.2. Paramagnetism

Paramagnetism a kind of magnetism characteristic of materials weakly attracted by a strong magnet, what named and extensively investigated by the British scientist Michael Faraday beginning in 1845. Most elements and some compounds are paramagnetic. Strong Paramagnetism

is exhibited by compounds containing iron, palladium, platinum, and the rare-earth elements. In such compounds, the atoms of these elements have some inner electron shells that are incomplete, causing their unpaired electrons to spin like tops and orbit like satellites, thus making the atoms a permanent magnet tending to align with and hence strengthen an applied magnetic field [16].

Strong Paramagnetism decreases with rising temperature because of the de-alignment produced by the greater random motion of the atomic magnets. Weak Paramagnetism, independent of temperature, is found in many metallic elements in the solid state, such as sodium and the other alkali metals, because an applied magnetic field affects the spin of some of the loosely bound conduction electrons. The value of susceptibility (a measure of the relative amount of induced magnetism) for paramagnetic materials is always positive and at room temperature is typically about 1/100,000 to 1/10,000 for weakly paramagnetic substances and about 1/10,000 to 1/100 for strongly paramagnetic substances [16].

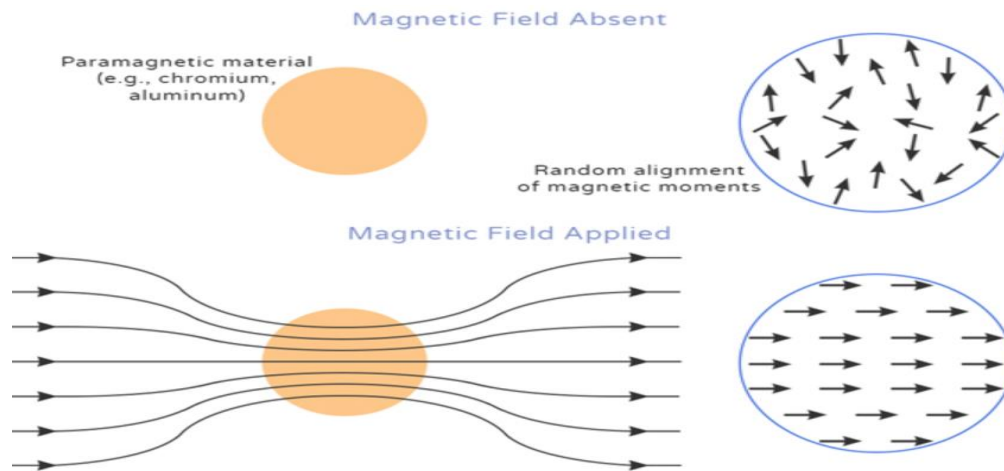


Figure II.5. Behavior in a Paramagnetism material

### II.5.3. Ferromagnetism

Ferromagnetism is a physical phenomenon in which certain electrically uncharged materials strongly attract others. Two materials found in nature, lodestone (or magnetite, an oxide of iron ( $Fe_3O_4$ )) and iron, have the ability to acquire such attractive powers, and they are often called natural ferromagnets. They were discovered more than 2,000 years ago, and all early scientific studies of magnetism were conducted on these materials [16].

Ferromagnetism is a kind of magnetism that is associated with iron, cobalt, nickel, and some alloys or compounds containing one or more of these elements. It also occurs in gadolinium and a few other rare-earth elements. In contrast to other substances, ferromagnetic materials are magnetized easily, and in strong magnetic fields, the magnetization approaches a definite limit called saturation [16].

When a field is applied and then removed, the magnetization does not return to its original value; this phenomenon is referred to as hysteresis. When heated to a certain temperature called the Curie point, which is different for each substance, ferromagnetic materials lose their characteristic properties and cease to be magnetic; however, they become ferromagnetic again on cooling [16].

The magnetism in ferromagnetic materials is caused by the alignment patterns of their constituent atoms, which act as elementary electromagnets. Some species of atoms possess a magnetic moment; that is, such an atom itself is an elementary electromagnet produced by the motion of electrons about its nucleus and by the spin of those electrons. Below the Curie point, atoms that behave as tiny magnets in ferromagnetic materials spontaneously align themselves. They become oriented in the same direction, so that their magnetic fields reinforce each other [16].

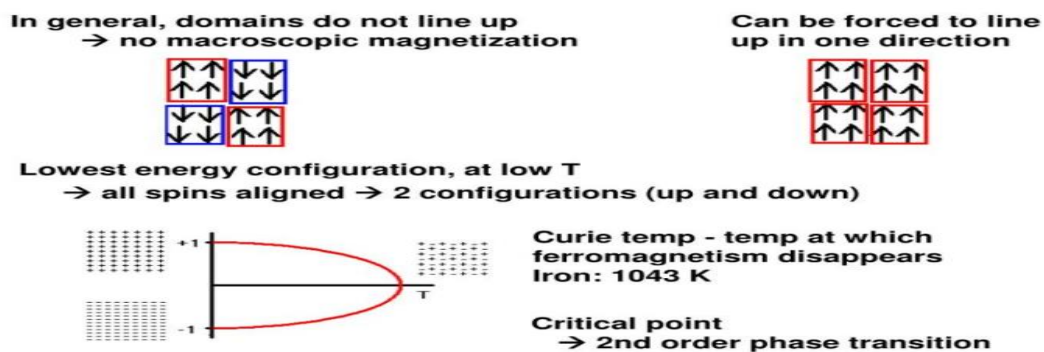


Figure II.6. Behavior in a Ferromagnetism material

## II.6. Hysteresis

The property of ferromagnetic materials that describes the relationship between magnetization and the strength of the magnetic field is called hysteresis. The magnetization of the specimen increases from zero to higher values and attains its maximum value at a point referred to as saturation magnetization. When we further increase magnetic field  $H$ , there is no further increment in magnetic moment. When we decrease magnetic field  $H$  to zero, the magnetization  $M$  attains point  $Q$ , referred to as residual magnetization. Further, if we change the magnetic field from zero to negative values, the magnetization of the material becomes zero at a point  $R$ , where the magnetic field  $H_c$  is referred to as the coercivity of the specimen. If we increase magnetic field  $H$  in the reverse direction, magnetization of material reaches its peak value at a point  $S$ . The area of the loop indicates the amount of energy wasted in one cycle of operation. The hysteresis loop is the loop traced out by magnetization in a ferromagnetic or ferromagnetic material as the magnetic field is cycled [14].

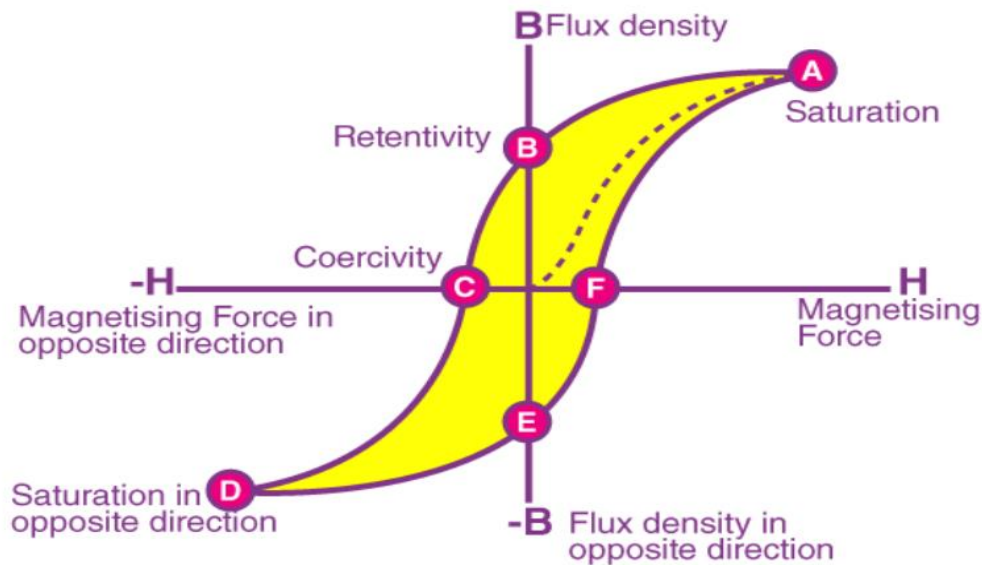


Figure II.7. Hysteresis Loop

### II.6.1. Coercive Field $\vec{H}_c$

Two different definitions of coercive field are provided:  $\vec{H}_{cB}$  is the field required to bring the induction to a zero value starting from the saturated state, and  $H_{cJ}$  is the field required to reduce to zero the polarization  $J$  (i.e. magnetization  $M$ ). It is always  $\vec{H}_{c1} > \vec{H}_{cB}$  [12].

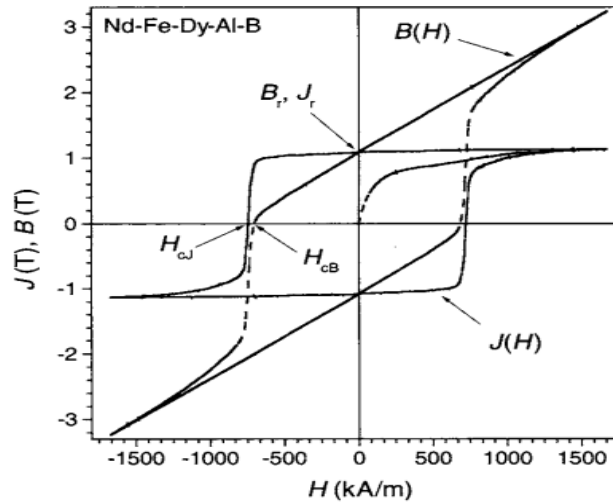


Figure II.8. Explication of Coercive Field

### II.6.2. Remanent Induction $\vec{B}_r$

The value of induction, which occurs, once the material is magnetized and then the magnetizing field is decreased to zero [22].

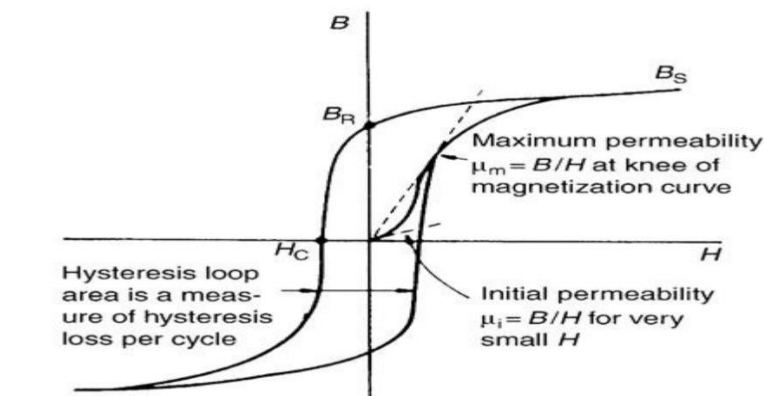


Figure II.9. B-H diagram showing saturation ( $B_s$ ), remanent induction flux density ( $B_r$ ), Coercive field strength ( $H_c$ ), and a trail up from the unmagnetized material.

### II.6.3. Hysteresis Mechanical

Hysteresis loss refers to the energy dissipation phenomenon in materials exhibiting magnetic hysteresis. When an external magnetic field is applied to a material, the magnetic domains within the material align themselves with the direction of the applied field. However, not all domains can align perfectly due to various factors, such as imperfections in the material's crystal structure, thermal vibrations, and magnetic domain wall movements [14].

As a result, when the external magnetic field is removed, some magnetization remains in the material. This residual magnetization must be overcome by demagnetizing the material thoroughly. The energy required to do this work dissipates as heat, resulting in hysteresis loss [14].

The magnitude of hysteresis loss depends on several factors, including the magnetic properties of the material, frequency of the applied magnetic field, and temperature. Materials with high coercivity and high retentivity tend to exhibit higher hysteresis losses. Reducing hysteresis loss is essential in applications such as transformers and electric motors, where efficiency is crucial. [14].

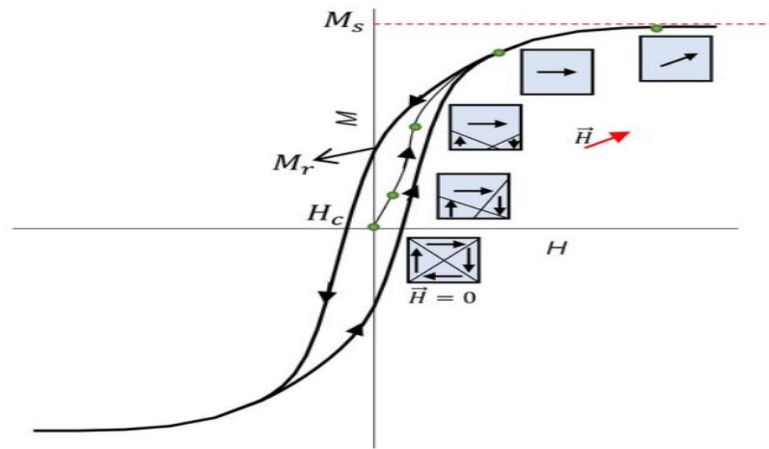


Figure II.10. Explication of Hysteresis Mechanical

## II.7. Soft and Hard Magnetic Materials

Soft and hard magnetic materials possess distinct magnetic properties that determine their suitability for different applications. Soft magnetic materials, with their high permeability and low coercivity, are ideal for electromagnetic devices and AC applications, such as transformers, inductors, and chokes. On the other hand, hard magnetic materials, with their high coercivity and residual magnetism, are perfect for permanent magnets, magnetic sensors, and data storage devices. Understanding the properties and applications of these materials allows engineers and designers to optimize the performance of various magnetic and electromagnetic systems [16].

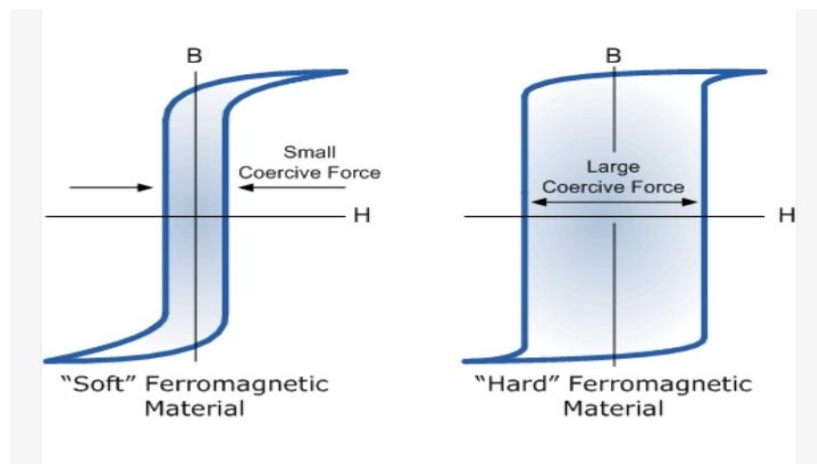


Figure II.11. Hysteresis mechanical in Soft and Hard Magnetic Materials

## II.8. Non-grain oriented iron and silicon iron sheets

Non-Grain-Oriented (NGO) Iron Sheets, also known as Non-Oriented Electrical Steel, have magnetic properties that are as isotropic as possible, meaning they have similar magnetic properties in all directions. They are often used in electrical applications like motors and transformers due to their energy-saving properties when optimally applied, these sheets are used for the construction of all Armored magnetic circuits, operating in a variable induction regime [17].

**II.8.1. Non-Oriented Fully Processed Electrical Steel**

Non-oriented, fully processed electrical steel has varying silicon levels that range from 0.5% to 3.25% Si. It has uniform magnetic properties in all directions. This type of electrical steel does not require recrystallization processes to develop its properties. The low silicon alloy grades provide better magnetic permeability and thermal conductivity. For high alloy grades, better performance is expected at high frequencies, with very low losses. This type is excellent for magnetic circuits in motors, transformers, and electrical system housings. This fully processed type provides difficulty in punchability due to a completed annealing process. Organic coatings are added to improve lubrication in the punching process [17].

**II.8.2 Non-oriented semi-processed electrical steel**

Non-oriented semi-processed electrical steels are largely non-silicon alloyed steel and are annealed at low temperatures after the final cold rolling. The end-user, however, has to provide the final stress-relief anneal according to the steel's intended application. The punchability of this electrical steel type is better than that of the non-oriented, fully processed type, so organic coatings are not required. Non-oriented semi-processed grades are good core materials for small rotors, stators, and small power transformers [17].

**II.8.3. Principles of fabrication**

NO FeSi alloys have an approximately isotropic grain texture, and they are produced in a great variety of grades that contain between 0.5 and 3.25% silicon plus up to 0.5% aluminum and manganese up to 0.3%, which are added to improve the resistivity and reduce the temperature of primary recrystallization without having an important influence on the mechanical properties. Al also prevents aging by N precipitation, stabilizing it through the formation of AlN second phases. The higher grades are delivered as fully processed materials, and they are obtained according to the following procedure [17]:

- Melting, degassing, and continuous casting of slabs.
- reheating (1000 – 1250 °C) and hot rolling to a thickness of 1.8 – 2.3 mm.

- pickling and cold rolling to an intermediate gauge.
- Intermediate annealing (750 – 900 °C).
- Cold rolling to final gauge (0.65 – 0.35 mm).
- Decarburization and re-crystallization annealing (830 – 900 °C).
- Final grain-growth annealing (850 – 1100 °C).
- Coating, punching, and core assemblage.

Compared with semi-processed products, improved punchability can be provided in fully processed NO FeSi electrical steels by the addition of a phosphate-based or chromate-based organic coating that acts as a lubricant when stamping and gives some insulation to the base scale. Semi-processed electrical steel products have a higher level of carbon than fully processed materials because, after the final cold rolling, they are generally subjected to a lower-temperature decarburizing annealing. In order to obtain additional decarburization and optimize the magnetic properties, the end user will subsequently stress-relief anneal the material in a wet decarburizing atmosphere [17].

After the mill decarburization anneal, samples are cut into specimens, decarburized at about 800 °C for at least one hour, and tested to grade the coil. The impurities, included in the material, the grain size, the crystallographic texture, and the residual or applied stresses can be controlled in order to improve the magnetic properties of NO Fe-Si alloys [17].

## **II.9. Grain-Oriented Iron-Silicon Sheets**

Grain-oriented iron-silicon sheets, also known as grain-oriented electrical steel, are crucial in producing energy-efficient transformers and high-performance generators. They are typically used in the cores of distribution transformers and have a goss texture that is essential for their magnetic properties. These sheets are processed to develop optimal properties in the rolling direction and usually contain about 3% silicon [19].

### **II.9.1. Principles of fabrication**

Two families of oriented grain sheets are currently available on the market:

-classic sheets [19].

-more efficient, high permeability sheets.

The different stages of manufacturing conventional sheets are shown in the following Table II.2:

**Table II.2. Different stages of manufacturing conventional sheets**

steps	Operation
1	Preparation of steel for the desired analysis
2	Continuous casting-obtaining slabs
3	Heating of slabs in stringer furnaces ( $T \geq 1350^\circ\text{C}$ )
4	Hot rolling on a strip train ( $e = 2 \text{ mm}$ )
5	Pickling and first cold rolling ( $e = 0.7 \text{ mm}$ )
6	Intermediate annealing
7	Second cold rolling to final thickness ( $e = 0.30 \text{ mm}$ )
8	Decarburization annealing in a very slightly oxidizing atmosphere
9	Coating with magnesia and drying
10	Static secondary recrystallization annealing ( $1175^\circ\text{C}$ )
11	Washing brushing and phosphating annealing

### II.9.2. Insulation of grain-oriented sheets

A series of coaters are used to apply insulation coating liquid to the top and bottom of a plate. Grain-oriented electrical steel has two layers of coating, a base coating of dark brown Forsterite ( $Mg_2SiO_4$ ) as the main ingredient and a transparent insulating coating containing phosphates [20]

### II.10. Overview of Iron Losses Models

An overview of the most popular techniques for calculating iron losses is presented in the Figure II.12. Three groups comprise this sorting model. The iron losses models from the first group are derived directly from Steinmetz's original formula. Under the second category, models attempt to divide total iron losses into multiple categories depending on the influence of physical factors (such as frequency dependence, rotating and variable flux density behavior, harmonic analysis, etc.). The last group consists of mathematical models of hysteresis losses. These models are

intended to provide an empirical or mathematical description of the hysteresis behavior of magnetic materials [11].

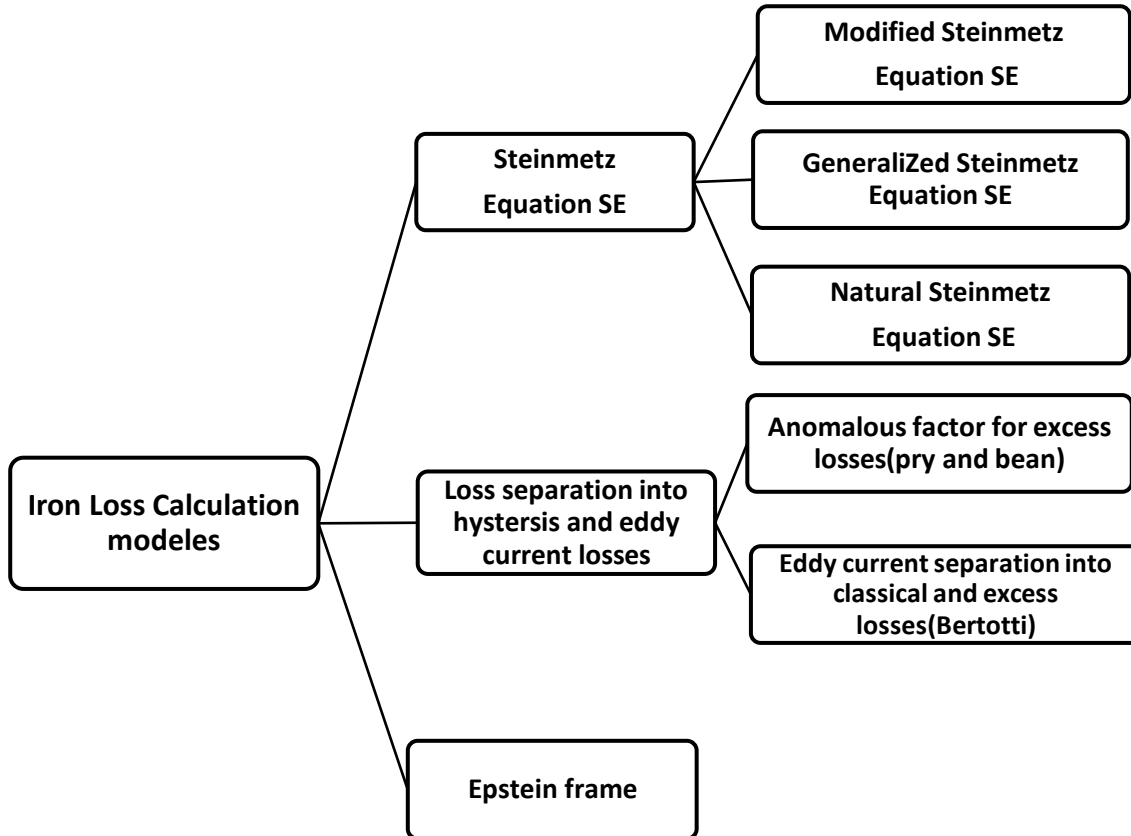


Figure II.12. Model approaches to determine iron losses in electrical machines.

### II.10.1. Steinmetz Equation

The Steinmetz equation (SE) serves as the basis for the first set of models [11]:

$$p_{Fe} = C_{SE} f^\alpha B^\beta \quad (\text{II.17})$$

Where  $p_{Fe}$  is the symbol of iron loss in W/kg,  $B$  is the peak value of the magnetic flux density in the sheet, and  $f$  is the frequency of the periodic signal. The three coefficients  $C_{SE}$ ,  $\alpha$  and  $\beta$  are determined by fitting a loss model to the measured data. Since the classical Steinmetz equation (II.17) only applies to sinusoidal flux densities, several modifications have been made in recent decades to extend the classical Steinmetz equation to non-sinusoidal flux density waveforms

caused, for example, by power electronic circuits. One modification of the Steinmetz equation for calculating core losses for arbitrary flux density waveforms is called the modified Steinmetz equation (MSE). The idea of MSE is to introduce an equivalent frequency that depends on the macroscopic demagnetization coefficient ( $dM/dt$ ). Because the rate of demagnetization is proportional to the rate of change of flux density ( $dB/dt$ ), the equivalent frequency based on this rate of change is defined as [11]:

$$f_{eq} = \frac{2}{\Delta B^2 \pi^2} \int_0^T \left( \frac{dB}{dt} \right)^2 dt \quad (\text{II.18})$$

With  $\Delta B = B_{max} - B_{min}$ . Combining (II.18) with the Steinmetz equation in (II.17) yields

$$p_{Fe} = CSE f_{eq}^{\alpha-1} \hat{B}^{\beta f} \quad (\text{II.19})$$

DC bias pre-magnetization can also be taken into account by introducing a second correction factor. This factor includes two more factors that need to be resolved: measurements at various frequencies and magnetizations. The disadvantage of MSE is that it loses accuracy for waveforms with a small fraction of the fundamental frequency. A newer modification of the Steinmetz equation is the so-called generalized Steinmetz equation (GSE), described and compared with the modified Steinmetz equation [11].

This modification of the Steinmetz equation is based on the assumption that the instantaneous iron loss is a single-valued function of the flux density  $B$  and the rate of change of the flux density  $dB/dt$ , without taking into account the history of the flux density waveform.

A formula is derived that uses this single-valued function and combines it with the Steinmetz coefficients (II.17) of it gives [11]:

$$p_{Fe} = \frac{1}{T} \int_0^T C_{GSE} \left[ \frac{dB}{dt} \right]^{\alpha} [B(t)]^{\beta-\alpha} dt \quad (\text{II.20})$$

Where  $C_{GSE}$  is a coefficient in (II.17) that is connected to CSE. One benefit of the GSE over the MSE is that it has a DC-bias sensitivity without requiring extra measurements or coefficients.

Moreover, an equivalent frequency or amplitude that can be applied to the classical Steinmetz equation (much like the MSE) can be derived using the GSE. Several strategies are suggested for this purpose [11].

The accuracy limitation of the GSE arises when the flux density's third or nearly higher harmonic component becomes significant, which is a drawback. If the flux density waveform has multiple peaks, then this is the case. In such cases, it may be necessary to consider analytical hysteresis loss models due to the minor loops in the hysteresis loop. The previously derived GSE is optimized for the so-called improved Generalized Steinmetz Equation (iGSE) in order to solve this issue [11].

In order to consider the minor loops in the full major hysteresis loop for the loss calculation, the iGSE splits the waveform into one major and one or more minor loops. In light of this, a recursive algorithm is provided wherein the flux density waveform is split into major and minor loops, and the iron losses are computed independently for each identified loop  $x$  by [11]:

$$p_{Fe_x} = \frac{1}{T} \int_0^T C_{SE} [dB/dt]^{\beta-\alpha} dt \quad (II.21)$$

Where  $\Delta B$  represents the flux density of the waveform's current major or minor loop from peak to peak. Because the iGSE is a function of  $\Delta B$  rather than  $B(t)$ , one drawback of the iGSE is that it lacks the DC-bias sensitivity of the GSE. An analogous methodology to the iGSE has been released as the Natural Steinmetz Extension (NSE), which additionally considers the flux density value  $\Delta B$  from peak to peak [11].

Account:

$$p_{Fe} = \left(\frac{\Delta B}{2}\right)^{\beta-\alpha} \frac{C_{SE}}{T} \int_0^T \left[\frac{dB}{dt}\right]^{\alpha} dt \quad (II.22)$$

There is no separation of the waveform into major and minor loops. Rather, it is applied directly to the entire period's waveform (ignoring any minor loops in the hysteresis loop). In actuality, the impact of rectangular switching waveforms is the main focus. In summary, the various methods based on the Steinmetz equation and their coefficients provide an easy and quick way to estimate the iron losses without requiring previous measurements of the material being used. Either the manufacturers directly supply the Steinmetz coefficients, or it is simple to obtain them by fitting the Epstein frame measurement curves [11].

The introduced approaches have a drawback in that there is known variation in the Steinmetz coefficients with frequency. Therefore, it may be challenging to identify appropriate

coefficients that produce good results over the entire frequency range of the applied waveform for waveforms with high harmonic content. Additionally, the accuracy is generally worse for wide frequency ranges when compared to the Preisach hysteresis loss models shown in Section (II.21), in particular at low frequencies. Since the hysteresis effect is mostly to blame for the losses, they essentially become independent on the waveform. It should be noted that the MSE model was the only one examined for electrical machine lamination steel sheets. The other enhanced models based on Steinmetz were created with an emphasis on ferrites at higher frequencies and have not been tested for common silicon-iron alloys, which are typically utilized in electrical machinery [11].

### II.10.2. Standard losses separation approach

A different kind of iron loss equation divides the iron losses into various physical components in addition to the various extensions of the Steinmetz equation. the losses based on the amplitude of the flux density ( $\hat{B}^2$ ), and the variation's relationship to frequency ( $f$  and  $f^2$ ) Thus, the losses can be classified as (dynamic) eddy current losses and (static) hysteresis losses [11]:

$$p_{Fe} = p_{hyst} + p_{ec} = C_{hyst}f\hat{B}^2 + C_{ec}f^2\hat{B}^2 \quad (II.23)$$

It is assumed that the hysteresis losses at low frequencies ( $f \rightarrow 0$  Hz) are proportional to the hysteresis loop area of the material in (II.23), where  $C_{hyst}$  and  $C_{ec}$  are the hysteresis and eddy current coefficients, respectively. It is possible to approximate the eddy current component of the losses PEC using Maxwell's equations. This leads to [11]:

$$p_{ec} = \frac{d^2(dB(t)/dt)^2}{12\rho\gamma} \quad (II.24)$$

where  $d$  is the thickness of the lamination sheet,  $\rho$  and  $\gamma$  are the specific resistivity and material density of the lamination sheets, respectively, and  $B(t)$  is the flux density as a function of time [11].

For a number of nickel-iron alloys, equation (II.23) has been shown to be accurate; however, for silicon-iron alloys, it is inaccurate. This is why Pry and Bean introduced an empirical correction factor  $\eta_{exc}$ , also known as the excess loss factor (sometimes called the anomalous loss factor). It extends (II.23) to [11]:

$$p_{Fe} = p_{hyst} + \eta_a p_{ec} = C_{hyst} f \hat{B}^2 + \eta_{exc} C_{ec} f^2 \hat{B}^2 \quad (\text{II.25})$$

Using  $\eta_{exc} = \frac{P_{ec\_measured}}{P_{ec\_calculated}} > 1$

In silicon-iron alloys with thin grain orientation,  $\eta_{exc}$  values range from 2 to 3. Adding an extra loss term  $P_{exc}$  to (II.23) to account for the excess losses, as a function of flux density and frequency is another way to improve it. The static hysteresis losses ( $p_{hyst}$ ), dynamic eddy current losses ( $p_{ec}$ ), and excess losses ( $p_{exc}$ ) are the three terms that make up the iron loss formula ( $p_{Fe}$ ) [11].

$$p_{Fe} = p_{hyst} + p_{ec} + p_{exc} = C_{hyst} f \hat{B}^2 + C_{ec} f^2 \hat{B}^2 + C_{exc} f^{1.5} \hat{B}^{1.5} \quad (\text{II.26})$$

Bertotti developed a theory that resulted in a statistical model to calculate the iron losses by introducing so-called magnetic objects. This model led to a physical description and function of the loss factor  $C_{exc}$  in terms of the active magnetic objects and the domain wall motion, since the excess losses in (II.26) are still based on empirical factors: [11]

$$C_{exc} = \sqrt{SV_0 \sigma G} \quad (\text{II.27})$$

In equation (II.27),  $S$  represents the lamination sample's cross sectional area,  $\sigma$  denotes the lamination sheets' electric conductivity, and  $G \approx 0.136$  is a dimensionless coefficient of eddy current damping. [11]

Grain size is taken into consideration while characterizing the statistical distribution of the local coercive fields with  $V_0$ . According to recent studies, the first term in (II.26) concerning the flux density squared dependency does not really fit the hysteresis losses of highly alloyed silicon iron lamination sheets and other alloys. Consequently, an additional fitting coefficient  $\alpha$  is added, typically ranging from 1.6 to 2.2 in the case of ferromagnetic materials and alloys. [11]

Adding this factor results in the following equation, which is now frequently utilized with either  $\alpha = 2$  or a variable  $\alpha$  in the post-processing computations of finite element software:

$$p_{Fe} = C_{hyst} f \hat{B}^2 + C_{ec} f^2 \hat{B}^2 + C_{exc} f^{1.5} \hat{B}^{1.5} \quad (\text{II.28})$$

### II.10.3. Epstein Frame

There are many ways to measure iron loss in steel laminations, in our project we used a test called the Epstein frame test on electrical steel sheet type M800-50A

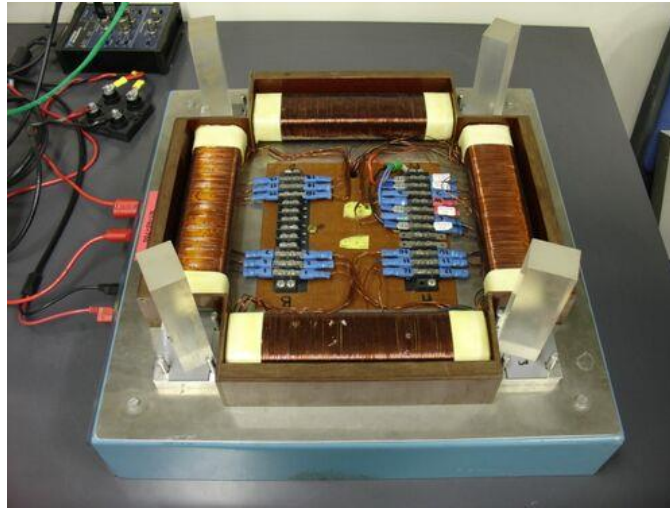


Figure II.13. Coils in epstein frame

The magnetic characteristics of soft magnetic materials are measured using an Epstein frame, referred to as an Epstein square, which is a standard measurement tool, The Epstein frame is a 25 cm square frame, which comprises a primary and a secondary winding, The measurement setup (see Figure II.14) consist of a power supply (PS), a shunt resistor  $R_s$ , a standard Epstein frame, a data acquisition with analog to digital converter (ADC) and digital to analog converter (DAC) devices, and a PC which controls the process and stores measurement data. For the measurement input data like the characteristics of the sample and the testing conditions are required [23].

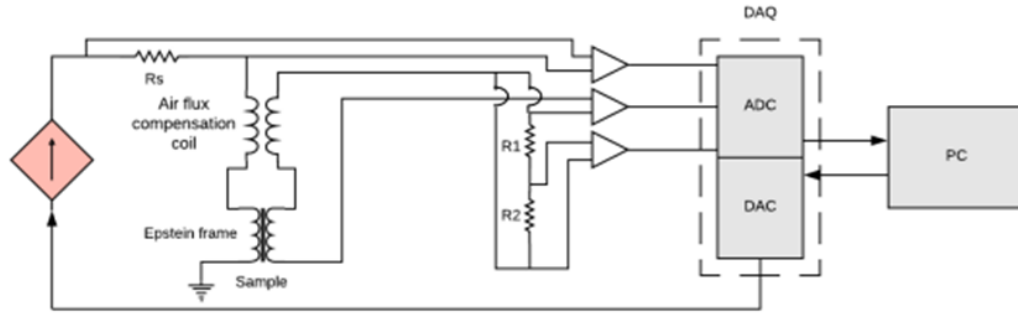


Figure II.14. Epstein frame measurement system

### II.10.3. Method of work the epstein frame

This non-linear and hysteretic behavior manifests itself when measuring the material. To carry out this measurement, a primary coil imposes a sinusoidal flux within a closed magnetic circuit made up of the material to be characterized. The voltage is also measured across a secondary coil also surrounding the sample. Faraday's law (II.29) makes it possible to make the link between voltage and induction if we put it in the form of (II.30), with  $N_2$  the number of turns of the secondary coil, which surrounds the sample and does not deliver current,  $V_2$  the voltage across the secondary coil,  $S$  the section of the sample, and  $B$  the induction in the sample. The integration of the voltage across the secondary coil is then sufficient to determine the induction [9].

$$e = -\frac{d\phi}{dt} \quad (\text{II.29})$$

$$V_2 = -N_2 \frac{dB}{dt} S \quad (\text{II.30})$$

Measuring the current flowing through the primary coil allows, using Ampère's theorem (II.31), to determine the field  $H$  [9].

$$\oint \vec{H} \cdot d\vec{l} = N_1 \cdot i \quad (\text{II.31})$$

it is then enough to measure the value of the current as soon as the number of turns of the primary coil  $N_1$  and the length  $l$  are known [9].

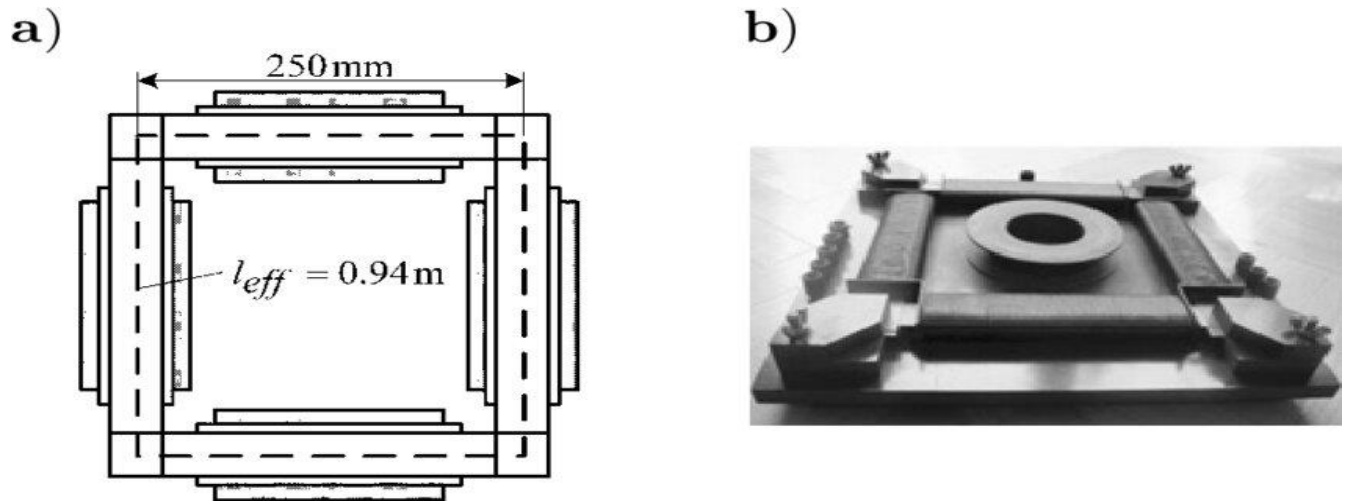


Figure II.15. Epstein frame

## II.11. Conclusion

Magnetic materials play a vital role in technical and industrial fields, from the generation and transmission of electrical power to computing and storage uses. Understanding the magnetic properties of these materials and how to calculate iron losses resulting from their use is fundamental to improving the efficiency of electrical appliances.

Iron losses, which include hysteric losses and eddy current losses, greatly affect the performance and efficiency of magnetic systems. Therefore, loss separation models and models based on the Steinmetz and Bertotti equation are the most convenient and appropriate for quick and approximate iron loss calculations and comparison of different materials for specific electrical equipment. While the frame Epstein is based on laboratory measurements, which makes it the most accurate

By applying these common methods for calculating iron losses, engineers can design more efficient and sustainable magnetic systems. Improving magnetic materials and reducing iron losses contributes greatly to the development of advanced and efficient technologies, resulting in energy saving, cost reduction and overall performance improvement of electrical appliances.

**CHAPTER III**

**ELECTRO-INDUSTRIES**

**COMPANY**

### III.1. Introduction

Electro-Industries is a company that specializes in the design, manufacture, and marketing of industrial electrical equipment (distribution transformers, electric motors, and generator sets).

We will introduce the company where we finished our end-of-study internship in this chapter. We will go over the various steps involved in producing induction motors as well as the various workshops that the motors go through in the manufacturing process

### III.2. History of the company

Electro-industries are the result of the reorganization of the industry operated in Algeria between 1980 and 2000, which led in 1999 to the restructuring of the former ENEL (National Electro-Technical Industries Company) in a number of EPA/SPA. The plant was conducted as part of a product contract with German partners SIEMENS for the product and FRITZ WERNER for engineering and construction. Infrastructure is carried out by Algerian companies ECOTEC COSIDER and BATIMETAL.



Figure III.1. Logo of Electro-industries

### III.3. Presentation of the company

Electro-Industries company has an area of 45 hectares and is located on national road N°12, 30 km from the capital of the state of Tizi-Ouzou, and 8 km from the commune of Azazga 913 /5 000 Electro-Industries products are produced and controlled according to DIN standards (degrees of protection for electric motors), VDE (regulations relating to electrical machines) and comply with European CE recommendations and the strict internal standards recommended by the licensor Siemens. The level of their quality has been approved by local customers (Sonelgaz, Enmtp, Eniem, Kahrif, etc.) and foreign customers (Russia, African countries, Senegal, Mali... etc.)



Figure III.2. Satellite view of the company website

Electro-Industries Company is specialized in manufacturing and commercializing:

a) - Electrical motors:

Three-phase motors of 0.25W to 400KW and single-phase ones of 0.55KW to 2.2KW.

Three-phase two-speed asynchronous motors of 0.55KW to 7.8KW.

Single-phase asynchronous motors for conditioning systems 50W, 120W, 140W and 145W.

b) - Synchronous alternators of 17.5KVA to 200KVA.

c) - Transformers from 50KVA to 2000KVA.

d) - Generator sets of 17.5 to 200KVA.

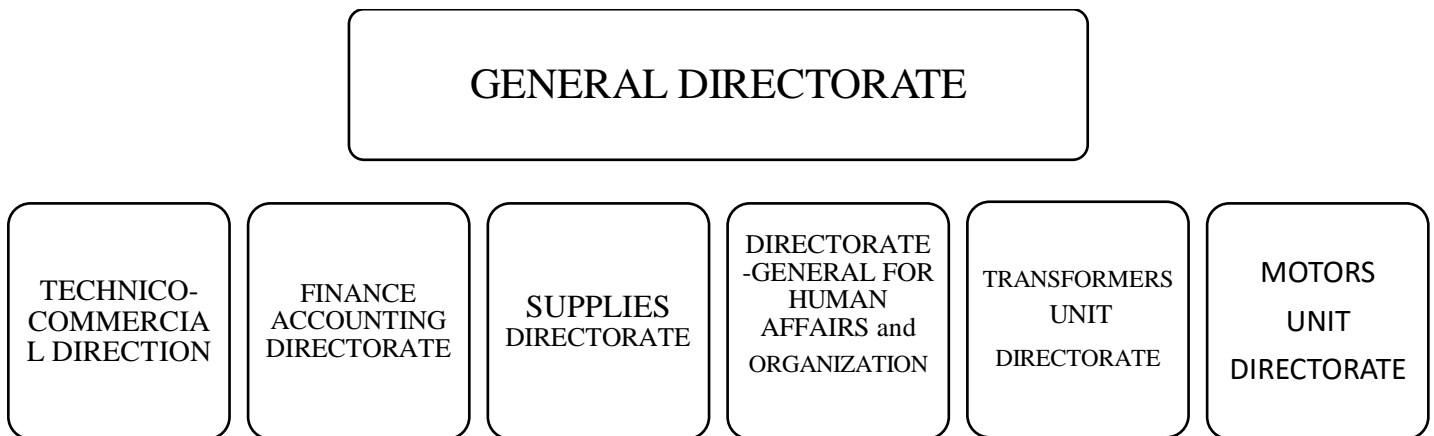


Figure III.3. Factory units

### III.4. Presentation of the motors unit

The motors unit manufactures asynchronous motors with different powers and speeds. To ensure their quality of production, the motors unit has five mechanical manufacturing workshops in which mechanical and electrical control stations are incorporated to validate the conformity of each manufactured part used in the production of each type of motor.

The following diagram shows us that the UMA is made up of different workshops:

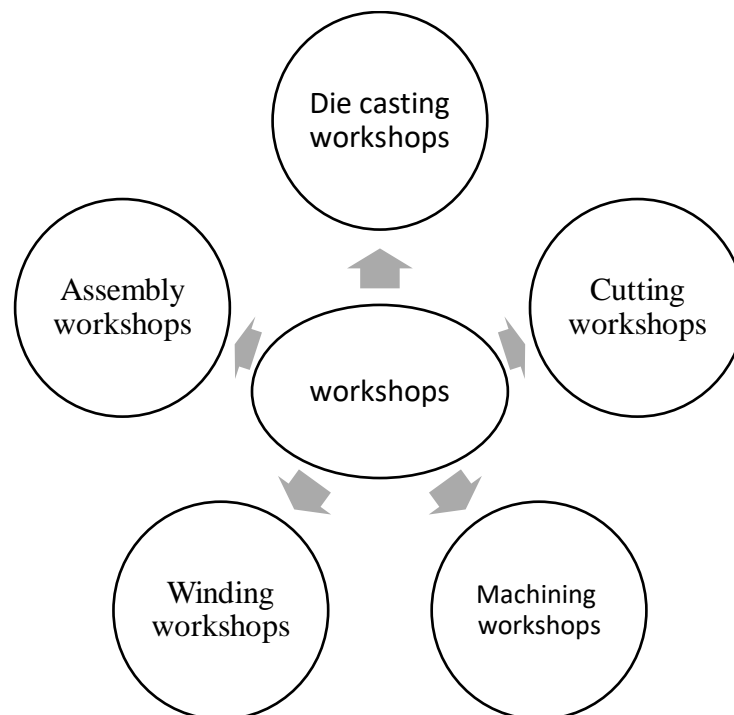


Figure III.4. UMA different workshops

### III.5. Cutting workshops

In this workshop, we carry out all the transformation work on used sheets for the manufacture of parts, namely:

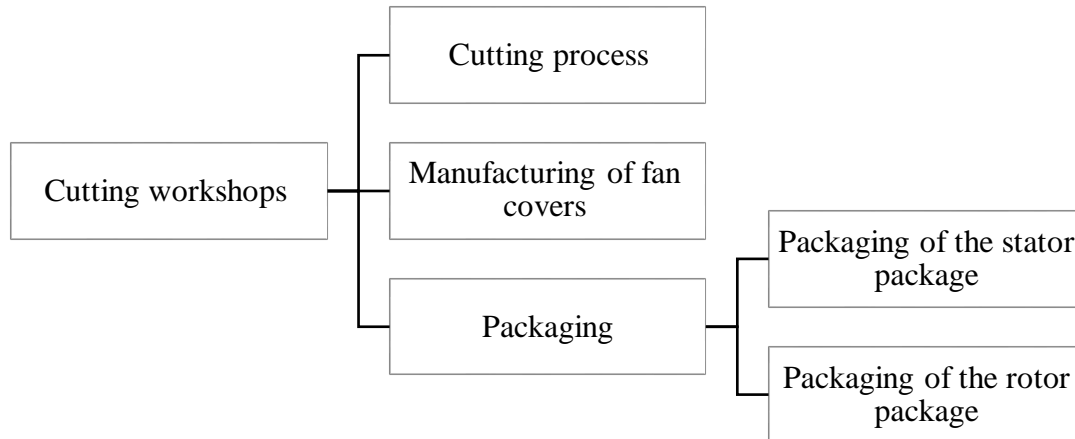


Figure III.5. Basic stages of the cutting workshop.

### III.5.1. Cutting process

The most popular process in this workshop is that of successive automatic cutting with a rapid press. This process allows the stator and rotor sheets to be cut and slotted in the same cycle according to the command issued to the machine. Once cut and slotted, the stator and rotor sheets are evacuated to the outside of the machine by conveyors and then stacked separately.

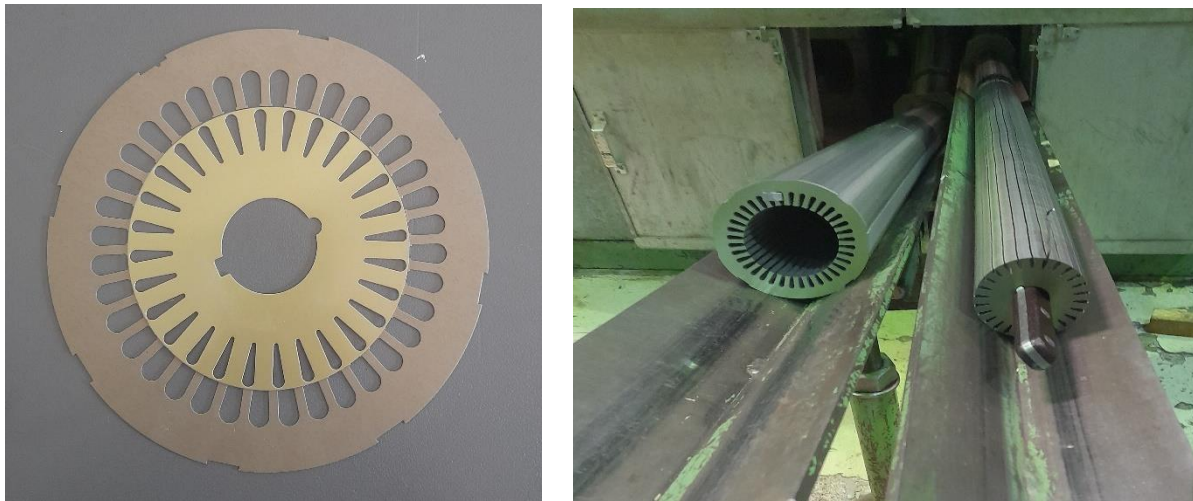


Figure III.6. Pictures from cutting process

### III.5.2. Packaging

It is carried out after stacking the sheets according to the length of the stator or the rotor package, the operation is carried out using a tool mounted on a packaging press to obtain the

requested length, and then the sheets are held with staples placed in the grooves before being pressed them using four jacks



**Figure III.7. Packaging of the stator package**

### **III.5.3. Manufacturing of fan covers**

From the sheets form of steel discs, the stamping is done by the stamping machine, and for the flat part, it will be pierced in the form of a grid by a punch matrix to allow the removal of heat during motor operation.



**Figure III.8. fan covers**

### **III.6. Die casting workshops**

In this stage, all the parts used in the manufacture of the aluminum version of the motors, such as:

-99.5% pure aluminum rotor injection

-production of parts in pure aluminum alloy by (silicon, manganese, and copper) as carcasses, flanges (AS, BS), terminal boxes, and terminal box covers.



Figure III.9. Housing

### III.7. Machining workshops

In this workshop, the rotor shafts are manufactured as well as machining. parts such as the flange, rotor, casing, etc.

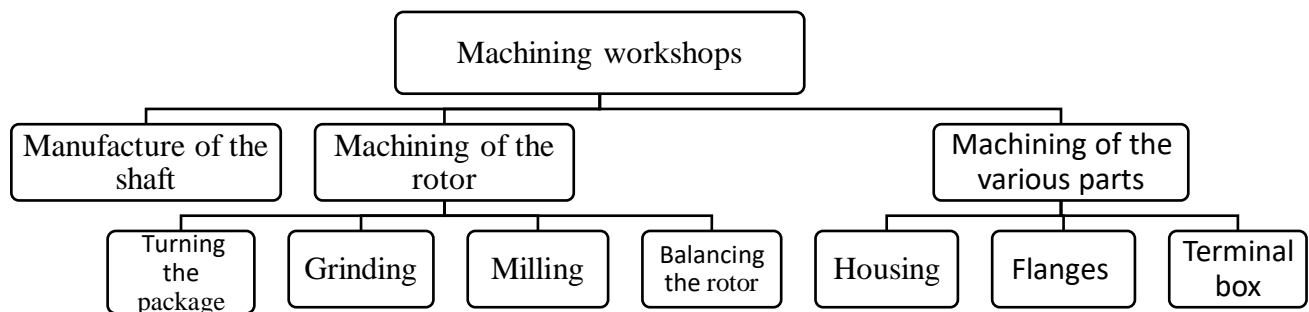


Figure III.10. The basic stages of machining workshops

### III.7.1. Manufacture of the shaft

Once the steel is positively tested, the shafts are cut using a mechanical saw or an automatic saw. The shaft in its raw state passes to the machining center to be centered; this operation consists of drilling two holes, which serve as a reference to be able to turn our rotor on a very precise axis.



Figure III.11. Machining workshops

### III.8. Winding workshops

The winding workshop is divided into three sectors:

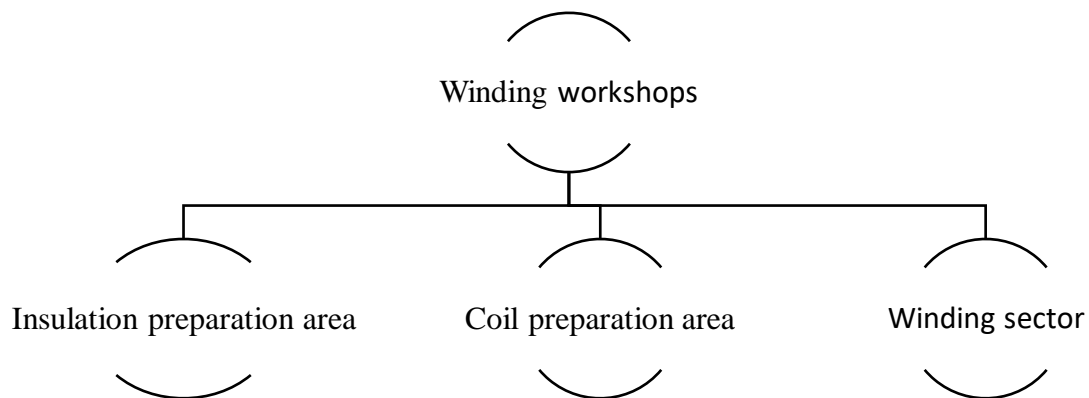


Figure III.12. Basic stages of Winding workshops

#### III.8.1. Insulation preparation sector

In this sector, all the insulators for all the machines are prepared in different models depending on where they are needed. The insulators used by the Electro-industries guarantee conforming quality to international standards

### III.8.2. Coil preparation sector

The coils are made using templates mounted on the machines rotary (winders), which are adjusted according to the number of turns per bundle.

### III.8.3. Winding stator preparation sector

This is the sector where the stator coil manufacturing process takes place, from the insertion of the slot channels to the impregnation

- a. insertion of the slot channels.
- b. Inserting the coils into the stator.
- c. Connection.
- d. Connection of coils and connection cables.
- e. Shrinking and pressing of coil heads.
- f. Control.
- g. Impregnation.



Figure III.13. Winding workshops

**III.9. Assembly workshop**

There are two essential sectors in this workshop.

**III.9.1. Pre-assembly sector**

The operations carried out in this sector are:

- Oil the inside of the casing to facilitate the insertion of the stator package.
- Fitting the package with a press.
- Lengthening and turning of the centering edges of the AS and BS side carcasses Milling the legs to find the exact axle height.
- Painting the inside diameter of the stator with a coat of anti-rust paint.

**III.9.2. Final assembly sector**

In this sector, the following operations are carried out:

- Installation of the BS rated inner bearing cover to ensure good motor sealing
- Fitting of bearings already lubricated on AS and BS sides with a vertical press and location of the key on AS side
- Screw the bearing covers into the flange, this allows the bearing to be enclosed between these two parts.
- Location of the key on the BS side and fitting of the fan with the same press then insertion of the stop ring (clip clamp) for the fan.
- Integration of the complete rotor in the stator and fixing of the BS rated flange with defects.
- Location of the washers (compensation washers and spring washers) on the AS side flange to avoid axial play of the rotor.
- Fixing the flange on the carcass with defects as well as mounting the engine cover Preparing of the terminal box and fixing the connection cables on the terminal board.



Figure III.14. Assembly workshop

### III.10. Final test

Once the product is finished, it undergoes a certain number of electrical checks:

- hand and eyes test
- Resistance measurement
- Idle running tests
- Tests with rotor locked
- Tests with load



Figure III.15. Resistance measurement and tests with load

**III.11. Conclusion**

Finally, we really learned a lot about the construction of the induction motor, from where we saw why and how the electric machine, of course, is considered an essential machine on the entire line of the industry with regard to its usefulness and its good characteristics: its performance, its solidity, its ease of repair and transport, and its being more economical compared to other machines.

# **CHAPTER IV**

## **CALCULATION OF IRON LOSSES IN A 2.2 KW INDUCTION MOTOR**

**IV.1. Introduction**

In the fourth chapter, we studied the characteristic of silicon iron sheets, where we used the company's Epstein framework to extract these properties, which are represented by iron loss as a function of flux density at different frequencies. In addition to studying the loss of iron in the engine using the Steinmetz and Bertotti equations and comparing them. We also compared the loss between two types of silicon iron sheets M400-50A and M800-50A various methods of calculation.

We also used Motor-CAD software to simulate the magnetic and thermal behavior of a 2.2 kW asynchronous motor. Motor-CAD is a modeling program designed specifically for electric motors, which allows you to simulate their electromagnetic and thermal performance.

We can simulate the behavior of the motor in normal operation by analyzing the magnetic field and temperature distribution between different parts of the motor body. This makes it possible to evaluate the electromagnetic and thermal performance of the motor.

**IV.2. Presentation of software motor-CAD**

Motor-CAD is a computer program for designing motors that was made by Motor Design Limited. It helps design and analyze motors thanks to its three integrated modules:

**E-Magnetic:** is a 2D finite element module for accurate prediction of electromagnetic and electrical performance.

**Thermal:** is a finite element thermal analysis module for the study of heating and cooling of motors. It allows the user to try a variety of cooling methods on the motor and determine the best one for a given operating environment.

**Lab:** is a virtual test module that includes rapid calculation of yield and loss maps and simulation of operating cycles

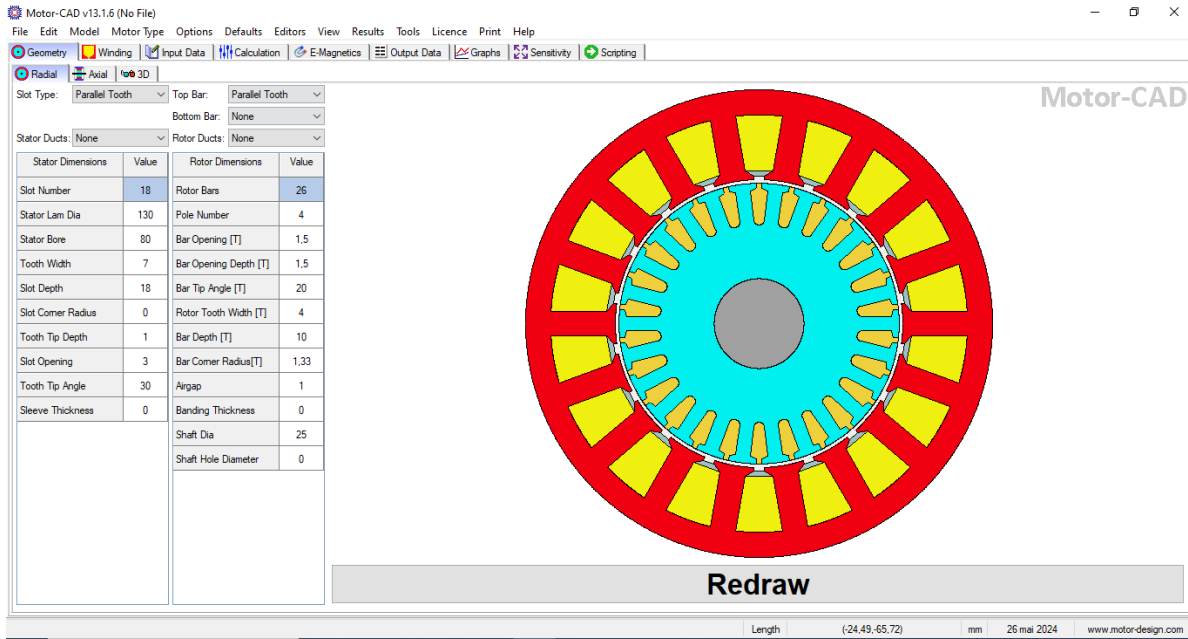


Figure IV.1. ANSYS Motor-CAD Software Window

Part one: Calculating iron losses

IV.3. Epstein Frame

The Electro-Industries company owns an Epstein frame type 25 cm (Figure IV.2). We have used it in order to measure the value of losses in iron for steel sheets of the type M800-50A, following the same steps described in chapter II

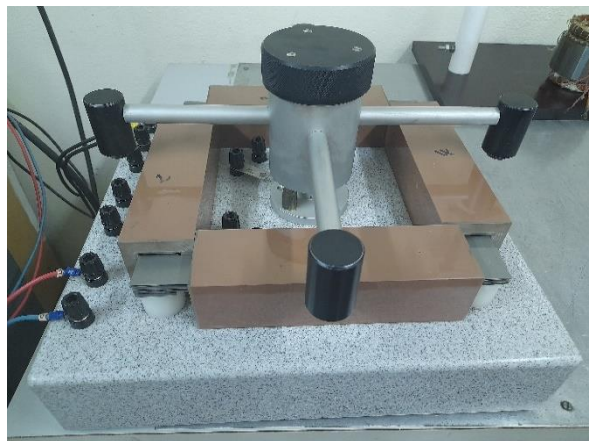


Figure IV.2. Epstein Frame in the company Electro-Industries

#### IV.4. Steel sheet M800-50A

We worked at the company with steel sheet type M800-50A, is a specific type of magnetic steel characterized by a core loss of 8 W/kg at a frequency of 50Hz and thickness of 0.5mm, where M stands for “magnetic”, and A refers to the type of steel sheet, as well as to the quality of the material’s

After entering the results of the iron losses and the flux density for different frequencies obtained from a test on the Epstein frame, the method used to calculate the losses in this case is the Bertotti method and Steinmetz .

#### IV.5. Steinmetz and Bertotti equations

After adding the values of the frequency, flux density, and iron losses to the motor-CAD, they gave us values of the constants ( $K_{eddy}$ ,  $K_h$ ) for the Steinmetz equation, as well as ( $K_h$ ,  $K_{exe}$ ) for the Bertotti equation. We used these constants in calculating iron losses for different values of frequency (30, 50, 60, 100, 200) for each value of flux density (0.5, 1, 1.5) by using the previous equation (IV.1, IV.2):

##### Steinmetz equation

$$W_{Fe} = K_h \times f \times B^{(\alpha+\beta B)} + 2\pi^2 K_{eddy} \times f^2 \times B^2 \quad (IV.1)$$

##### Bertotti equation

$$W_{Fe} = K_h \times f \times B^\alpha + K_{eddy} \times f^2 \times B^2 + K_{exe} \times f^{1.5} \times B^{1.5} \quad (IV.2)$$

With

$$K_{eddy} = \frac{(\text{lamination thickness})^2}{12 \cdot \text{density} \cdot \text{ele resistivity}} \quad (IV.3)$$

Where

$$\text{Density} = 7650 \text{ (kg/m}^3\text{)}$$

$$\text{Ele resistivity} = 2.3 \times 10^{-7} \text{ (Ohm.m)}$$

We obtain the results shown in the following tables:

Table IV.1. Steinmetz loss method being used for Steel sheet M800-50A

<b>Steinmetz coefficient</b>	Hysteresis loss coefficient( $K_h$ )	0.05318
	Eddy current loss coefficient( $K_{eddy}$ )	$10^{-5}$
	Alpha exponent for hysteresis loss	1.713
	Beta exponent for hysteresis loss	0
<b>Bertotti coefficient</b>	Hysteresis loss coefficient( $K_h$ )	0.007231
	Alpha exponent for hysteresis loss	3.447
	Eddy current loss coefficient( $K_{eddy}$ )	$1.183 \times 10^{-5}$
	Excess loss coefficient ( $K_{exc}$ )	0.007605

Table IV.2. Core losses vs magnetic flux density for different method at 30Hz

Flux density [T]	Bertotti[W/kg]	Steinmetz[W/kg]	Epstein Frame[W/kg]
0.5	0.4643	0.5310	0.4546
1	1.4772	1.773	1.313
1.5	3.1973	3.595	3.050

Table IV.3. Core losses vs magnetic flux density for different method at 50 Hz

Flux density [T]	Bertotti[W/kg]	Steinmetz[W/kg]	Epstein Frame[W/kg]
0.5	0.9912	0.9344	0.796
1	3.08	3.152	2.418
1.5	6.469	6.435	6.029

Table IV.4. Core losses vs magnetic flux density for different method at 60 Hz

Flux density [T]	Bertotti[W/kg]	Steinmetz[W/kg]	Epstein Frame[W/kg]
0.5	1.3001	1.1509	1.00
1	4.0111	3.9014	3.03
1.5	8.34476	7.9895	6.62

Table IV.5. Core losses vs magnetic flux density for different method at 100 Hz

Flux density [T]	Bertotti[W/kg]	Steinmetz[W/kg]	Epstein Frame[W/kg]
0.5	2.7847	2.1156	1.8810
1	8.4469	7.2919	5.97407
1.5	17.164	15.0923	10.466

Table IV.6. Core losses vs magnetic flux density for different method at 200 Hz

Flux density [T]	Bertotti[W/kg]	Steinmetz[W/kg]	Epstein Frame[W/kg]
0.5	7.8564	5.2181	4.7563
1	23,43	18.5317	15,33
1.5	46.4370	39,0674	37,74

We also we obtain a graph representing the iron losses vs flux density Figure (IV.3) and Figure (IV.4):

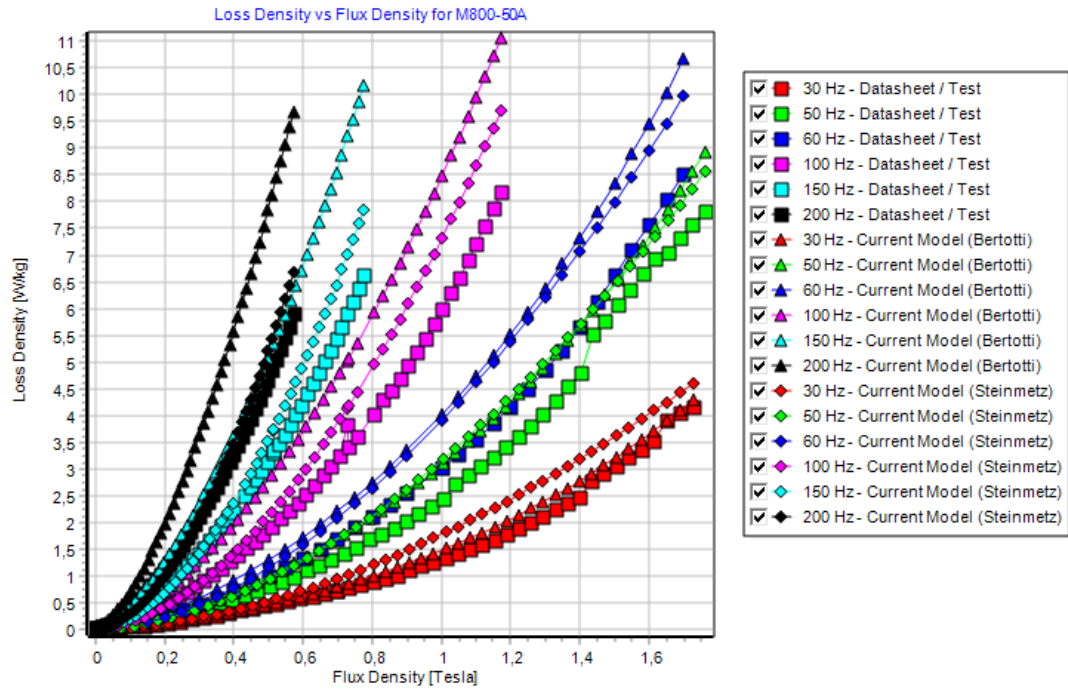


Figure IV.3. Specific losses curve for M800-50A sheet from 30Hz to 200Hz

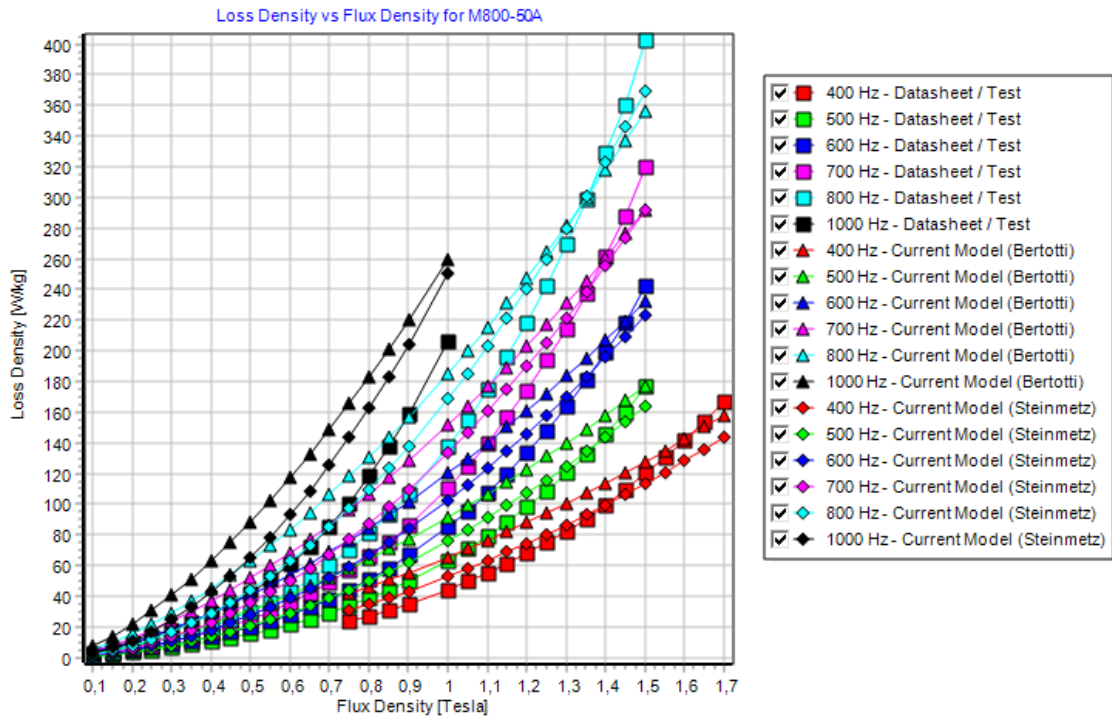


Figure IV.4. Specific losses curve for M800-50A sheet from 400Hz to 1000Hz

After looking at the results of the previous tables for various frequencies we notice that every time the value of the frequency or flux density increases, the value of the iron losses increases, this indicates that both frequency and magnetic flux density have an impact on iron losses in electrical machinery.

The accuracy of the Steinmetz and Bertotti iron loss models and the Epstein frame is an important consideration in the design and analysis of electrical machines. The Bertotti model offers better precision than the Steinmetz model, for high-frequency applications.

For applications in which simplicity and fast estimates are sufficient, the Steinmetz equation may be sufficient. However, to get higher accuracy, especially in scenarios that involve various frequencies, complex wave forms, or materials with large abnormal losses, the Bertotti equation is the most convenient.

If the maximum accuracy is required to measure the magnetic losses of a specific material under specific operating conditions, then the Epstein frame is the most accurate tool.

#### IV.6. Steel sheet M400-50A

By using the data within the Motor-CAD program, we extracted the different flux density points for M400-50A steel sheets and the following tables represent the iron loss in different ways and frequencies.

**Table IV.7. Steinmetz loss method being used for Steel sheet M400-50A**

<b>Steinmetz coefficient</b>	Hysteresis loss coefficient(Kh)	0.03663
	Eddy current loss coefficient( $K_{eddy}$ )	$5.441 \times 10^{-6}$
	Alpha exponent for hysteresis loss	2.715
	Beta exponent for hysteresis loss	0
<b>Bertotti coefficient</b>	Hysteresis loss coefficient(Kh)	0.003351
	Alpha exponent for hysteresis loss	3.813
	Eddy current loss coefficient( $K_{eddy}$ )	$6.4839 \times 10^{-6}$
	Excess loss coefficient (Kexc)	0.004153

Table IV.8. Core losses vs magnetic flux density for different method at 50Hz

Flux density [T]	Bertotti[W/kg]	Steinmetz[W/kg]	Epstein Frame[W/kg]
0.5	0.535099	0.346065	0.46
1	1.65207	2.1	1.46
1.5	3.52021	6.11087	3.42

Table IV.9. Core losses vs magnetic flux density for different method at 60 Hz

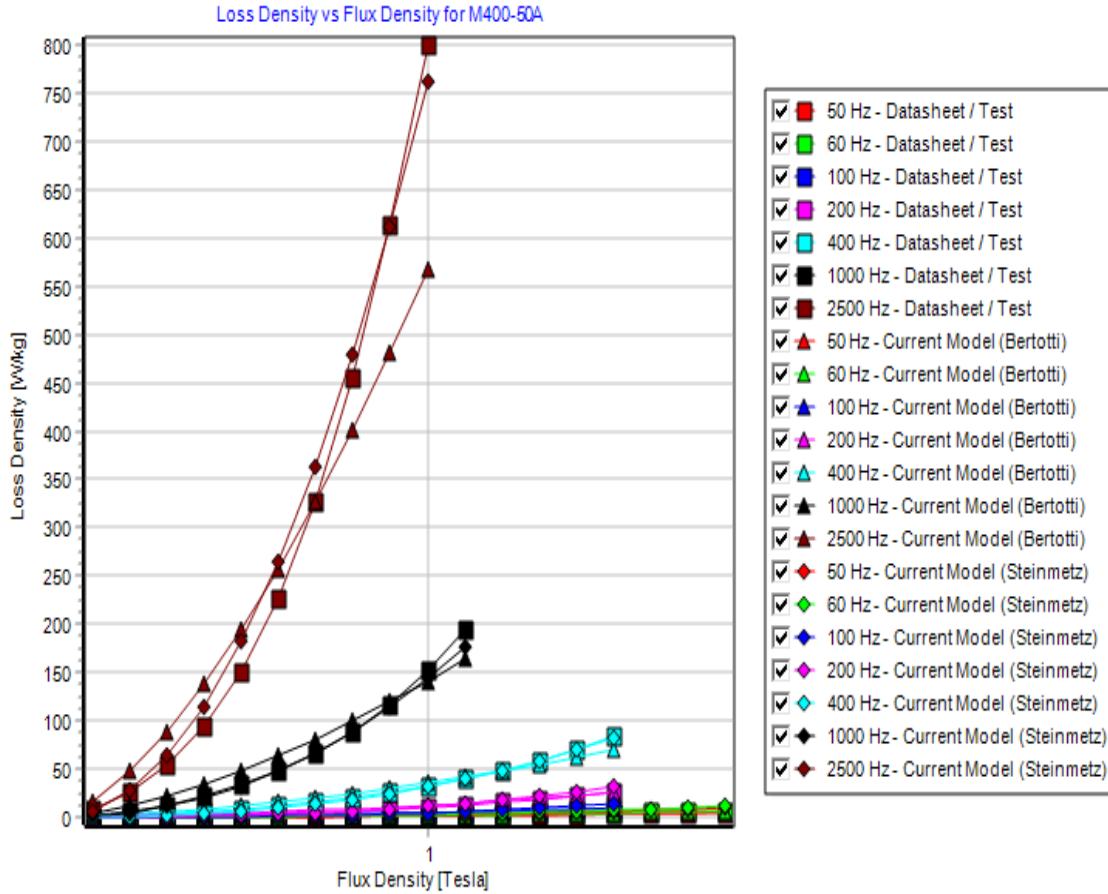
Flux density [T]	Bertotti[W/kg]	Steinmetz[W/kg]	Epstein Frame[W/kg]
0.5	0.702549	0.431389	0,573
1	2.15454	2.58444	1.85
1.5	4.54196	7.47804	4.34

Table IV.10. Core losses vs magnetic flux density for different method at 100 Hz

Flux density [T]	Bertotti[W/kg]	Steinmetz[W/kg]	Epstein Frame[W/kg]
0.5	1.50836	0.826382	1,102
1	4.55294	4.73701	3.72
1.5	9.34801	13.43	8.79

Table IV.11. Core losses vs magnetic flux density for different method at 200 Hz

Flux density [T]	Bertotti[W/kg]	Steinmetz[W/kg]	Epstein Frame[W/kg]
0.5	4.26553	2.18977	2.87
1	12.676	11.622	10,4
1.5	25.3083	31.6931	25.3



Figures IV.5. Loss density vs flux density for M400-50A

**IV.7. Comparison between steel sheets M800-50A and M400-50A**

We took a fixed point of flux density (0.5, 1) for different frequencies (50, 60, 100, 200) to compare the iron losses produced by each steel sheet for the Epstein frame and the Steinmetz and Bertotti equations.

Table IV.12. Comparison the value of iron losses between steel sheets

M800-50A and M400-50A for 0.5 T

Frequency [Hz]	Bertotti [W/kg]		Steinmetz [W/kg]		Epstein Frame [W/kg]	
	M800-50A	M400-50A	M800-50A	M400-50A	M800-50A	M400-50A
<b>50</b>	0.9912	0.535099	0.9344	0.346065	0.796	0.46
<b>60</b>	1.3001	0.702549	1.1509	0.431389	1.00	0.573
<b>100</b>	2.7847	1.50836	2.1156	0.826382	1.8810	1.102
<b>200</b>	7.8564	4.26553	5.2181	2.18977	4.7563	2.87

Table IV.13. Comparison the value of iron losses between steel sheets

M800-50A and M400-50A for 1T

Frequency [Hz]	Bertotti [W/kg]		Steinmetz [W/kg]		Epstein Frame [W/kg]	
	M800-50A	M400-50A	M800-50A	M400-50A	M800-50A	M400-50A
<b>50</b>	3.08	1.65207	3.152	2.1	2.418	1.46
<b>60</b>	4.0111	2.15454	3.9014	2.58444	3.03	1.85
<b>100</b>	8.4469	4.55294	7.2919	4.73701	5.97407	3.72
<b>200</b>	23,43	12.676	18.5317	11.622	15,33	10.4

After looking at the results of the previous tables, we note that the value of iron losses in steel sheets M400-50A is small, approximately 50% in front of the loss value of M800-50A type steel sheets for all studies (Epstein frame and the Steinmetz and Bertotti equations).

### Part two Study on induction motor type 2.2 kW

#### IV.8. Presentation of the induction motor

In our project we study, a three-phase asynchronous squirrel cage machine, with a power of 2.2kW tetra-polar, manufactured by the company Electro-Industries of Azazga. The geometric and physical parameters of the machine are given in the table below (IV.24)

Table IV.14. Specifications of the Machine Studied

Setting	Symbol	Value	Unit
Nominal power	$P_{input}$	2.2	KW
Nominal voltage	$U_n$	380	V
Nominal current	$I_n$	4.5	A
Nominal torque	$T_n$	14.9	N.m
Nominal rotation speed	$N_n$	1410	Tr/min
Frequency	$f$	50	Hz
Number of phases	$q$	3	-
Number of poles	$2p$	4	-
Insulation class	-	F(155°C°)	-
Mass	$m$	20	kg



Figure IV.6. Housing



Figure IV.7. Rotor



Figure IV.8. Stator



Figure IV.9. Induction motor

#### IV.9. Machine geometry

We used the available parameters of the 2.2 kw motor to create the geometry of the machine using the Motor-CAD software. The figures below show the machine's geometry.

Motor-CAD

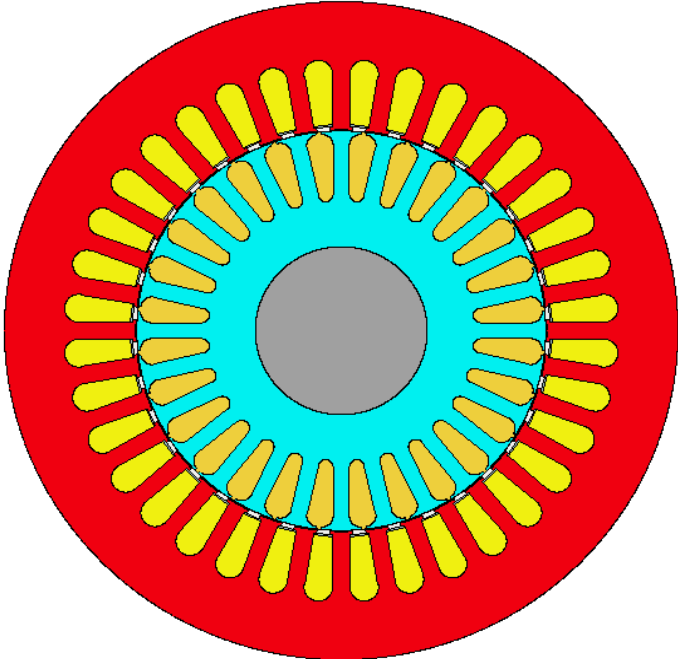


Figure IV.10. Radial geometry of induction motor

Motor-CAD

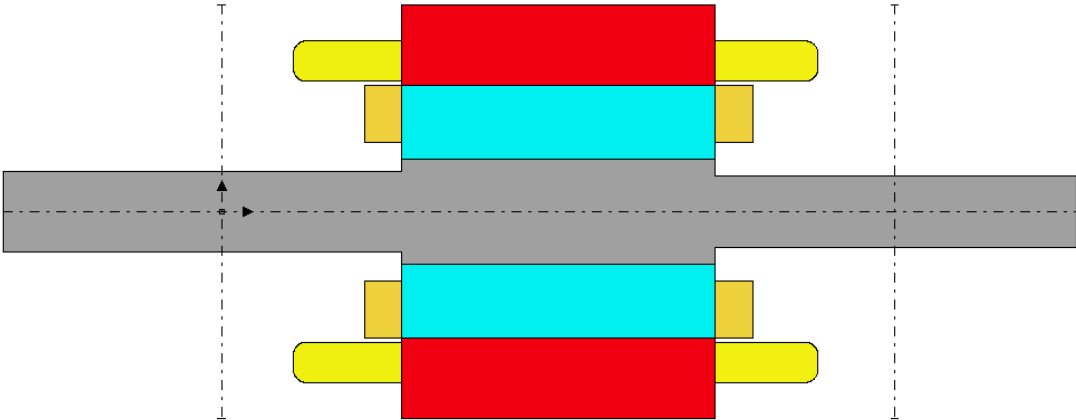


Figure IV.11. Axial geometry of induction motor

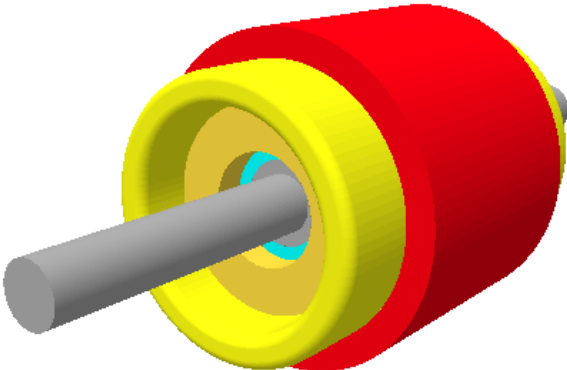


Figure IV.12. 3D View of induction motor

**IV.10. Pattenm distribution**

We followed the parameters to design our winding on the software, the Figure (IV.13) and Figure (IV.14) show the winding's radial pattenm and linear pattenm distribution:

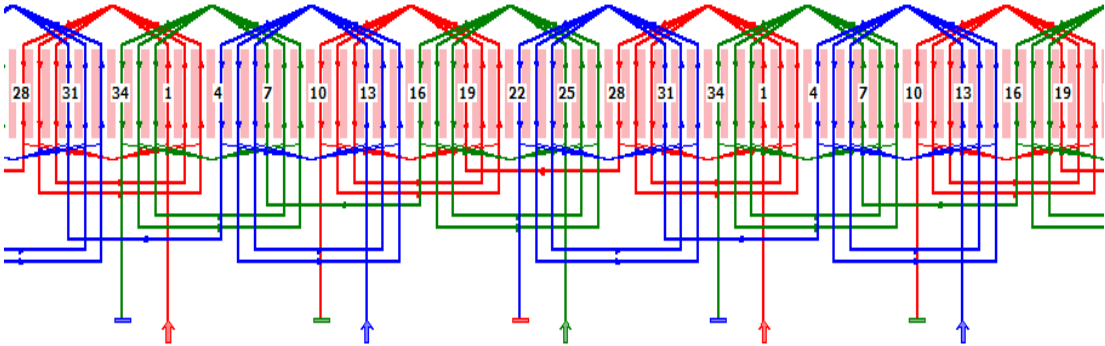


Figure IV.13. Linear Pattenm Distribution

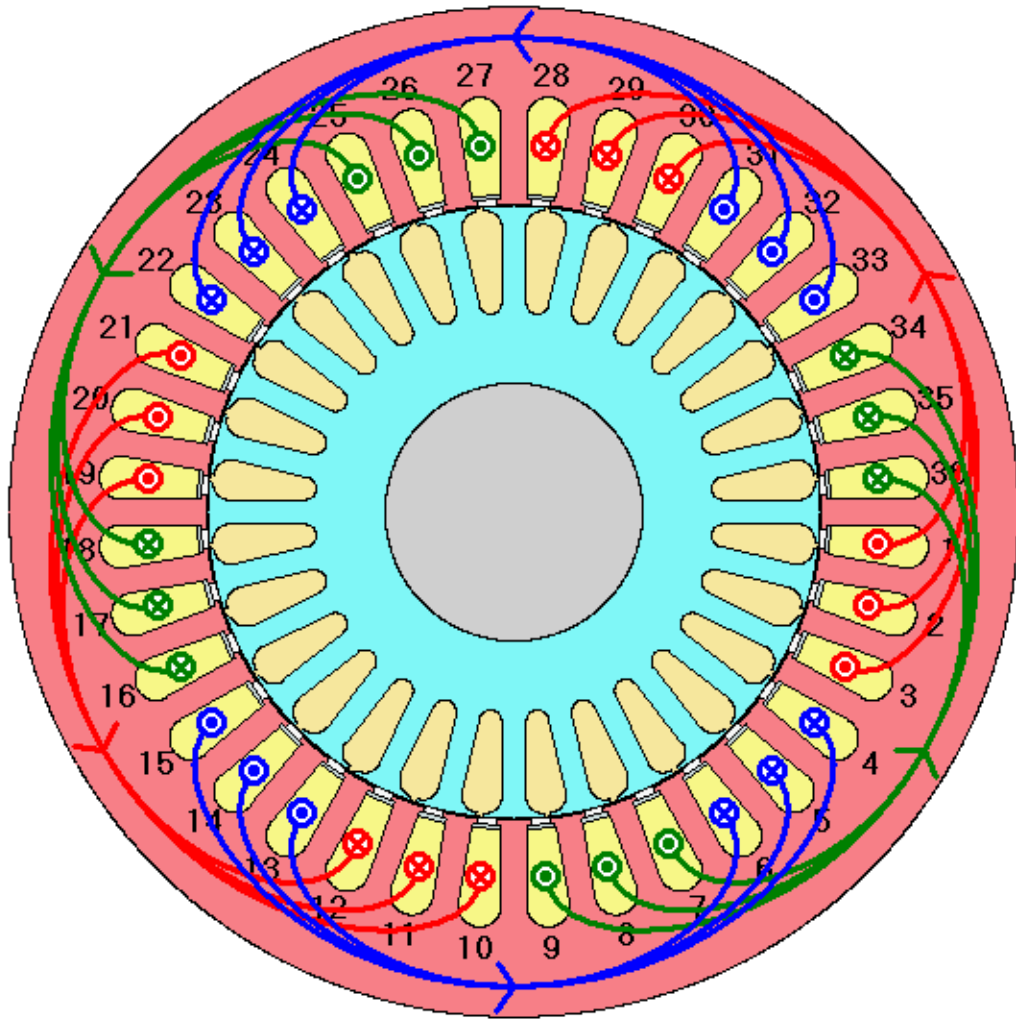


Figure IV.14. Radial Pattern Distribution

#### IV.11. Curve of first magnetization

We obtain the first magnetization curve for ferromagnetic materials when they are exposed to a variable magnetic field for the first time, the curve  $B - H$  Figure (IV.15) represents the relationship between the magnetic induction ( $B$ ) and the magnetic field ( $H$ ) for a steel sheet M800-50A (50Hz)

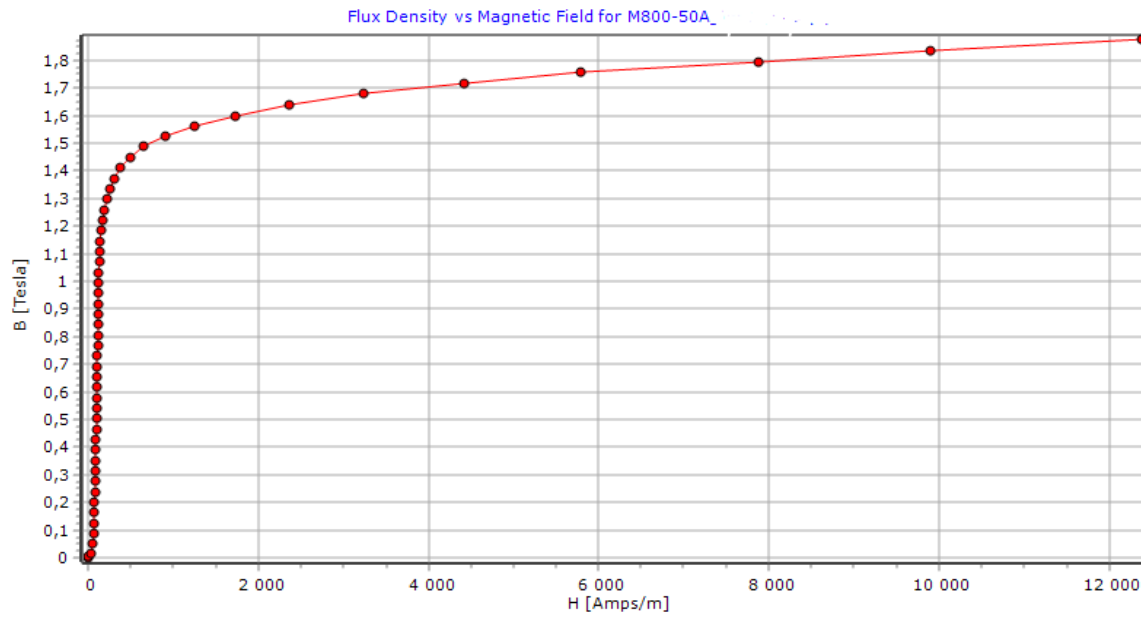


Figure IV.15. Curve of first magnetization

Figure (IV.15) also shows how the material responds to an increasing external magnetic field. At first, as the magnetic field increases, the magnetic induction also increases. As the magnetic field increases, the magnetic induction reaches its maximum value which corresponds to the saturation state.

## IV.12. Electromagnetic simulation results

### IV.12.1. Mesh

Motor-Cad determines the flow distribution through the machine using the finite element method, the figure (IV.16) represent the mesh by the finished element network of the motor, we observe that the mesh is concentrated more in the slot and maintenance areas, this is because the

air gap is where the electromagnetic interaction and the slot hold the coils of conductor wires, which are the source of the current used for the creation of the rotating field.

**Motor-CAD**

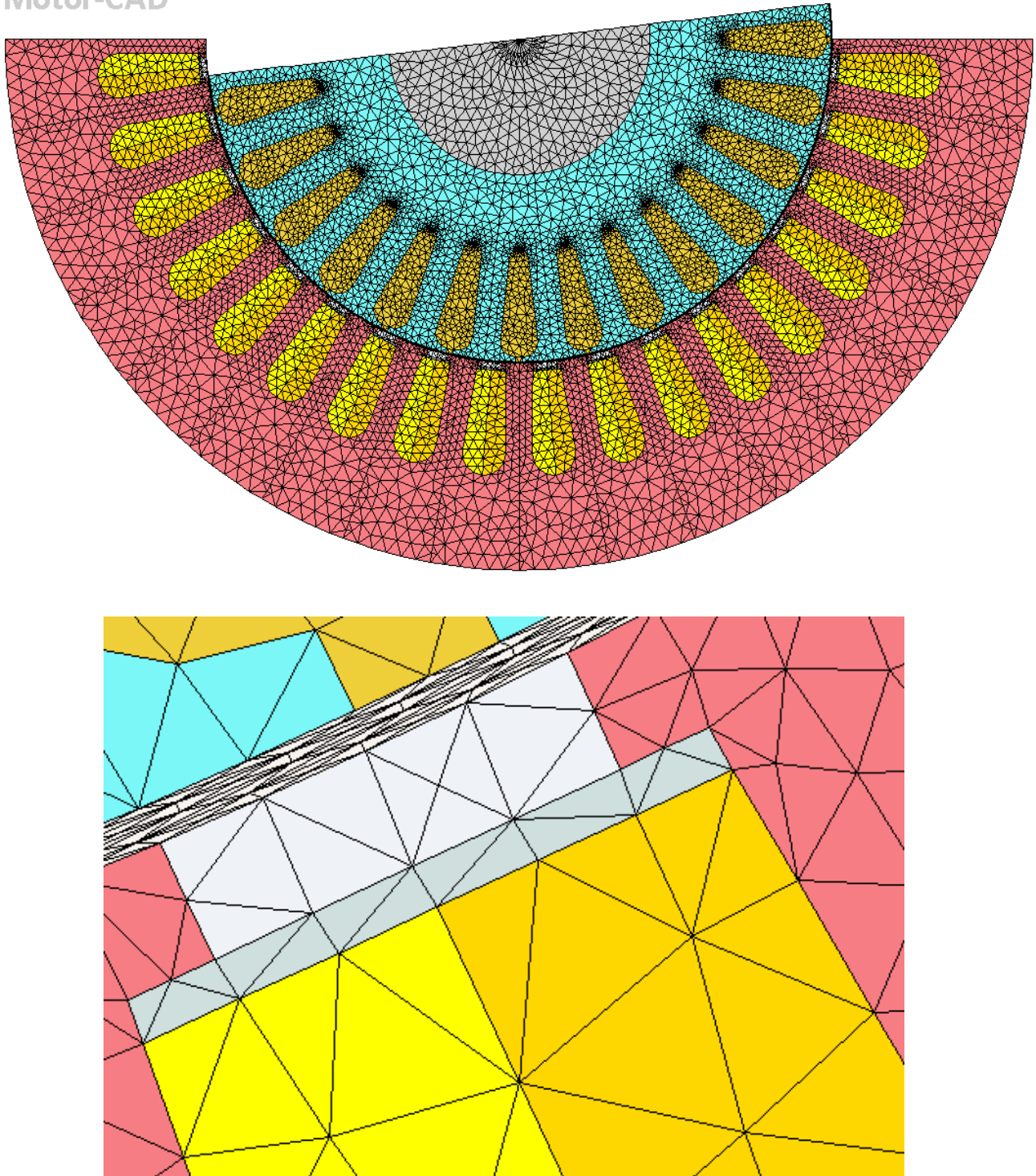


**Figure IV.16. Mesh of the motor**

### IV.12.2. Magnetic field cartography

Figure (IV.17) shows us the distribution of the field and induction magnetic, the induction values are close to the values that are put into the first curve of magnetization. Furthermore, we note that the induction is more concentrated in the vicinity of angularly shaped regions.

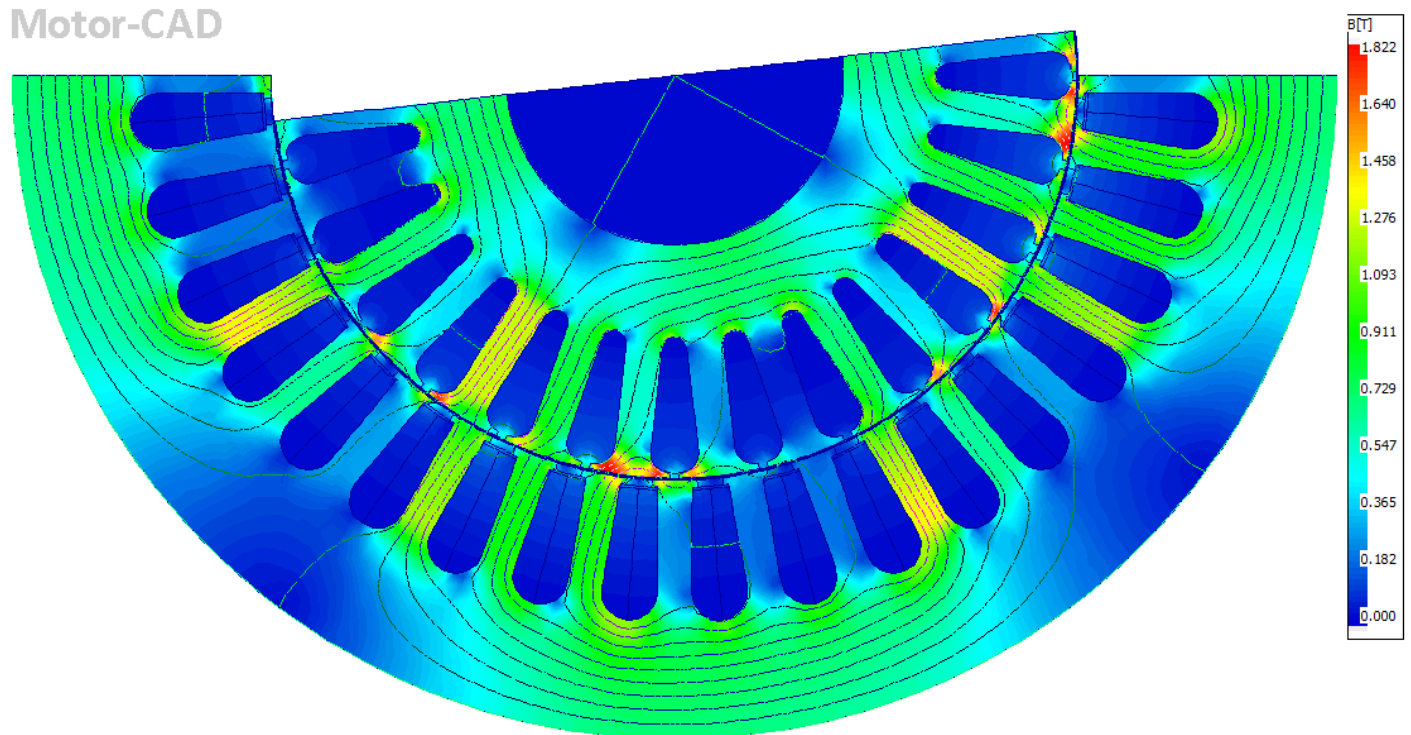


Figure IV.17. Distribution of the magnetic field

### IV.12.3. Electromagnetic characteristics

It is evident that the speeds achieved correspond to those of a class F motor in the National Electrical Manufacturers Association (NEMA) classification, which pertains to asynchronous motors with deep slots.

Figures (IV.18) and (IV.19) present the electrical properties of the motor:

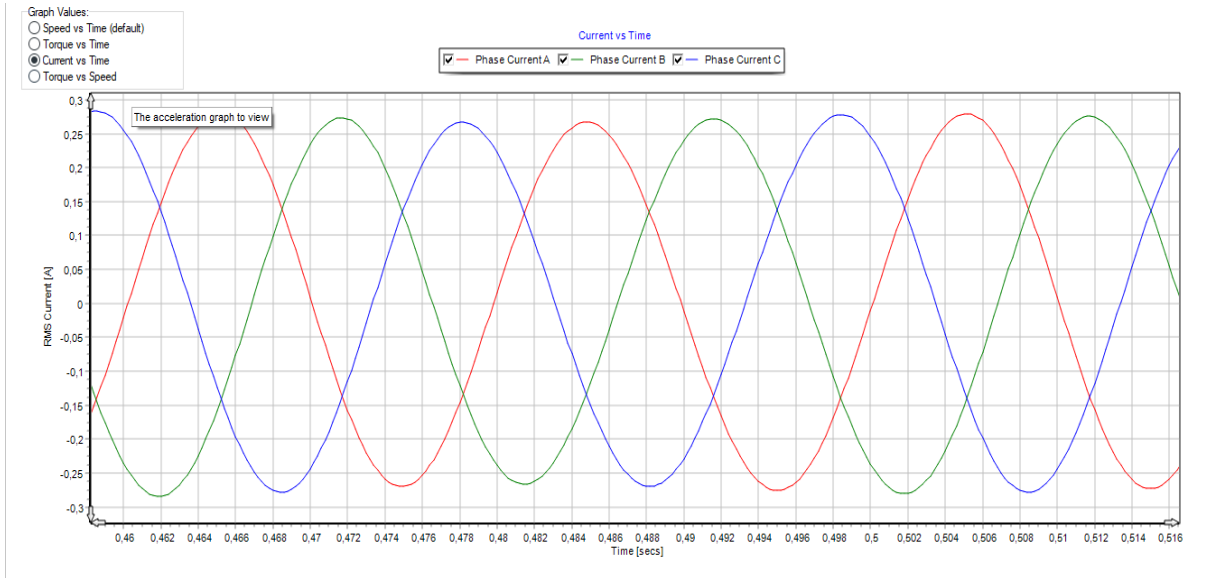


Figure IV.18. Stator current waveform

The machine's terminal currents are phase-shifted by  $120^\circ$  from one another and are exactly sinusoidal. They are well-balanced and have the same maximum value

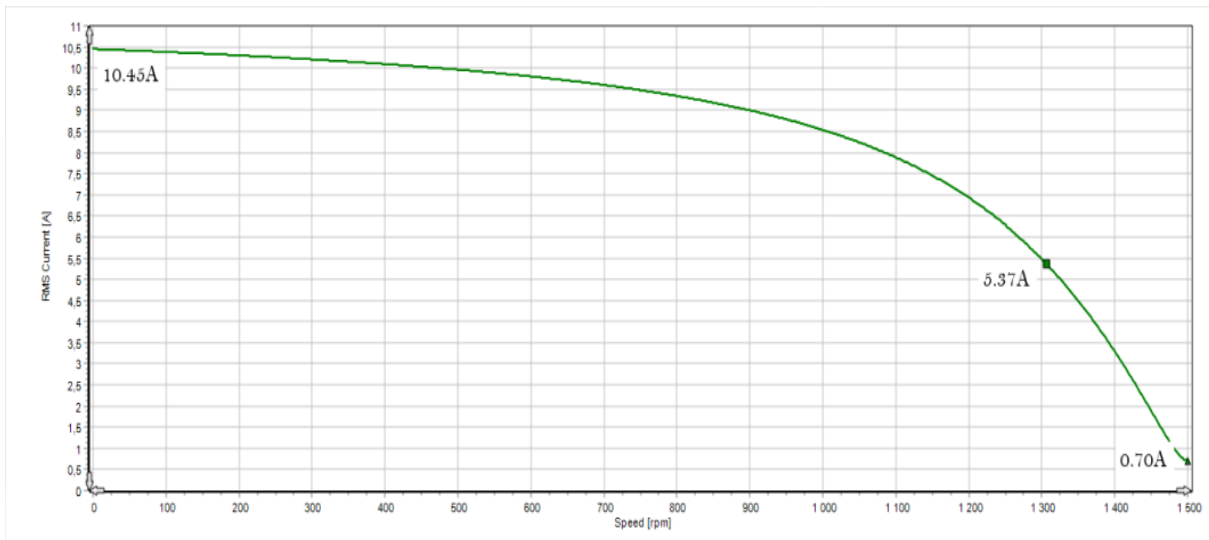
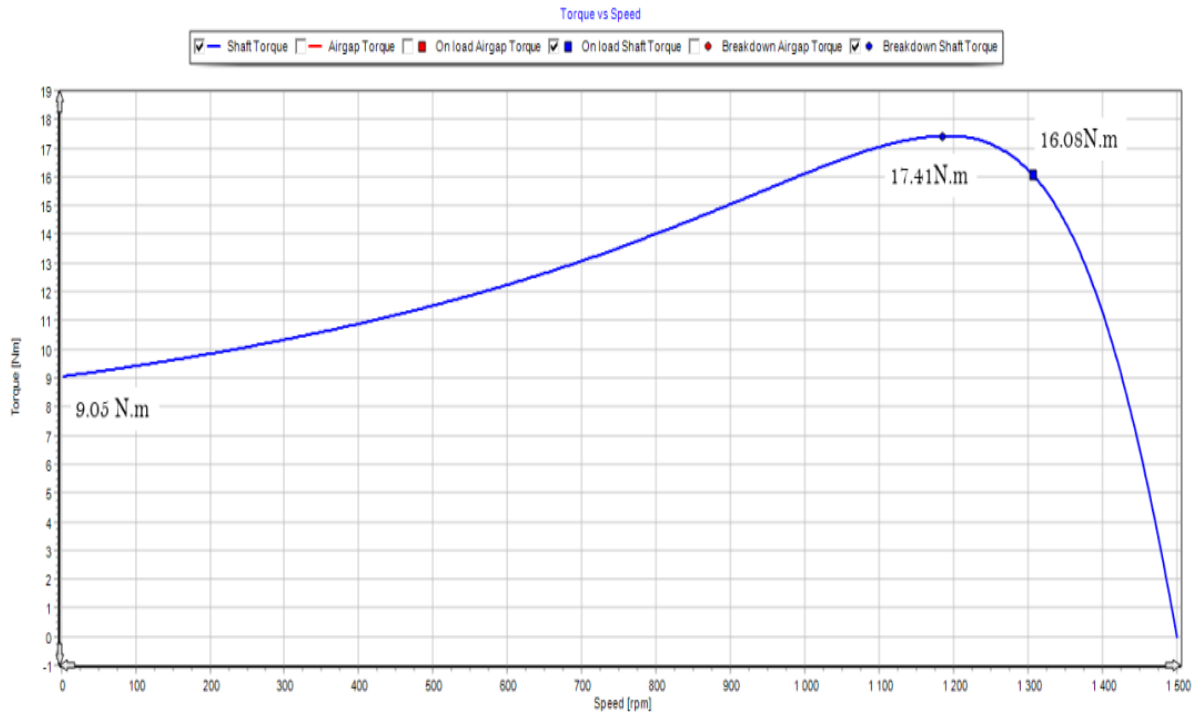


Figure IV.19. Line current versus speed

Figure (IV.19) shows no load Line current of 0.7 A as well as the nominal current of 10.45 A, and on load line current of 5.57 A.

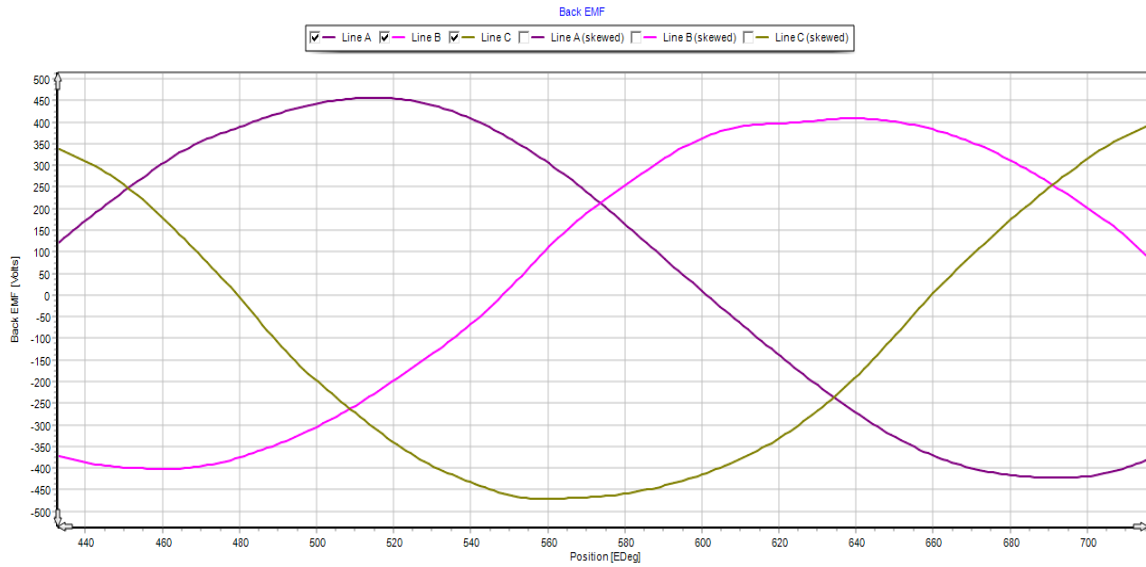
Figures (IV.20) present the mechanical properties of the motor:



**Figures IV.20. Torque versus speed**

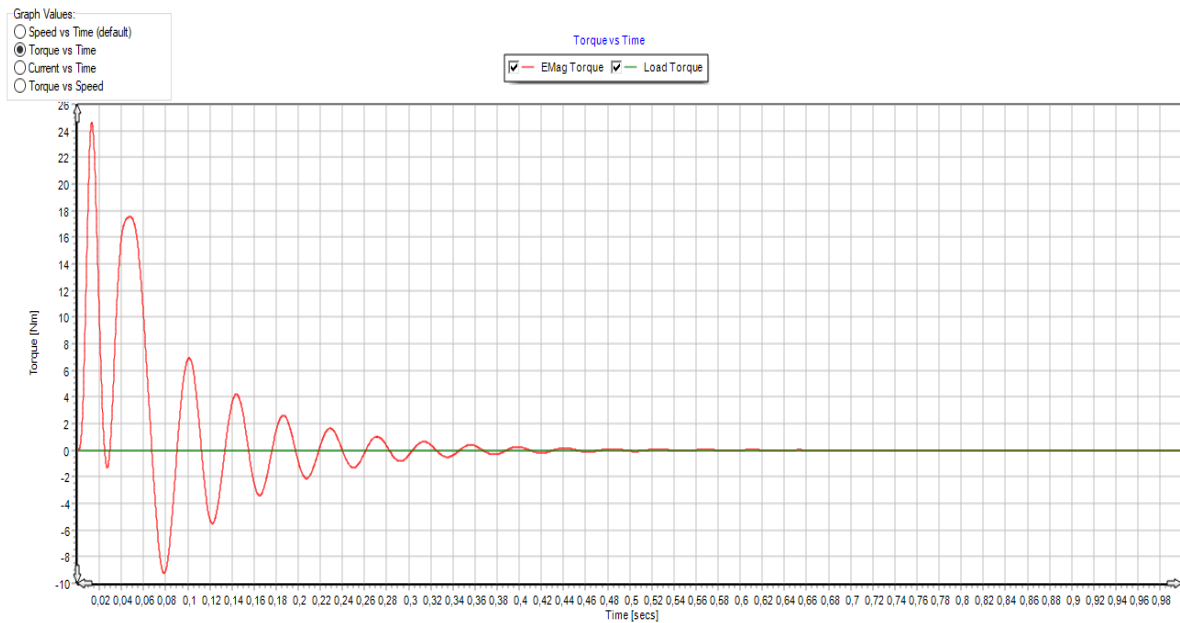
This figure indicates that the motor's starting torque is 9.05 N.m., its maximum torque is 17.41 N.m., and its nominal torque is 16.08 N.m.

When an induction motor works, it creates a force called electromotive force (EMF) according to the relative motion between the stator and rotor windings, This EMF opposes the applied voltage and is called "back EMF", the back EMF is caused by the rotor windings cutting through the magnetic field produced by the stator windings, figures (IV.21) present the Single load point back FEM position



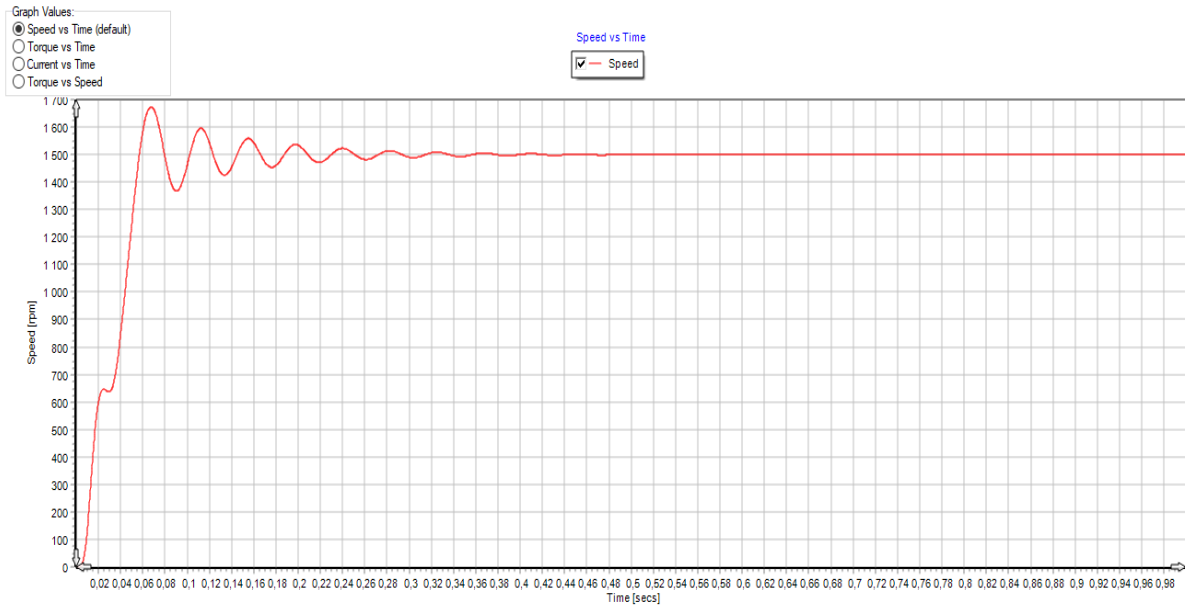
Figures IV.21. Single load point back FEM position

IV.12.4. Magnetodynamic characteristics



Figures IV.22. Torque variation curve as a function of time

The torque versus time curve demonstrates how well the simulated motor reacts when load torque is applied

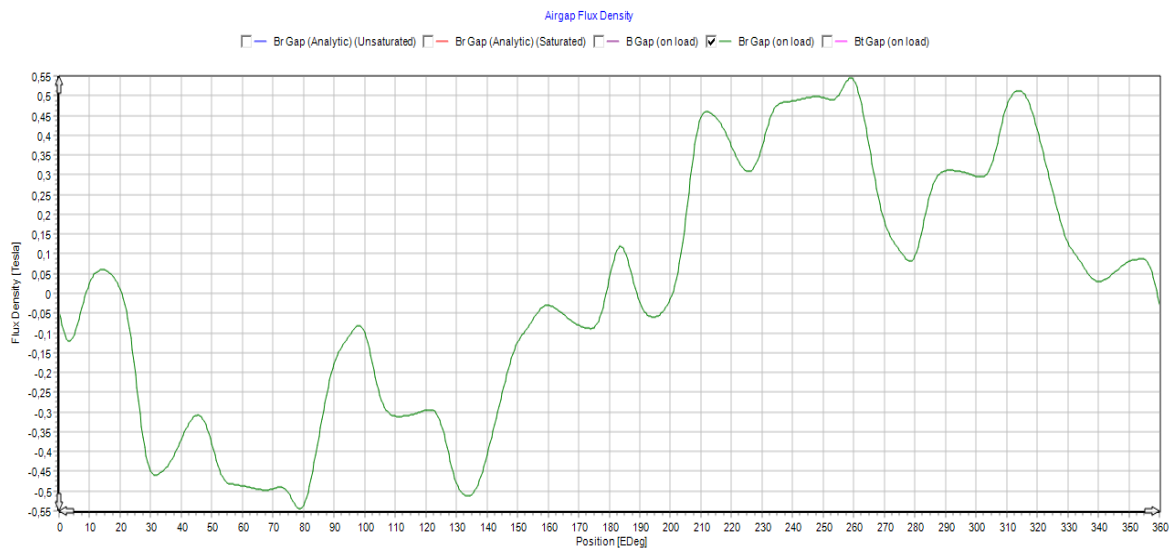


Figures IV.23. Rotation speed curve as a function of time

It can be seen from the two previous graphs that our design complies with the asynchronous motor under study's operating principle and that the simulated values match the experimental values found through a variety of factory tests.

### IV.13. Airgap flux density

The figure below represents the distribution of flux density in the air gap in our motor.



Figures IV.24. Distribution of flux density in the airgap

When we look at figure (Figures IV.24), we can see that it doesn't look perfectly sinusoidal, this is because of the discontinuity of the airgap.

#### IV.14. Losses in the induction motor

##### IV.14.1. In the stator

Table IV.15. Losses in the stator

The Losses		Value [W]	
Iron losses	Hysteresis losses	In the stator back	30,59
		In the stator tooth	19,21
	Eddy current losses	In the stator back	4,468
		In the stator tooth	3,2

##### IV.14.2. In the rotor

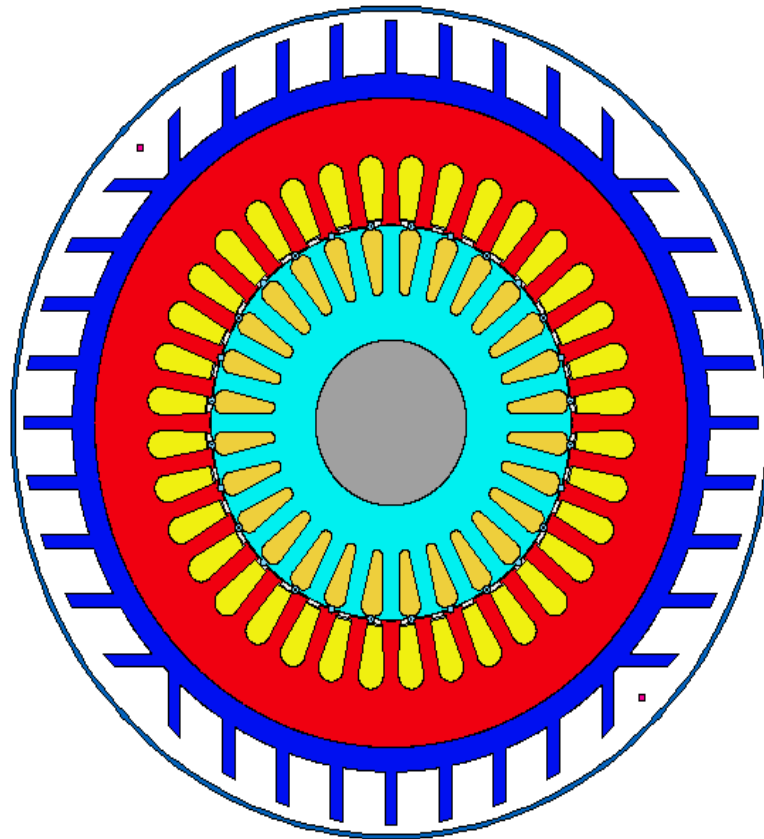
Table IV.16. Losses in the rotor

The losses		Value[W]	
Iron losses	Hysteresis losses	In the rotor back	4,943
		In the rotor tooth	6,942
	Eddy Current losses	In the rotor back	0,5235
		In the rotor tooth	1,006

## IV.15. Thermal study

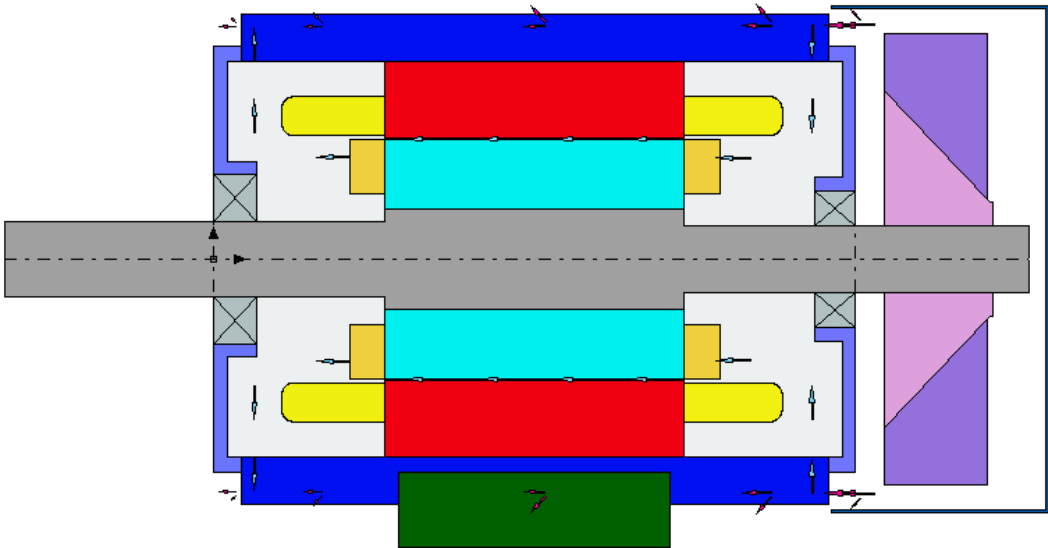
### IV.15.1. Geometry of the squirrel cage asynchronous machine

We presented the machine's cooling circuit and carcass for the thermal analysis. The motor with casing is shown in radial, axial, and three-dimensional views in the figures below.

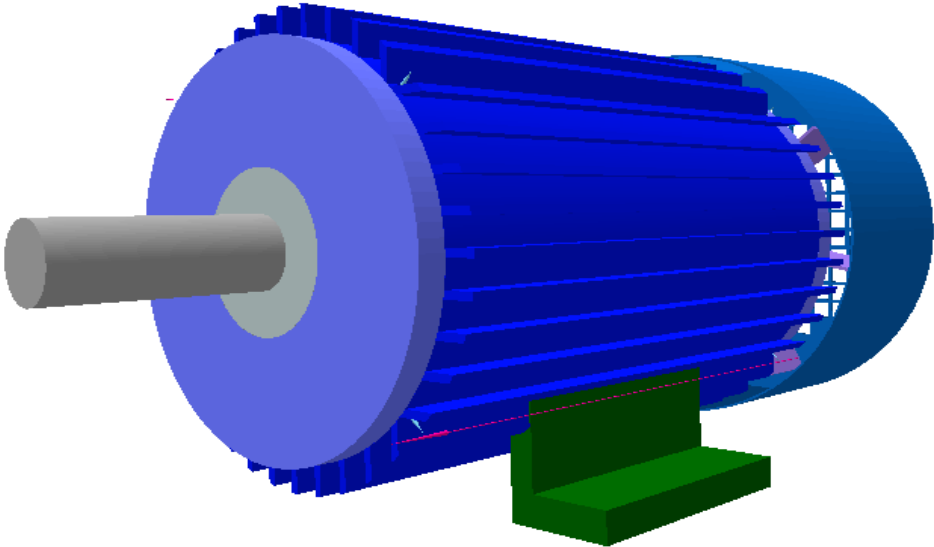


Motor-CAD

Figures IV.25. Radial geometry of a squirrel cage asynchronous motor according to ansys Motor-CAD



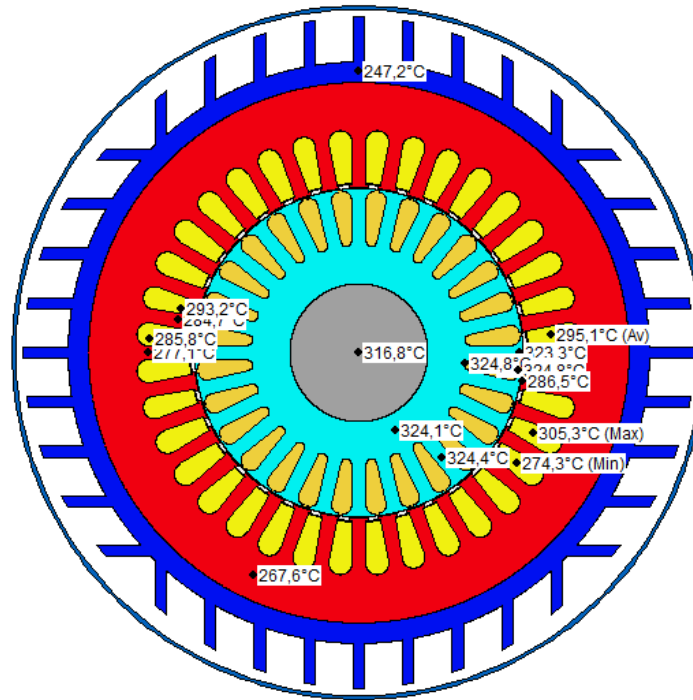
Figures IV.26. Axial geometry of a squirrel cage asynchronous motor according to Ansys Motor-CAD



Figures IV.27. 3D view of the induction motor

### IV.15.2. Temperature distribution without of a cooling circuit

In this application, we introduced a motor casing without a cooling circuit, the following figures (IV.28) show the temperature distribution as well as its evolution over time in different parts of our motor:



Motor-CAD

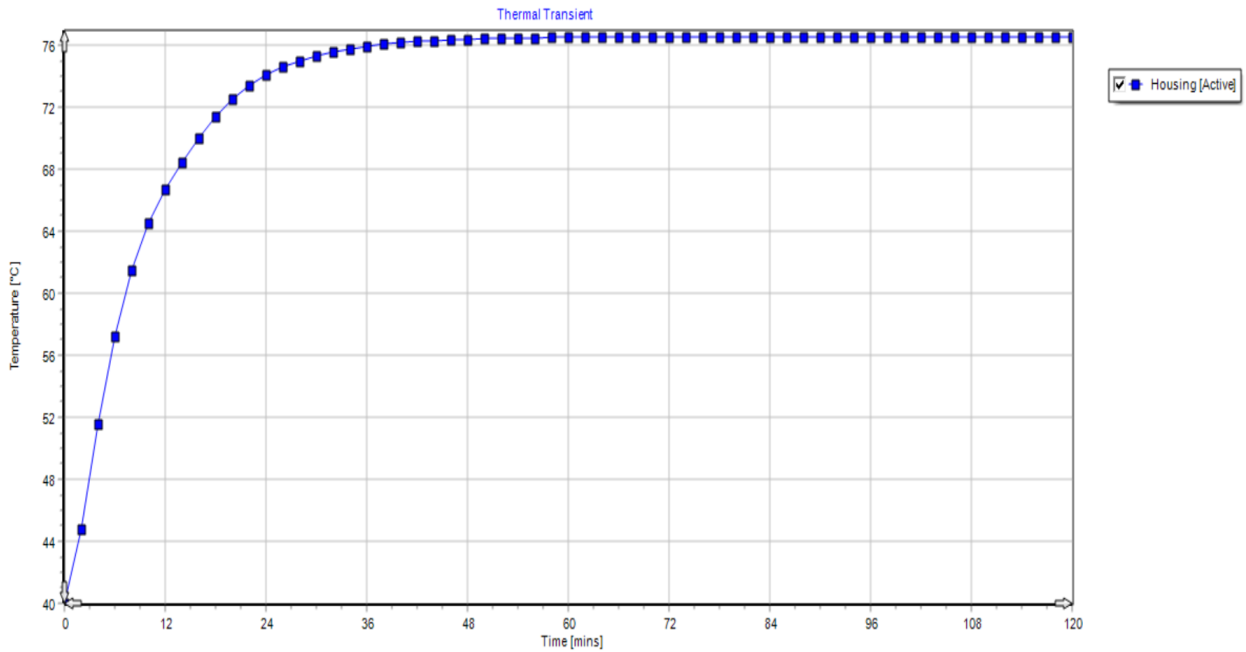
Figures IV.28. Radial view of motor temperature distribution by ansys Motor-CAD

### IV.15.3. Temperature distribution with cooling circuit

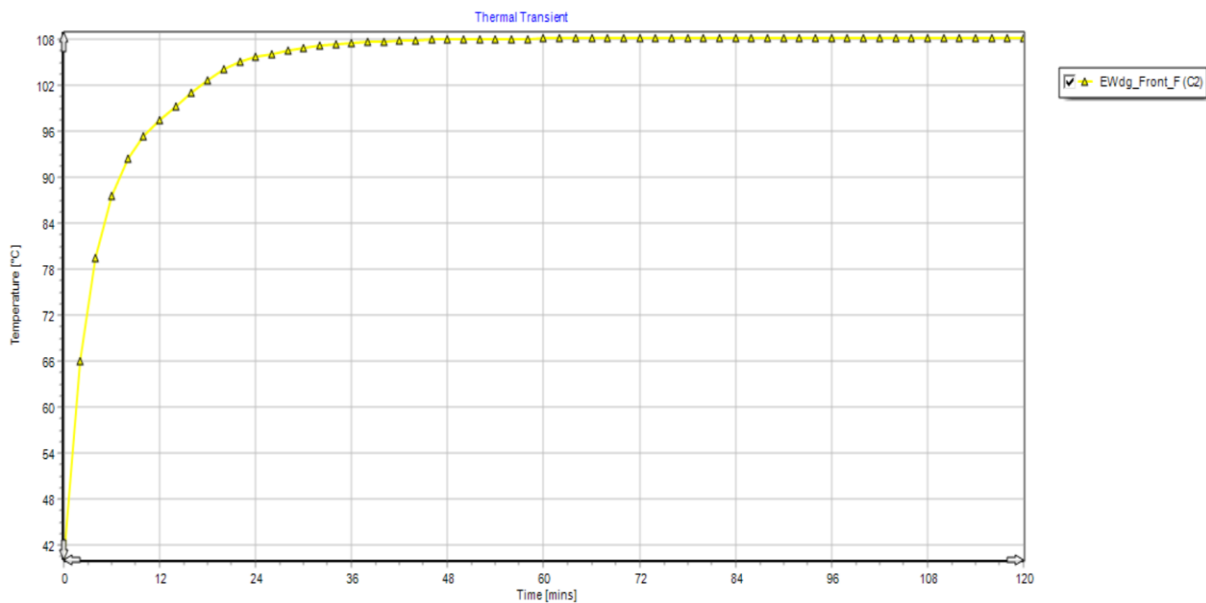
The cooling circuit was added to this application, which we used in this motor blown-over (self-ventilated) cooling type. The following figures (IV.29 and IV.30) show the temperature distribution and its temporal evolution in various motor components:



The performance of a machine is largely limited by overheating, and high machine temperatures present the risk of destroying the insulation and thus causing a series of faults in the machine, this is why the motor cooling process is very important in order to ensure engine safety which in turn will improve the efficiency of the machine.



Figures IV.31. Temperature variation in the motor housing



Figures IV.32. Temperature variation in the motor end winding front (C2)

We note from Figures IV.32 and IV.31 that the temperature values obtained by the study are consistent with those that were actually given to us in the factory

#### **IV.16. Conclusion**

In this chapter, we simulated a 2.2 kW asynchronous motor and performed its electromagnetic and thermal analysis. Benefits from reducing iron losses in electric motors include increased stability, noise reduction, temperature control, energy savings, and efficiency. To accomplish these objectives, engineers and designers concentrate on optimizing motor designs. Since iron losses affect overall motor performance, a balanced strategy is necessary for the best possible motor operation.

# **GENERAL CONCLUSION**

## GENERAL CONCLUSION

Electric cars offer significant environmental and economic benefits, such as zero emissions, lower operating costs, and reduced maintenance. However, they also face challenges like high initial costs, limited charging infrastructure, and environmental concerns related to battery production and disposal.

Electric motors in electric cars are pivotal to the functionality and efficiency of these vehicles. Unlike internal combustion engines, electric motors operate by converting electrical energy stored in batteries into mechanical energy, providing a smooth and instant torque that enhances acceleration and overall driving experience. They are typically more efficient than gasoline engines, as they generate less heat and have fewer moving parts, which reduces maintenance needs and increases longevity. Additionally, electric motors contribute to a quieter ride and lower emissions, aligning with the growing demand for sustainable transportation solutions. Innovations in motor design, such as advancements in permanent magnet and induction motor technologies, continue to improve the performance and range of electric vehicles, making them an increasingly viable alternative to traditional cars.

Losses in electric motors are a critical factor affecting their efficiency and performance, with iron losses being a significant component. Iron losses, also known as core losses, occur in the motor's magnetic core and consist of hysteresis and eddy current losses. Hysteresis losses arise due to the repeated magnetization and demagnetization of the core material, while eddy current losses are caused by circulating currents induced within the core. These losses lead to energy dissipation in the form of heat, reducing the motor's efficiency. Minimizing iron losses is essential for improving motor performance, which can be achieved through the use of high-quality magnetic materials, optimizing the core design, and implementing advanced control strategies. Addressing iron losses is particularly important in electric vehicles, where maximizing motor efficiency directly contributes to extending the vehicle's range and enhancing overall energy efficiency.

In the first chapter, we explored the history of electric cars and motors, the relationship between motors and batteries, and the types of electric motors used in electric vehicles, highlighting the prevalence of induction motors due to their good torque and low manufacturing cost. We also studied iron losses and their impact on motor efficiency, emphasizing the importance of minimizing these losses. The second chapter covered the types of magnetic materials, their properties, and

methods for calculating iron losses, such as the Steinmetz and Bertotti equations, with the Epstein framework being the most accurate. We presented in the third chapter how the Electro-Industries company producing induction motors from the first unit to the last one, where it works with high precision in order to manufacture an induction motors that meets international standards. The fourth chapter focused on the properties of M800-50A silicon iron sheets, using the Epstein framework to analyze iron losses at different frequencies, comparing losses between M400-50A and M800-50A sheets, and conducting electromagnetic and thermal simulations for a 2.2kW asynchronous motor.

Modeling iron losses in rotating electric motors is essential in various stages of motor design, performance analysis, control system development, and maintenance. It helps improve efficiency, manage heat, reduce costs, optimize performance, ensure compliance with standards, and enhance reliability and longevity. By understanding and minimizing iron losses, engineers can create more effective and durable electric motors.

# **BIBLIOGRAPHY**

## BIBLIOGRAPHY

- [1] Raff, D. M. (2018). GM and the Evolving Industrial Organization of American Automobile Manufacturing in the Interwar Years. In *Coping with Variety* (pp. 35-57). Routledge.
- [2] Ntombela, M., Musasa, K., & Moloji, K. (2023). A comprehensive review for battery electric vehicles (BEV) drive circuits technology, operations, and challenges. *World Electric Vehicle Journal*, 14(7), 195.
- [3] Ramya, K. C., Ramani, J. G., Sridevi, A., Rai, R. S., & Shirley, D. R. A. (2022). Analysis of the different types of electric motors used in electric vehicles. *E-Mobility: A New Era in Automotive Technology*, 43-57.
- [4] Zeaiter, A. (2020). Thermal modeling and cooling of electric motors: Application to the propulsion of hybrid aircraft (Doctoral dissertation, ISAE-ENSMA Ecole Nationale Supérieure de Mécanique et D'aérotechnique-Poitiers).
- [5] Hughes, A. (2005). *Electric motors and drives: fundamentals*. Elsevier Science & Technology.
- [6] Asmane, T., & Menad, O. (2016). Evaluation of iron losses in an asynchronous cage machine (Doctoral dissertation, Mouloud Mammeri University).
- [7] Bylia, B., & Taous, A. (2017). Calculation of iron losses in the asynchronous machine (Doctoral dissertation, Mouloud Mammeri University).
- [8] OSWOS, (2024). Losses in Electric Motors, <https://oswos.com/motor-losses/>.
- [9] Frias, A. (2015). Minimization of iron losses in electric traction machines through modeling and optimization (Doctoral dissertation, Université Grenoble Alpes).
- [10] Hämäläinen, H. (2013). Identification of some additional loss components in high-power low-voltage permanent magnet generators.
- [11] Krings, A. (2014). Iron losses in electrical machines-influence of material properties, manufacturing processes, and inverter operation (Doctoral dissertation, KTH Royal Institute of Technology).

- [12] O'handley, R. C. (1999). *Modern magnetic materials: principles and applications* (p. 768).
- [13] Bernreuther, W., & Suzuki, M. (1991). The electric dipole moment of the electron. *Reviews of Modern Physics*, 63(2), 313.
- [14] Fiorillo, F., Appino, C., Pasquale, M., & Bertotti, G. (2006). Hysteresis in magnetic materials. *The Science of Hysteresis*, 3, 1-190.
- [15] Cullity, B. D., & Graham, C. D. (2011). *Introduction to magnetic materials*. John Wiley & Sons.
- [16] Harris, I. R., & Williams, A. J. (2009). *Magnetic materials. Material science and engineering*, 2, 49-84.
- [17] Ros-Yáñez, T., Ruiz, D., Barros, J., & Houbaert, Y. (2004). Advances in the production of high-silicon electrical steel by thermomechanical processing and by immersion and diffusion annealing. *Journal of alloys and compounds*, 369(1-2), 125-130.
- [18] Mănescu, V. E. R. O. N. I. C. A., Păltânea, G. H. E. O. R. G. H. E., & Gavrilă, H. O. R. I. A. (2014). Non-oriented silicon iron alloys-state of the art and challenges. *Rev. Roum. Sci. Techn. - Electrotechn. et Energ.*, 59(4), 371-380.
- [19] Gao, L., Zeng, L., Yang, J., & Pei, R. (2020). Application of grain-oriented electrical steel used in super-high speed electric machines. *AIP advances*, 10(1).
- [20] Hur, N., Park, S., Sharma, P. A., Ahn, J. S., Guha, S., & Cheong, S. W. (2004). Electric polarization reversal and memory in a multiferroic material induced by magnetic fields. *Nature*, 429(6990), 392-395.
- [22] Jiles, D. (2015). *Introduction to magnetism and magnetic materials*. CRC press.
- [23] Reimets, N. (2018). Revamp of the Epstein frame measurement system for characterising magnetic materials (No. CERN-STUDENTS-Note-2018-122).

# **ABSTRACT**

## ABSTRACT

From all the electric motors types, the induction motor is the most common. Therefore, it is not a surprise to notice that it is still the subject of many research aiming to improve its modeling and optimize its design. Despite its simplicity of manufacture and implementation, modeling and calculating the induction motor is not easy.

The objective of this work is study and account the iron losses in an induction motor in No-Load test by measuring the Iron losses on steel sheet type M800-50A using Epstein frame, and calculating them again by using Steinmetz, Bertotti equation for different values of frequency and flux density, and the comparison between the iron losses produced by each steel sheet type M800-50A and M400-50A for the Epstein frame and the Steinmetz and Bertotti equations

**Key words:** Induction Motor, No-Load, Steinmetz, Bertotti equation, sheet type, Epstein frame.

## RESUME

De tous les types de moteurs électriques, le moteur à induction est le plus répandu. Il n'est donc pas surprenant de constater qu'il fait encore l'objet de nombreuses recherches visant à améliorer sa modélisation et à optimiser sa conception. Malgré sa simplicité de fabrication et de mise en œuvre, la modélisation et le calcul du moteur à induction ne sont pas aisés.

L'objectif de ce travail est d'étudier et de prendre en compte les pertes de fer dans un moteur à induction lors d'un test à vide en mesurant les pertes de fer sur une tôle d'acier de type M800-50A à l'aide d'un cadre Epstein, et en les calculant à nouveau en utilisant l'équation de Steinmetz et de Bertotti pour différentes valeurs de fréquence et de densité de flux, et la comparaison entre les pertes de fer produites par chaque tôle d'acier de type M800-50A et M400-50A pour le cadre d'Epstein et les équations de Steinmetz et Bertotti

**Mots clés :** Moteur à induction, Sans charge, Steinmetz, équation de Bertotti, Type de tôle, Cadre Epstein

## ملخص

من بين جميع أنواع المحركات الكهربائية، يُعتبر المحرك الحثي الأكثر شيوعًا. لذلك، ليس من مفاجأة أنه ما زال موضوع العديد من الأبحاث التي تهدف إلى تحسين نمذجته وتحسين تصميمه. على الرغم من بساطة تصنيعه وتنفيذه، فإن نمذجة وحساب محرك الحثي ليس أمرًا سهلاً.

هدف هذا العمل هو دراسة وحساب خسائر الحديد في محرك التيار الحثي في اختبار في الفراغ من خلال قياس خسائر الحديد باستخدام إطار إيشتاين ، وحسابها مرة أخرى باستخدام معادلات ستاينميرز وبرتوتي M800-50A على ورقة فولاذية من نوع M800- لقيم مختلفة من التردد وكثافة التدفق المغناطيسي. ثم يتم مقارنة خسائر الحديد التي تنتجها كل ورقة فولاذية من نوع

باستخدام إطار إيشتاين ومعادلات ستاينميرز وبرتوتي M400-50A و 50A

الكلمات المفتاحية: المحرك الحثي، اختبار في الفراغ، معادلات ستاينميرز وبرتوتي ورقة فولاذية، إطار إيشتاين